University of South Carolina
Scholar Commons

Theses and Dissertations

1-1-2013

High Quality Silicon Carbide Epitaxial Growth by Novel Fluorosilane Gas Chemistry For Next Generation High Power Electronics

Tawhid Rana
University of South Carolina - Columbia

Follow this and additional works at: http://scholarcommons.sc.edu/etd

Recommended Citation
Rana, T.(2013). *High Quality Silicon Carbide Epitaxial Growth by Novel Fluorosilane Gas Chemistry For Next Generation High Power Electronics.* (Doctoral dissertation). Retrieved from http://scholarcommons.sc.edu/etd/2432

This Open Access Dissertation is brought to you for free and open access by Scholar Commons. It has been accepted for inclusion in Theses and Dissertations by an authorized administrator of Scholar Commons. For more information, please contact SCHOLARC@mailbox.sc.edu.

HIGH QUALITY SILICON CARBIDE EPITAXIAL GROWTH BY NOVEL FLUOROSILANE GAS CHEMISTRY FOR NEXT GENERATION HIGH POWER ELECTRONICS

by

Tawhid Ahmed Rana

Bachelor of Science
University of Dhaka, 2003

Master of Science
University of Dhaka, 2005

Submitted in Partial Fulfillment of the Requirements

For the Degree of Doctor of Philosophy in

Electrical Engineering

College of Engineering and Computing

University of South Carolina

2013

Accepted by:

Tangali S. Sudarshan, Major Professor

Grigory Simin, Committee Member

M.V.S. Chandrashekhar, Committee Member

Anthony Reynolds, Committee Member

Lacy Ford, Vice Provost and Dean of Graduate Studies

© Copyright by Tawhid Ahmed Rana, 2013
All Rights Reserved.

DEDICATION

This dissertation is dedicated to the memory of my beloved mother *Salma Binte Noor*.

ACKNOWLEDGEMENTS

Completion of a PhD program is an odyssey which consists of not only joyful moments and successes but also failures and frustrations. However, at the end, the joy of a completion always overwhelms everything else. I will always remember Professor Sudarshan for his friendliness, positive attitude and cheerfulness during this time. Without his positive energy it would be impossible for me to overcoming the difficulties and finish my PhD. I would like to say thanks to Professor Sudarshan for encouraging me in pursuing new ideas and providing me with the necessary supports in realizing these ideas by various tools.

Besides Professor Sudarshan, Professor M.V.S. Chandrashekhar was the person who always stood beside me by supporting new ideas and giving his valuable suggestions, which significantly improved the content of the PhD dissertation.

I would like to thank to my colleagues and-lab members Dr. Haizheng Song, Amitesh Shrivastava, Iftekhar Chowdhury, Dr. Peter Muzykov, David Metts, Biplob K. Daas, Mohammad Islam (Jewel), Sabih Omar, Kevin Daniels and Shamaita Shetu for their technical help and sample characterizations. I would like to say thanks to my friends and family members in USA and in Bangladesh for their support during this time.

I thankfully acknowledge my parents for their selfless support. I am greatly thankful to my father Md. Obaidullah, who always ensured me the best quality education.

South Carolina is a place rich in natural beauty and wonderful people. I will specially remember the beautiful Congaree River, which was located very near to the USC. The main idea of my PhD topic is the result of a simple thought which was sparked in my mind while I was observing the rocks interacting with the water stream in this heavenly Congaree River. I will always cherish my beautiful memories in South Carolina in my heart and I hope I can take my experiences that I gained here to the next level in my upcoming career.

ABSTRACT

High quality, thick (~100μm), low doped and low defect density SiC epitaxial films are essential for high voltage (blocking voltage >10kV), light, compact and reliable next generation power devices. One of the significant challenges in obtaining high quality thick SiC epitaxial films is to restrict/eliminate the Si gas-phase nucleation or aerosol formation during growth. The generated aerosol particles adversely influence growth by reducing the growth rate due to precursor losses, and also affect crystal quality, since the Si droplets are carried to the crystal growth surface. Moreover, liquid aerosol particles adhere to the various reactor parts (parasitic deposition), and contribute to their severe degradation during epitaxial growth. These parasitic depositions are generally loosely bound, and can be carried to the growth surface during growth as particulates, resulting in degradation of crystal quality by introducing defects in the growing epitaxial layers. The aforesaid condition is specifically severe at higher precursor gas flow rates or in long duration growth required to achieve high quality thick epitaxy since parasitic deposition and related particulate formation are also increased at these growth conditions. At this parasitic deposition enhanced condition, the cost of growth is also expected to increase due to frequent replacement of degraded reactor parts. Hence, cost effective, high quality thick epitaxy is not achievable until the particle generation in the reactor is suppressed effectively in high temperature SiC CVD. To investigate the critical issues of parasitic deposition and nucleation related particle generation, intensive comparative study was

performed for the first time for different conventional silane and chloro-silane gases. Based on the study of these precursors, a novel Si precursor gas tetrafluorosilane (SiF_4) was proposed to be a superior Si precursor gas specifically suitable for high temperature SiC CVD. Initially, SiF_4 is compared to DCS without any propane addition during growth. It was found that without propane SiF_4 with only hydrogen, no Si deposition takes place in the reactor (only etches the SiC), whereas DCS deposits severe Si on the surface making the reactor parts unusable. The ability of SiF_4 not to deposit Si in the reactor is unique and found to be very useful to achieve high quality SiC epitaxy at high temperatures in the cleanest possible growth environment. The chemistry of SiF_4 gas precursor is utilized to eliminate Si gas phase nucleation and Si parasitic deposition during silicon carbide (SiC) epitaxial growth, otherwise unachievable in similar growth conditions using conventional silane (SiH_4) and dichlorosilane ($SiCl_2H_2$/DCS) precursors. Higher Si-F bond strength (565 kJ/mol) in SiF_4 prevents early gas decomposition and Si cluster formation, essential for high temperature SiC CVD, and yet enables growth of high quality epitaxy in an improved particulate suppressed growth condition. High quality, thick 4H-SiC epilayers >100 um have been demonstrated using SiF_4 with excellent surface morphology, polytype uniformity, crystallinity and low defect density needed for reliable high power devices.

TABLE OF CONTENTS

DEDICATION iii

ACKNOWLEDGEMENTS iv

ABSTRACT vi

LIST OF TABLES xi

LIST OF FIGURES xii

LIST OF SYMBOLS xviii

LIST OF ABBREVIATIONS xix

CHAPTER 1: SILICON CARBIDE 1

1.1 INTRODUCTION 1

1.2 PROPERTIES OF SIC 7

1.3 SIC CRYSTAL FUNDAMENTAL 11

1.4 GROWTH RATES ON DIFFERENT OFF CUT ANGLES 17

1.5 GROWTH MECHANISM 18

1.6 ETCHING PROCESS 21

1.7 DEFECTS 22

1.8 FORMATION AND CONVERSION OF BPD 25

1.9 MORPHOLOGICAL DEFECTS 29

CHAPTER 2: STUDY OF SIC EPITAXIAL GROWTH USING SILANE AND DICHLOROSILANE GASES 33

2.1 INTRODUCTION 33

PART I: ANALYTICAL MODEL 38

2.2 DIFFUSIVITY 38

2.3 GROWTH RATE CALCULATION 42

PART II: SIMULATION AND EXPERIMENTAL STUDY 47

2.4 INFLUENCE OF GROWTH PRESSURE 47

2.5 EXPERIMENTAL SETUP 48

2.6 DECOMPOSITION OF SILANE AND DCS INTO ELEMENTAL SILICON 50

2.7 GROWTH RATE VERSUS PRESSURE 53

2.8 VARIATION OF DOPING CONCENTRATION WITH PRESSURE 57

2.9 VARIATION OF SURFACE MORPHOLOGY WITH GROWTH PRESSURES 61

CHAPTER 3: SIC EPITAXIAL GROWTH USING FLUORINATED SILANE (SiF_4) 65

3.1 INTRODUCTION 65

3.2 EXPERIMENTAL SETUP 73

3.3 THERMO-CHEMICAL STUDY OF SiH_4, SiH_2Cl_2 AND SiF_4 76

3.4. STUDY OF PARASITIC DEPOSITION USING SiH_4, SiH_2Cl_2 AND SiF_4 81

3.5. COMPARISON OF EPITAXIAL GROWTHS USING SiH_4, SiH_2Cl_2AND SiF_4 82

CHAPTER 4: SIC SURFACE PREPERATION (ETCHING) BY SiF_4 89

4.1 INTRODUCTION 89

4.2 EXPERIMENTAL 96

4.3 RESULTS AND DISCUSSION 99

CHAPTER 5: EFECT OF C/SI RATIOS ON EPILAYERS GROWN ON VARIOUS OFF-CUT SUBSTRATES USING TETRAFLUOROSILANE GAS 113

5.1 INTRODUCTION 113

5.2 RESULTS AND DISCUSSION 119

5.3 C/SI VS. SURFACE MORPHOLOGY 136

SUMMARY AND FUTURE PROSPECTS 147

REFERENCES 153

APPENDIX A -SILICON CARBIDE CRYSTAL PLANES AND DIRECTIONS 160

APPENDIX B – EPITAXIAL GRAPHENE GROWTH BY SiF_4 GAS 161

APPENDIX C – SAFETY ISSUES USING SiF_4 GAS 162

APENDIX D – DRAWING OF SPLIT TUBE ASSEMBLY 163

APPENDIX E – CHEMICAL VAPOR DEPOSITION MANUAL 166

LIST OF TABLES

Table 1.1 Properties of various semiconductor materials 7

Table 2.1 Experimental and theoretical values of the diffusivities of various gas molecules in the silane-propane and DCS-propane CVD chemistries at STP................. 41

Table 2.2 Comparison of analytical calculation of diffusivity, boundary layer thickness and growth rate for Silane and DCS. 46

Table 2.3 Dissociation bonding energies (Huheey, 1972) for various bonds related to silicon carbide growth. 51

Table 3.1 Comparison of epilayer quality using various precursors for (T= 1550°C, P= 300 torr, H_2 flow rate = 6 slm, C/Si =~1 and growth duration = 1hr; substrate E_2(TO)/E_1(TO) or 4H/3C peak ratio = ~32, substrate doping = ~$1x10^{19}$-N-type and substrate XRD FWHM = ~20 arcsec). 83

Table 4.1 Dissociation bonding energies of various bonds found in Si precursors......... 96

Table 4.2 Free formation energy (kcal/mol) for various SiC etching reactions calculated from JANAF thermo-chemical data [21] (kinetics.nist.gov/janaf/)............................... 101

Table 5.1 Current commercial specification of 3" and 4" diameter wafers.................... 118

Table 5.2 : Metric for doping $\Delta N = N_D - (-N_A) = N_D + N_A$ of epilayer using various gases. 122

Table 5.3 AFM surface analysis of epilayers grown on different off cuts. 138

LIST OF FIGURES

Figure 1.1 Three possible stacking sequences of silicon carbide 12

Figure 1.2 SiC polytypes seen from different directions. 13

Figure 1.3 Step structure of SiC for various off cuts of 4H-SiC (towards[1120])........... 15

Figure 1.4 3D image of a kink produced due to off cut of a substrate (Si face). 16

Figure 1.5 Kink shape for the off cut towards a) [1120] and b) [1100] directions. 17

Figure 1.6 Modeled growth efficiency (qualitative indication of growth rate) as a function of off cut angles. 18

Figure 1.7 a) Bottom (towards [0001] x-ray view) of formed 3c on (0001) plane shows ABC stacking sequence of 3C on (0001) plane. b) Two possible sequences (twins) of formation of cubic crystal on (0001) planes of 4H off cut samples x. inclusion shows ABC sequence and y. inclusion shows ACB sequence. 19

Figure 1.8 Step by step animation of a step flow growth and 3C inclusion during step flow growth. 3C growths are showing in hexagonal structure for ease of drawing. 20

Figure 1.9 Lateral and vertical 3C growth on a 4° off cut terrace 21

Figure 1.10 Step by step etching process of a SiC off cut surface................................... 22

Figure 1.11 Various common SiC crystal defects delineated after KOH etching. Micropipe is a threading screw dislocation with a larger displacement. 23

Figure 1.12 Wastage of SiC material due to cutting at an angle towards [1120] direction. 24

Figure 1.13 BPD lines intersects the surface due to the off cut angle 26

Figure 1.14 Propagation and conversion of Basal Plane Dislocation (Zhang & Sudarshan, 2005) 26

Figure 1.15 A simple analogy to BPD propagation and conversion................................ 27

Figure 1.16 BPD propagation and conversion due to the variation of their directions. ... 28

Figure 1.17 Triangular defects and inverted pyramids on 4°, 4H-SiC epitaxial growth. . 30

Figure 1.18 a) Nomarsky images of Si particles on a 4H-SiC wafer. b) Nomarsky image of the epilaery grown for the same place and magnified images of the positions corresponding the the circles (insets) after etching. AFM image is shown for a pit (#9) found in the epilayer. 31

Figure 2.1 Theoretically calculated (a) diffusivity versus molecular weight plot calculated for various gases at 1 atm (760 torr) and 273°K, (b) diffusivity versus molecular weight plot for various gases at 300 torr and 1823°K (1550°C).. 39

Figure 2.2 a) Schematic of the CVD reactor used for growth calculation. b) Boundary layer at the solid-gas interface. 43

Figure 2.3 Schematic diagram and boundary conditions of the CVD furnace used in simulation. The sticking coefficient for the growth surface is assumed to be 1, i.e., growth species adsorbed on the substrate surface will participate in growth. 49

Figure 2.4 Simulation of Si partial pressure at various growth pressures. Suppression of Si formation in DCS is clearly seen at 30 torr. Temperatures at specific locations in the reactor are shown. 52

Figure 2.5 Growth rate versus pressure for a) silane and b) DCS precursors: simulation and experiments 53

Figure 2.6 Comparison of parasitic deposition for DCS and silane in the gas injector tube shown as PQ in Figure2.1 54

Figure 2.7 Doping concentration versus growth pressure. 59

Figure 2.8 (a) Simulated HCl partial pressure for various growth pressures for DCS. Temperatures at specific locations in the reactor are shown. (b) AFM surface roughness at various growth pressures for DCS precursor. (c) AFM images for epitaxy grown by silane precursor at various growth pressures. 62

Figure 3.1 Patented technology to suppress parasitic deposition by creating a buffer gas layer.. 68

Figure 3.2 (a) Reactor geometry showing the position of the split gas-injector tube (left). Split tube before growth and parasitic depositions after growth are shown for different silicon precursor gases with propane and hydrogen. The locations from where the parasitic deposition starts are marked as 1, 2 and 3 for silane, DCS and SiF_4 respectively. (b) Temperature profile in the reactor obtained using a simulation tool is shown. (c) Bar graph showing the masses of parasitic depositions on gas injector walls using silane, DCS and SiF_4 precursor gases *with* and *without* propane addition. An ~80% reduction of parasitic depositions for SiF_4 *with propane* and a ~100% reduction *without propane* was found. (T= 1550°C, P= 300 torr, H_2 flow rate = 6 slm, propane flow rate = 1.6 sccm, Si precursor flow rates = 5 sccm and duration = 1hr). 74

Figure 3.3Temperature versus Gibbs free energy of thermal decomposition reactions of SiH_4, SiH_2Cl_2 and SiF_4 showing very less favorable thermal decomposition reaction for SiF_4.. 78

Figure 3.4 Particles on epilayer surface grown using various gas precursors at similar growth condition. No large particle related defects are observed for the epilayer grown using SiF_4 even at higher flow rates. (T= 1550°C, P= 300 torr, H_2 flow rate = 6 slm and duration = 1hr). 83

Figure 3.5 AFM image of a 60um thick epilayer with excellent surface morphology grown using SiF_4... 85

Figure 3.6 Raman analysis for epilayers grown using (a) silane, (b) DCS and (c) SiF_4. A higher $E_2(TO)/E_1(TO)$ peak ratio for the epilayer grown using SiF_4 (c) indicates improved polytype uniformity compared to growths using silane (a) and DCS (b). High LOPC mode peak intensity for SiF_4 grown epilayer (c) is indicative of lower dopant incorporation compared to epilayers using silane (a) and DCS (b). 85

Figure 3.7 X-ray rocking curve of a epilayer grown using SiF_4 gas with a FWHM of ~7.5 arcsecond.. 86

Figure 3.8 Room temperature PL spectrum of a SiC epilayer grown using SiF_4 demonstrates peak at 3.17eV. 87

Figure 4.1 Surface and subsurface damages are shown I. Initial state II. Force is applied on the diamond particle and SiC crystal is deformed, initiating surface and subsurface damages.. 92

Figure 4.2. a) Electrochemical setup. b) Decoration of subsurface damages after electrochemical treatment of SiC wafers in $CuSO_4$ solution. 94

Figure 4.3 Etch rates using various precursor gases with various concentrations in H_2 gas with dominant reaction numbers found in Table 4.2. Both DCS and Propane mitigate the etching of hydrogen whereas TFS enhances the hydrogen etching. Etch rates using TFS increases at higher concentration. 100

Figure 4.4 Mechanism of SiC etching using TFS and H_2. I. Si and C of SiC dissociate and form Si (l) on the surface according to reactions 1 and 2 in Table 4.2, II. Si on the surface is removed by TFS (reaction 14, Table 4.2). In the absence of TFS, the removal of silicon would be by thermal evaporation (reaction 5, Table 4.2), which is much less favorable, and III. Hydrogen reacts and removes C by forming either CH_4 or C_3H_8 gases (reactions 10 and 11, Table 4.2). 106

Figure 4.5 Etch rates as a function of TFS concentration in H_2 gas for various off cut SiC substrates. A trend of slightly higher etch rates were observed for higher off cut substrates. 109

Figure 4.6 AFM surface morphology of SiC surfaces for 0°, 4° and 8° off cut substrates etched at various TFS gas concentrations in H_2. 110

Figure 5.1a) C/Si ratio versus doping graph for various off cut substrates using SiF_4 and C_3H_8 as precursor gases; b) Doping concentration versus C/Si ratio for various off cut substrates using silane. 121

Figure 5.2 Comparison of C/Si ratio vs. doping for SiF_4 and DCS showing the doping change is less affected for SiF_4 compared to DCS (8° off cut). 121

Figure 5.3 C/Si ratio distribution in the reactor (2D analysis) and distance versus C/Si ratio plot of the susceptor surface. 124

Figure 5.4 C/Si versus growth rate for various off cut substrates (3C growth is found above a C/Si ratio of 0.3 for on-axis substrates. 129

Figure 5.5 Increased 3C at the steps is shown due to the higher off cut substrates (a) compared to the lower off cut substrates (b) and considered to be the reason for lower 4H/3C for higher off cut substrates. 132

Figure 5.6 Raman analysis of various epilayers with different off cuts at different C/Si ratios 134

Figure 5.7 Bar graph showing the 4H/3C peak ratios found at various C/Si ratios for various off cut substrates. 4H/3C of the substrates (for all of cuts) are shown by dashed line. 135

Figure 5.8 AFM study of epilayers grown on 8° off cut substrates at various C/Si ratios showing no strong correlation. Roughness (r.m.s) is shown in nm. 136

Figure 5.9 Graphical illustration of macro and micro steps 137

Figure 5.10 AFM images of the epilayer sufaces (4° off cut) for varoius C/Si ratios showing variation of step bunching on the surface. 1D analysis (white line at the top of each images) of these surfaces are shown in Figure 5.8. 138

Figure 5.11 1D analysis of the epilayer surface for various C/Si ratios grown on 4° off cut substrates showing the variation of macro and micro steps as a function of C/Si ratios. 140

Figure 5.12 a) Roughness measured based on the macrostep peak and troughs (calculated manually) for different C/Si ratios. b) Roughness measured based on the microstep peaks and troughs (calculated manually) for different C/Si ratios. These figures demonstrates that macrostep height is a stronger function of C/Si ratio than the microstep height..... 141

Figure 5.13 (a) AFM images of the epitaxial growth on the vicinal on-axis surface at a C/Si ratio of 0.3. b) 1D scan analysis of the surface along [1120]. (b) Nomarski images of the surface at different C/Si ratios. 143

Figure A.1 Crystal directions on the basal plane of hexagonal SiC crystal.................... 160

Figure A.2 Various crystal planes of hexagonal SiC crystal 160

Figure B.1 Steps of the graphene growth by TFS (SiF_4) gas n an inert ambient............ 161

Figure D.1 Sketch of the injector. 163

Figure D.2 Sketch of injector split tube. 164

Figure D.3 Sketch of top plate of the gas injector. 165

Figure E.1 Block diagram of CVD system. 168

Figure E.2 CVD reactor system used for the experiments.. 168

Figure E.3 Rack-1, Rack-2 and Rack-3 of the CVD system at USC............................. 169

Figure E.4: CVD program by lab view 171

Figure E.5: MFC software (MKS controller) 171

Figure E.6: Profile viewer (Labview) 172

Figure E.7 Simplified block diagram of CVD system. 173

Figure E.8: pressure controller front panel. 174

Figure E.9: Varian turbo pump control panel 175

Figure E.10: Cold Cathode Pressure unit. 175

Figure E.11: Gas flow meter display unit. 176

Figure E.12: Temperature sensor display. 177

Figure E.13: Gas cylinder valves and meters... 179

LIST OF SYMBOLS

E Electric field (V/cm).

D Diffusivity (cm^2/sec)

C Capacitance

V Voltage

I Current

ϵ Relative permittivity.

LIST OF ABBREVIATIONS

AFM .... Atomic Force Microscopy

FTIR .... Fourier Transformed Infra Red spectroscopy

SEM .... Scanning Electron Microscopy

TFS .... Tetrafluorosilane

DCS .... Dichlorosilane

CHAPTER 1

SILICON CARBIDE

In this chapter, fundamental of silicon carbide (SiC) as an electronic material and its challenges in term of epitaxial growth will be explained. A 3D CAD model is used to elucidate various basic crystallographic terminologies through new imageries, essential for the understanding of silicon carbide crystal and its epitaxial growth. Growth rate dependency is predicted for different off cuts based on these geometric models. Conditions for homogeneous growth are explained. Various primary defects related to SiC epitaxy is discussed in this chapter. Propagation and conversion of Basal Plane Dislocation is discussed and it is shown that BPD aligned to the off cut direction has the greatest chance to propagate into the epitaxial layer. Finally, some of the important morphological defects and their origin during crystal growth are introduced in this chapter. We believe this chapter will be a good starting point for the beginner researchers in the field of SiC epitaxy and may also be beneficial for the experienced researcher in the field to review their basic concepts on SiC crystal and epitaxial growth.

1.1 INTRODUCTION

There is a continuous effort in modern engineering technologies to reduce the size of the electronic devices for the convenience of their use. Electronics used in our everyday life are already astonishingly compact and light compared to the technology,

which was available 10 years ago. Compact, light weight, cell phone, PDA and many other pocket gadgets are using computational speed in the range of GHz frequency with enormous amount of memories in the range of giga bytes (GBs). Most of the appliances in our everyday life operate in low power range, usually around 100 volts and few amperes. At this operating voltage, it is easier to make the electronics smaller since they operate at small power and lower temperatures. Voltage domain in the regime outside of our households is much higher, and making compact and light weight electronic devices in that high voltage regime is extremely challenging. Heavy machineries used in the industries operate at a much higher voltages usually in the range of kVs. The voltage used in the national grid is much higher in the range of 10kVs to 100s of kVs. After the power generation in a power plant, voltage in the grids stepped up much higher in the order of 100s kVs in order to reduce current induced joule heating losses during long distance transmission. These high voltage power sources are stepped down for commercial or household applications.

During the transmission and voltage conditioning process (e.g. step up, step down) energy is lost. Each year about 7% of the electric energy is lost only during transmission and distribution in US (www.eia.gov/tools/faqs/faq.cfm?id=105&t=3). The loss of energy will be much bigger if the losses at the customer end are also included (e.g. factories, houses, offices etc.). The picture of energy losses will be enormous and much worrisome if the total losses in the world are considered. These energy losses not only cost a huge amount of money every year but also affect the global climate of the world.

The USA produced about 4,106 billion kilowatt-hours of electricity in 2011. Among this electricity produced, 68% was generated from the fossil fuel

(www.eia.gov/tools/faqs/faq.cfm?id=427&t=3). These fossil fuels have effect on emitting green house gases (e.g. CO_2, CH_4), thus increasing the carbon footprint (Laurence A Write, 2011) and facilitating global warming. Hence, reducing the power loss of the electric system does not only reduce the cost but also helps to reduce environmental pollution for a better world.

Currently, the electric grid system is built on 100 years old infrastructure where the supply is one directional to the customer. In this system the power system (e.g. power plant) cannot update itself to generate power based on the necessity of the consumer usage. To make the electricity distribution and power consumption much more managed to reduce losses and utilize them more efficiently, an intelligent grid system is required in near future which is termed as 'Smart Grid'. According to DOE (Department of Energy, US), five technologies will mainly drive the Smart Grid of the future. They are (www.energy.gov): "

- Integrated communications, connecting components to open architecture for real-time information and control, allowing every part of the grid to both "talk" and "listen".
- Sensing and measurement technologies, to support faster and more accurate response, such as remote monitoring, time-of-use pricing and demand-side management
- Advanced components, to apply the latest research in superconductivity, storage, power electronics and diagnostics
- Advanced control methods, to monitor essential components, enabling rapid diagnosis and precise solutions appropriate to any event

- Improved interfaces and decision support, to amplify human decision making, transforming grid operators and mangers quite literally into visionaries when it comes seeing into their systems ”

In the smart grid system, the power supply to the clients are not one directional, rather both the central system and the appliances can interact and find the optimal power management for the efficient use of energy with minimum wastage. This process requires much increased control over high voltage electric grid system at every possible node so that they can be switched on/off or conditioned (e.g. voltage conversion etc.) more efficiently and frequently. This is not possible with existing bulk transformer based voltage conversion or bulky mechanical switch based switching system. To realize the proposed smart grid system semiconductor based compact switching and power conditioning is essential.

It can be understood easily that to realize five primary goals of Smart Grid technology, in future, huge amount of electronic circuitry is required which will be able to operate reliably at a much higher voltage than we use in our households, which is beyond the handling capacity of the current silicon based technologies.

Making small, compact, light weight devices, which can operate at high voltage, is not only highly demanded for Smart Grid systems but they are also essential for ships, air carriers, automobiles etc. The fuel cost of the carrier is directly related to the weight of the carrier and hence the total weight of the carrier should be as less as possible. With the current silicon based electronics, huge, bulky cooling units are required, which increases the weight of the carrier significantly and thus also increases the cost. There are only few

electronic materials that can be operated in the aforesaid high voltage (or power) regime, at least theoretically, and certainly silicon carbide is the leading material of consideration.

Silicon carbide is one of the most promising new semiconductor materials for the aforesaid applications. Silicon carbide is the choice of making high voltage, high power electronic applications due to its outstanding properties such as high band gap, high thermal conductivity, high breakdown electric field, low intrinsic carrier concentration etc. (Table 1.1). Due to these properties, SiC electronic devices can be made compact, light weight and yet operable at high voltage and high current condition. Despite these promising properties, SiC is not yet a popular material for device fabrication due to the difficulties to produce high quality single crystal materials. Though true exploitation of SiCs unique properties in electronic devices should excel the performance of Si based power devices in the current market, the primary goal of SiC material for electronic devices is not reached yet. Further, few SiC power devices present in the market are still much expensive than the Si based power devices. Despite reports on devices in various literatures over 10KV (Sundaresan, Sturdevant, Marripelly, Lieser, & Singh, 2012; Zhao, Alexandrov, & Li, 2003)and high temperature applications, commercially available product is still in the range of 1.2 KV and at ~100 - 175°C (www.cree.com/news-and-events/cree-news/press-releases/2013/march/2nd-gen-mosfet; www.genesicsemi.com/index.php/news/03-05-13)only. When a product is commercialized, the rating for the product (e.g. voltage current relation) must be strictly maintained and it should be highly reliable for day to day operation since human lives will be depending on these devices (e.g. uninterrupted power supply to houses, hospitals, schools, vehicles etc). The meaning of reliability is that the rating of an electronic device

will be guaranteed over a certain period time within an acceptable tolerance limit. Silicon carbide devices cannot ensure reliability for high voltage application until high quality SiC materials are available. Despite high demand for high power electronics, SiC based devices will not be sold like hot cakes for Smart Grids, ships, air carriers or automobiles until the reliability of the devices is guaranteed by reducing the defects in the material.

Defects in electronic materials result in uncertainty in the device operation rendering unpredictable change of the behavior of the devices over time and even unexpected failure. In nature, 'defects' (in biological organisms) are well handled which is in fact create diversity. Perhaps the term 'defect' does not even exist from nature's perspective. However, compared to the biological world in nature, human electronic technology is still primitive. The operation of the electronic devices has to be predicted within a 'well defined' regime governed by the crystal structure. It is extremely difficult for us to predict the behavior of the electronic devices if the periodicity of the crystal (i.e. the simplicity) is not preserved. In that consideration, for man-made electronic world, the crystal should be 'defect' free so that the outcome of the devices can be well defined for guaranteed reliability. The world we live now is based on electronic technologies. Hence scientists constantly strive to explore new materials for electronics and improve their crystal quality by reducing defects in them to uncover more hidden power in the nature for the benefits of human lives.

Table 1.1 Properties of various semiconductor materials[a]

Property	Si	GaAs	4H-SiC	6H-SiC	3C-SiC	2H-GaN
Bandgap (eV)	1.1	1.42	3.2	3.0	2.3	3.4
Relative dielectric constant	11.9	13.1	9.7	9.7	9.7	9.5
Breakdown field (MV cm^{-1}) @$N_D = 10^{17}$ cm^{-3}	0.6	0.6	3	3	1.8	2-3
Thermal Conductivity (W/cm/K)	1.5	0.5	3-5	3-5	3-5	1.3
Intrinsic carrier concentration (cm^{-3})	10^{10}	1.8 X 10^6	~4 x 10^{-8} [b]	~10^{-6} [b]	~10	~10^{-10}
Electron mobility @$N_D = 10^{16}$ cm^{-3}	1200	6500	‖ c-axis 800 ⊥ c-axis 800	‖ c-axis 60 ⊥ c-axis 400	750	900
Hole Mobility @$N_A = 10^{16}$ cm^{-3}	420	320	115	90	40	200
Saturated electron velocity (10^7 cms^{-1})	1.0	1.2	2	2	2.5	2.5

[a] Adapted from (Neudeck, 2006)
[b] calculated using Nc (4H) = 3.25 x $10^{15}T^{3/2}$, Nv (4H) = 4.8 x $10^{15}T^{3/2}$
and Nc (4H) = 3.25 x $10^{15}T^{3/2}$, Nv (4H) = 4.8 x $10^{15}T^{3/2}$ from the formula
$n_i = \sqrt{NcNv} e^{-Eg/2kT}$

1.2 PROPERTIES OF SIC

Before we proceed to the discussion of the properties of SiC in comparison to other semiconductor materials, we will discuss some basic semiconductor fundamentals which determine the high temperature and high voltage operability of semiconductor materials.

Considering the semiconductor is pure (no dopant), at a certain temperature, there will be a small part of the covalent electrons liberated from the bonds due to the thermal energy present (kT) and these electrons will become conduction electrons. These carriers

generated due to thermal energy are called intrinsic carriers. At room temperature, thermal energy is 0.026eV or 26meV which is considerably lower than the bandgap of the common electronic materials (e.g. bandgap of Si and 4H-SiC are 1.1 and 3.2 respectively). Bandgap energy of Si is 42 times higher than the thermal energy at room temperature whereas 123 times higher than SiC bandgap energy. As a result there will be much lower intrinsic carrier concentration present for SiC compared to Si at room temperature. The intrinsic carrier concentration of a semiconductor material decreases exponentially with bandgap (Pearton, 1997) by the following relation,

$$n = N_c e^{-(E_C - E_F)/kT} \qquad (1.1)$$

where N_C is the effective density of states. For regular electronic applications, dopant density determines the majority carrier concentration, whereas intrinsic carrier concentration will essentially be the minority carrier concentration. An increased minority carrier or intrinsic carrier concentration will increase the reverse bias leakage current of the device. Hence as the temperature increases, intrinsic carrier concentration will increase (see temperature relation in equation 1) and also the leakage current will increase. Higher bandgap of SiC and associated lower intrinsic carrier concentration (Table 1.1) gives SiC of its theoretical operational limit to 800°C compared to only 300°C of Si (Neudeck, 2006) .

There is another important consideration for high temperature operability which makes SiC to be unique compared to other semiconductor material. Thermal conductivity is the property of material to conduct heat (W/cm/K). During operation (i.e. resistive heating due to high current flow), it is necessary to efficiently conduct the thermal energy to the surrounding (e.g. heat sink or air) before it destroys the device. Localized heat in a

device is needed to be spread over the whole device surface and to the surrounding faster to prevent localized damage in an integrated circuit chip. This is an extremely important consideration for high power devices due to their high current operation and related heat generation. A much higher thermal conductivity (~5 W/cm/K) of SiC makes it unparalleled for high temperature operation in terms of heat management than other common semiconductor materials.

The second consideration for high power electronics is that how much voltage can be applied across a material without rupturing it. Maximum voltage that can be applied across a material depends on its breakdown electric field (V/cm). When electric field is applied across a semiconductor material, above a critical value, the material loses its ability to withstand or resist the force created by the electric field and as a result it raptures. As an analogy, similar phenomenon occurs during lightening spark on the sky when electric field exceeds the breakdown electric field of the air. Higher breakdown electric field is essential for high voltage operation of a material. Breakdown electric field of SiC is about 10 times higher than the breakdown electric field of Si indicates that similar thickness of SiC should block much higher voltage than Si. Breakdown voltage of a semiconductor rectifier depends on the breakdown or critical electric (E_{crit}) field as below:

$$V_B = \frac{\epsilon_S E_{crit}^2}{2qN} - \phi_{bi} \qquad (1.2)$$

As a result of high breakdown field and lower intrinsic carrier concentration, using SiC, the blocking voltage region can be made 10 times thinner and 10 times heavier doped for Si, thus giving a 100 fold benefit in reduced resistance of the blocking region for the same voltage rating (Bhatnagar & Baliga, 1993).

Despite the aforesaid advantage of SiC for high temperature operation, mobility of SiC is not very promising compared to GaAs, GaN or Si (Table 1.1) and hence SiC cannot compete for high speed devices with GaAs, GaN and may not be a choice for high frequency devices. It is to be mentioned that electron mobility of 6H SiC is isotropic unlike that of 4H-SiC, and is much lower to the direction parallel to c-axis (Table 1.1). Hence vertical device with 6H-SiC is not preferable and hence 4H-SiC triumphs over 6H-SiC for the choice of devices. Currently 4H-SiC draws the primary interest in the research community.

Gallium Nitride (GaN) is the strongest competitor for high voltage and high temperature applications in the field due to its high bandgap, low intrinsic carrier concentration, high breakdown field and higher mobility and saturated electron velocity. However, the thermal conductivity of GaN is lower compared to SiC and GaN may not be the best choice for high temperature devices in terms of heat management. However, the main drawback of commercialization of GaN high power devices is considered to be the lack of its substrates availability in the market. GaN substrates are very expensive. Currently a six inch wafer of Si is only about $25, whereas, only a two inch GaN wafer costs about $1900 (www.compoundsemiconductor.net/csc/indepth-details/19735741/GaN-substrates-to-challenge-silico.html) (on the other hand, for comparison, SiC substrate will cost around few hundred dollars for a 2” wafer). To avoid this exorbitant cost, GaN epilayers are usually grown over sapphire, SiC or Si. As a result, interface mismatch related defects are created which increases the leakage current (www.compoundsemiconductor.net/csc/features-details/19734837/Exploiting-the-high-temperature-promise-of-Si.html). However, GaN substrate technology is improving

rapidly. It is predicted that the price of GaN substrate will fall by 60% by the year 2020 (www.compoundsemiconductor.net/csc/indepth-details/19735741/GaN-substrates-to-challenge-silico.html). As GaN substrates are improved and become cheaper, it can be assumed that that the competition between SiC and GaN to be the choice high power electronic material will be much harder in near future unless SiC technology solves its critical challenges meanwhile.

1.3 SIC CRYSTAL FUNDAMENTAL

1.3.1 POLYTYPES

About 200 known polytypes are found for Silicon carbide (Matsunami & Kimoto, 1997). Different polytypes have different stacking sequences. To understand the SiC growth and related challenges it is essential to know its common polytypes in terms of stacking sequences, crystal directions, crystal planes etc. A crystal will behave differently from different directions. As an example, for 6H SiC, the mobility is different along different crystal directions (Neudeck, 2006). Crystal growth is different on different planes for growth rates, polytype replication (homogeneity) etc. To have a comprehensive understanding of growth related issues on different crystal planes we will first discuss about some important polytypes and their crystal structures for those polytypes which are very widely used in SiC technologies.

Let us discuss what polytype is. If one hexagonal close pack layer (Stack-1) is stacked over another hexagonal closed pack layer (Stack-2) as in Figure 1.2, there are three different possibilities they can be stacked one over another. These positions are termed as A, B and C as shown in Figure 1.2.

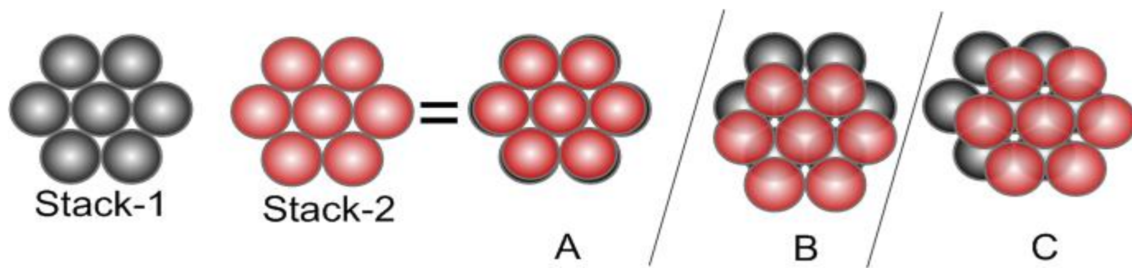

Figure 1.1 Three possible stacking sequences of silicon carbide

When SiC crystals are formed, the stacking order may take different sequences before they repeat. Hence, SiC crystals may have different properties despite the same atomic composition. This is called the polytypism. SiC polytypes are named based on the number of stacks before the sequence is repeated. Various common SiC polytypes, 2H, 3C, 4H and 6H are shown using 3D modeling in Figure 1.3 These polytypes are shown from different perspectives as if they are viewed by the audience (or seen by the gas molecules during the growth) from different directions. The relative sizes of the atoms are maintained in this Figure and heights of the bi-layers are kept proportional to give the reader 'a feel' of viewing real SiC crystals. The polytypes stacking sequences can be seen easily by observing Figure 1.3(a) and Figure 1.3. (b). However, for the similar polytypes, it is not possible for the viewers to know the polytype by just merely

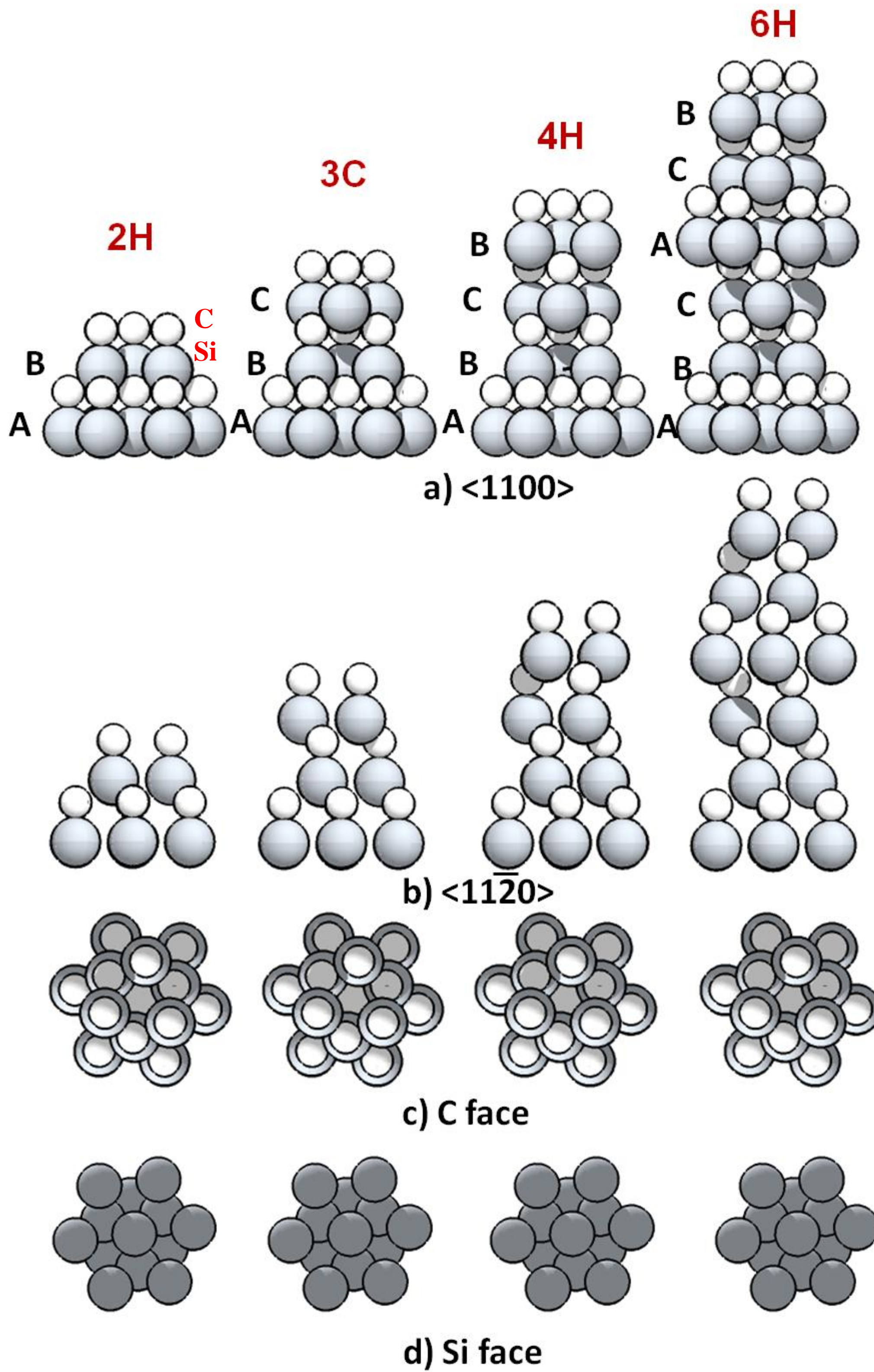

Figure 1.2 SiC polytypes seen from different directions.

observing the c planes (from top or bottom) in <c> direction as shown in Figure 1.3(c) and Figure 1.3(d). Readers are advised to see various directions in the SiC crystal in the Appendix.

Similarly, during the CVD growth, molecules 'see' the surface they approach the surface from different directions. Crystal growth on a c plane (or basal plane) can take any arbitrary polytype when gas molecules approach it as for us it is impossible to know the polytype from the c plane only (as Fig-3c and d). So, growth on a c-plane (0001) is highly unpredictable since it does not expose any template needed for polytype replication during growth. Homogeneous crystal is essential for devices and this problem can be solved by partially exposing the m planes to create a template for polytype imitation by cutting the original crystal boule at an angle which is called the off cut angle. Thus, to facilitate the homogeneous growth, steps are created by cutting the wafer at a certain angle and this is called step controlled epitaxy as described in (Matsunami & Kimoto, 1997) for silicon carbide epitaxy.

1.3.2 STEP CONTROLLED EPITAXY

To create the template for the imitation of the polytype during the crystal growth, it is essential to cut the crystal at an angle of usually 2°, 4°, 8°. Wafers are usually produced by cutting at an angle towards a certain direction which is usually $< 11\bar{2}0 >$ for SiC. Figure 1.4 shows the step sizes for different off cut angles. Using the 3D modeling software it was found that the step density will increase up to an off cut of 65.8 degree and reach its maximum step density for 4H-SiC. It can be inferred that the crystal quality will be the best in term of polytype uniformity at this angle since for this off cut, a highest number of templates are present due to highest number of kinks. An enlarged

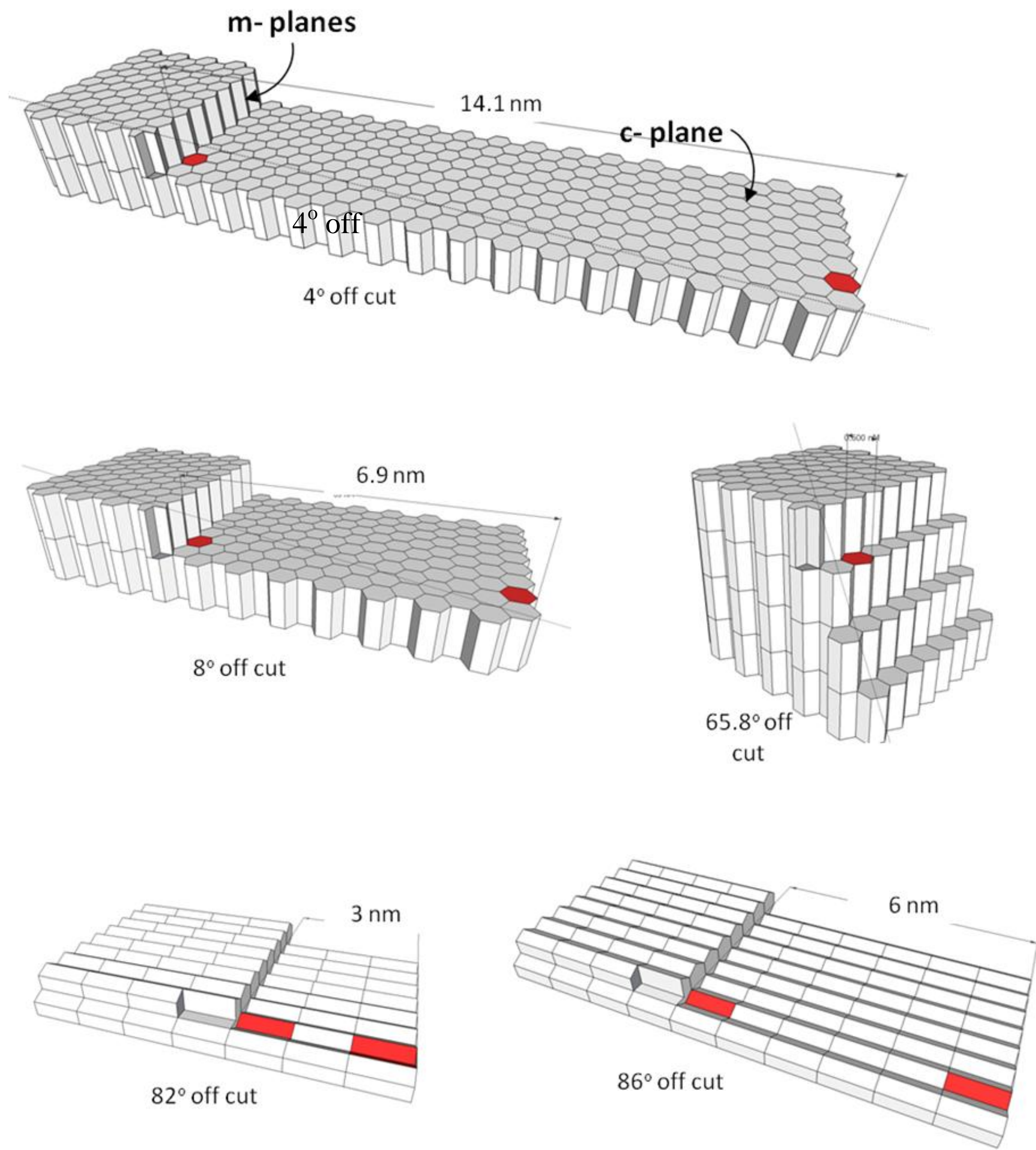

Figure 1.3 Step structure of SiC for various off cuts of 4H-SiC (towards$[11\bar{2}0]$)

image of the kink, where the ideal growth should take place is shown in Figure 1.5. When off cut is increased further, step density is reduced again, however this time, the crystal

plane on the surface changes. Step height is reduced and the surface of the terrace is not c plane anymore as seen for the off cuts of 82° and 86° in Figure 1.4.

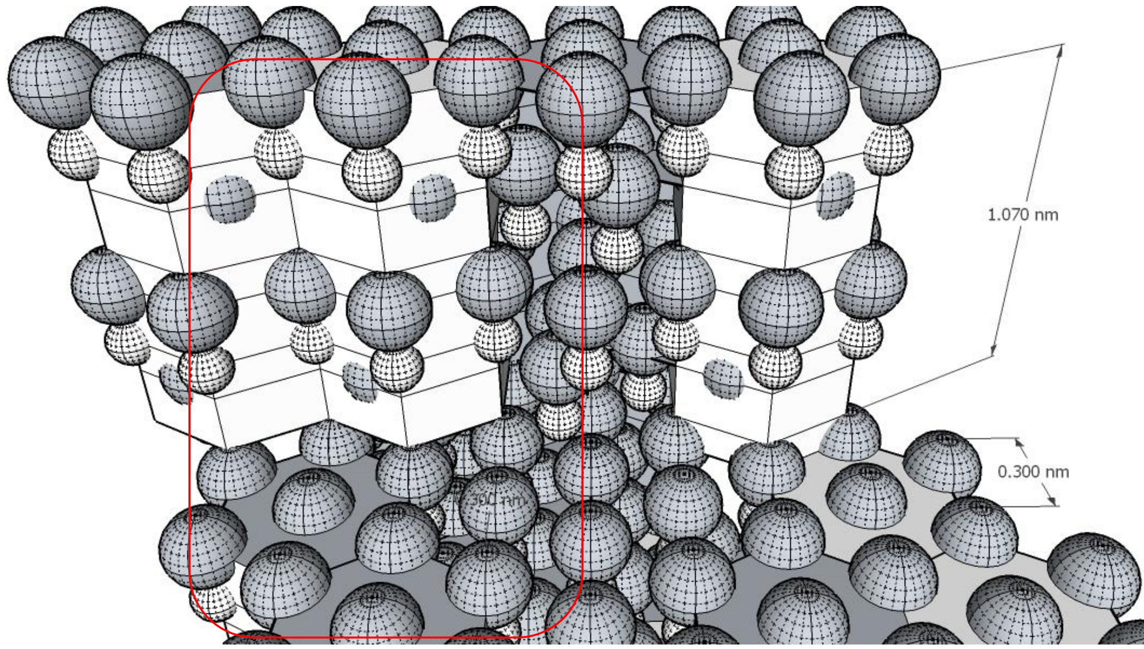

Figure 1.4 3D image of a kink produced due to off cut of a substrate (Si face).

How a kink might be different than a terrace can be apparent by observing Figure 1.5. At kinks both Si and C dangling bonds are present whereas the terrace is only terminated either by Si or C. At the kink dangling bond from both C and Si are present and hence kinks are energetically more favorable for homogeneous growth.

If the crystal is cut towards $< 11\bar{2}0 >$ direction, then the kink produced at the steps will look like Figure 1.6(a). On the other hand, if the crystal is cut towards <1100> direction, the kink will look like Figure 1.6(b). Even though in a perfect off cut, only a certain kind of steps Figure 1.6 (a) or (b) should exist, however, practically, the off cut is not perfect and it is possible that both type of steps may present on the surface due to

mis-cut. At higher off cuts one type of step will be dominant with higher density than the other. On the other hand, for lower off cut substrates, especially for the vicinal on axis substrate, the density of both types of steps might be comparable in density and the growth may take in both directions (isotropic) rendering anomaly in the step flow growth.

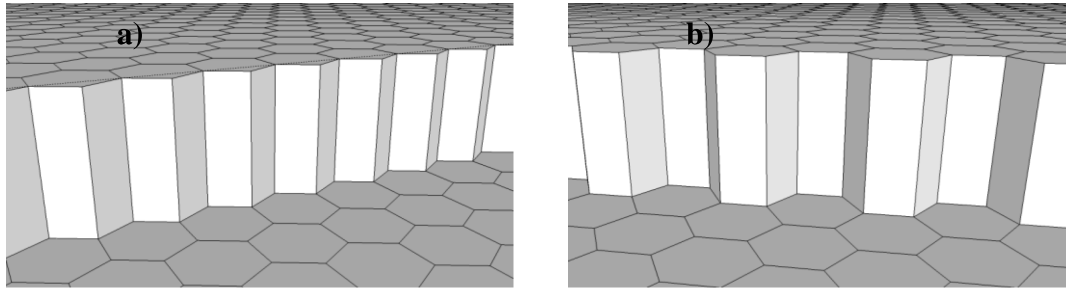

Figure 1.5 Kink shape for the off cut towards a) $[11\bar{2}0]$ and b) [1100] directions.

1.4 GROWTH RATES ON DIFFERENT OFF CUT ANGLES

Off cut substrates have a surface with c planes and m planes (Figure 1.4). The objective of the off cut is to provide template of the certain polytype to facilitate the homogeneous growth as discussed earlier. The activation energy required for the growth is very low at the kink (only 3 kcal/mol) compared to the higher activation energy required to grow on the terrace (20 kcal/mol) (Kimoto, Nishino, Yoo, & Matsunami, 1993). Hence, kinks produced due to off cut as shown in Figure 1.5 have the highest sticking coefficient for the growth and kinks work like a perfect sink during the growth. Since, growth takes place (or should take place for homogenous growth) mainly at the kinks due to very low activation energy at kinks, hence growth rate will be proportional to the kink density on the surface. Kink density on the surface is a function of off cut angle as shown in Figure 1.4. We used the 3D modeling tool to count the step number for

a certain length for various off cut angles and plot them in Figure 1.7. The y-axis in Figure 1.7 is analogous to the step density or kink density indicating the growth efficiency or growth rate. Step increment is not linear to the increase of off cut and does not change for all off cut angles. The off cut angles where there is a change in step density is shown by dots in Figure 1.7. It can be seen in Figure 1.7 that the kink density increases rapidly until ~10° off cut almost linearly and then changes slowly at above. There is a very little variation of step density in the range of off cut angles shown as A and B in Figure 1.7. Step density starts decreasing again above 65.8° off cut. Though a higher off cut will increase the growth rate, later in this chapter we will show that a device killing defect, BPD density increases for higher off cut substrates which is undesirable. Hence, there is a dilemma in selecting the right off cut angle for the epitaxial growth.

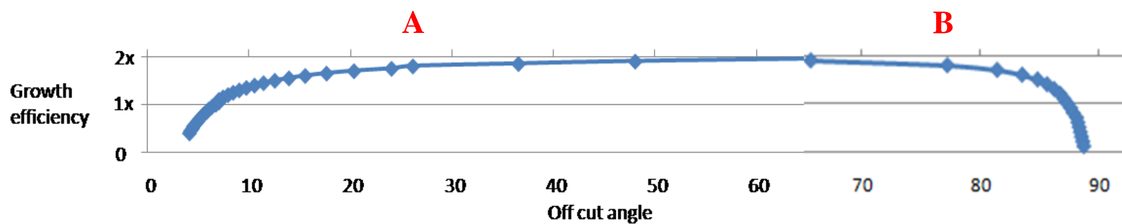

Figure 1.6 Modeled growth efficiency (qualitative indication of growth rate) as a function of off cut angles.

1.5 GROWTH MECHANISM

Growth on c plane (0001) is undesirable due to their tendency to form 3C polytype since it is the plane of (111) of a cubic crystal as well (Konstantinov, Hallin,

Pecz, Kordina, & Janzen, 1997)with a negligible lattice mismatch. 3C nucleation on the (0001) or c-plane and the possibility of forming 3C twins are visually depicted in Figure 1.8. As discussed earlier, the goal of cutting the substrate at a certain angle is to create the kinks where polytype sequence is exposed for imitation by the incoming gas molecules during the CVD process. However, c planes (terraces) on the surface as seen in Figure 1.4 are still present. Hence, the possibility of 3C formation remains during the growth. In an ideal condition 3C growth on c plane (Figure 1.8) should be completely suppressed.

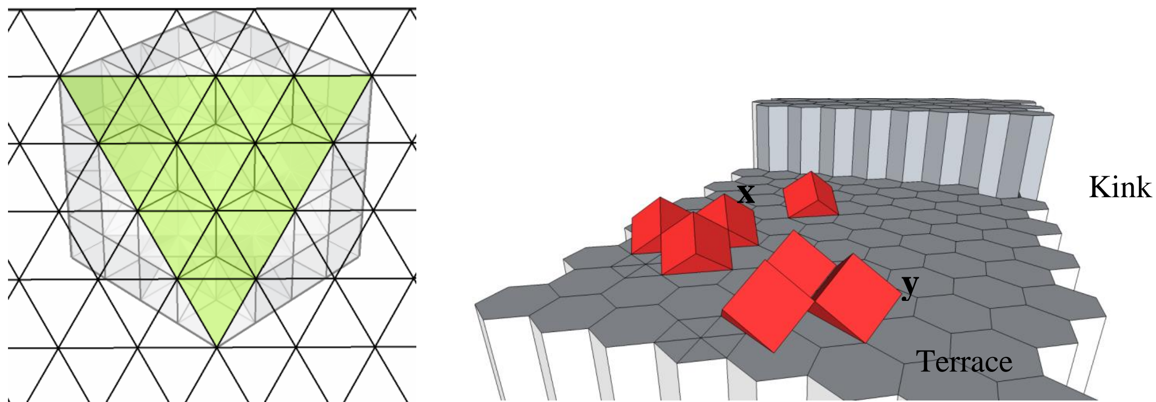

Figure 1.7 a) Bottom (towards [0001] x-ray view) of formed 3c on (0001) plane shows ABC stacking sequence of 3C on (0001) plane. b) Two possible sequences (twins) of formation of cubic crystal on (0001) planes of 4H off cut samples x. inclusion shows ABC sequence and y. inclusion shows ACB sequence.

The quality of epitaxy in terms of morphological defects (often 3C inclusion related defects) for a given condition will depend on the terrace length. At lower off cut, terrace or c-plane (0001) as seen in Figure 1.4 are longer. When 3C is nucleated on these longer terraces (0001), 3C growth on the terrace will have an interaction to the step flow growth by creating obstruction. This is illustrated in Figure 1.9 which is self explanatory.

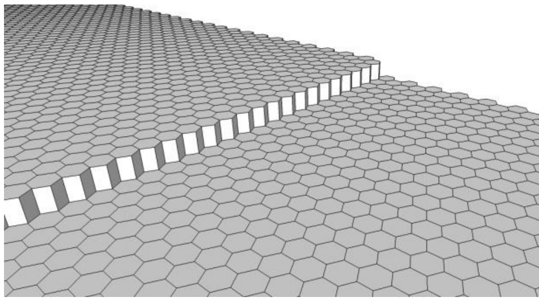

Time t_1 = just before the growth

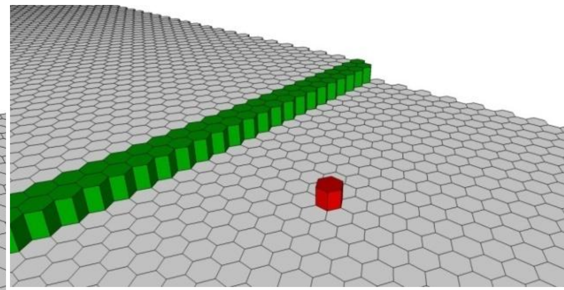

Time t_2: Lateral growth starts. 3c growth initiated

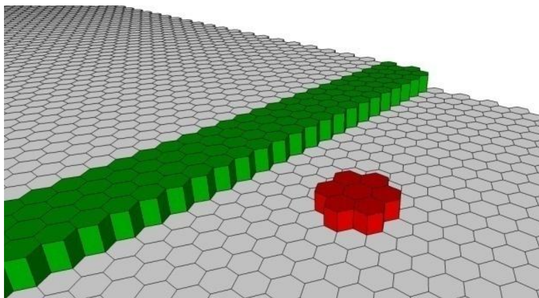

Time t_3: Both 4H and 3C lateral growth

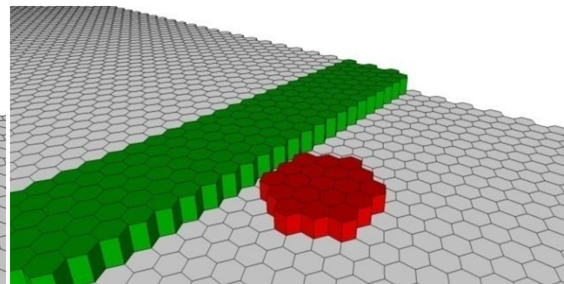

Time t_4: 3C grows in every direction

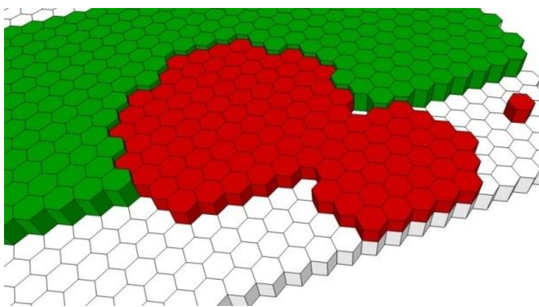

Time t_5: Initiation of other 3C

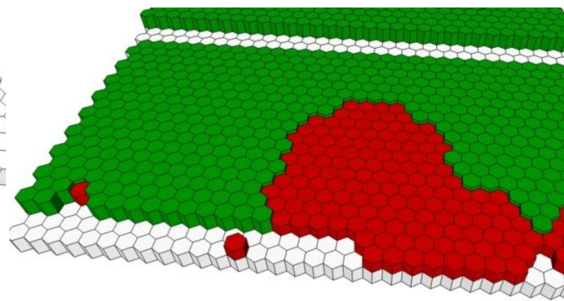

Time t_6: 3C growth expands and included

Figure 1.8 Step by step animation of a step flow growth and 3C inclusion during step flow growth. 3C growths are showing in hexagonal structure for ease of drawing.

Only lateral growth of 3C polytypes was shown in Figure 9. However c plane is also possible for vertical growth (towards [c]) for 3C growth (Figure 10), which will make the step flow growth process more complicated.

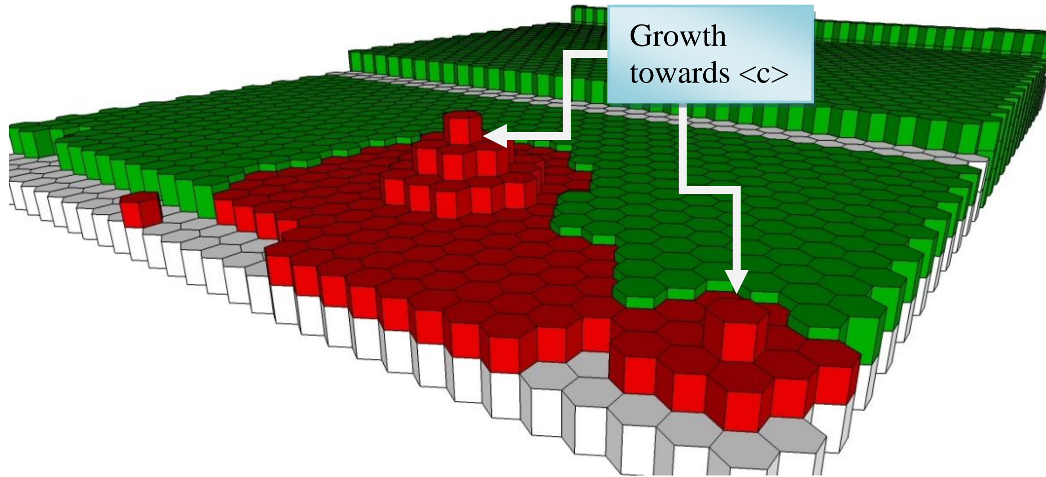

Figure 1.9 Lateral and vertical 3C growth on a 4° off cut terrace

1.6 ETCHING PROCESS

Etching is an essential part of the SiC epitaxial growth. An ideal etching condition will preserve the surface and should also be step mediated, taking place at the kinks. Unlike the growth towards $[11\bar{2}0]$ (if cut in this direction), the step flow during etching is towards [1120] direction. Similar like the growth, kinks has the higher reactivity for the etchant gas molecules since at the kink a complex arrangement of dangling bonds are present which are more reactive (please see Figure 1.5 for a better understanding of the atomic arrangement at the kink compared to the terrace). Hence the etching occurs more favorably at the kink and with a lateral movement than vertical. As an example, the ideal etching of the surface (shown in Fig-10) is elaborated step by step in Figure 1.11.

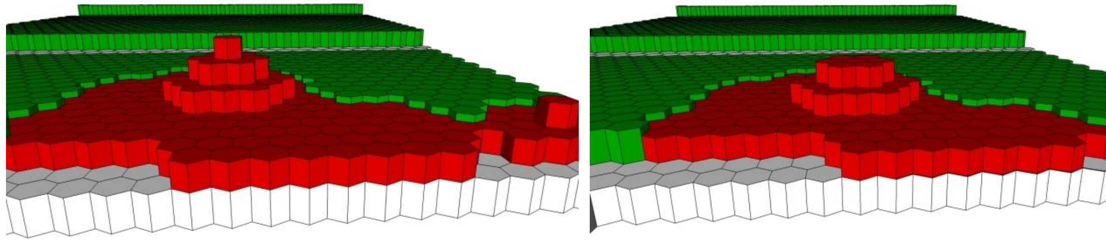

Time t_1: Initial condition

Time t_2: The topmost cell is removed first since it has highest number of m-planes exposed for reaction.

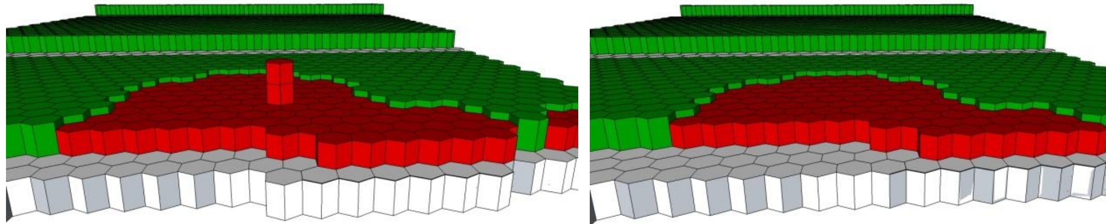

Time t_3: Lateral etching continues and the step edges moves towards [1120] direction

Time t_4: Any perturbation, scratch marks etc. will be flatten

Figure 1.10 Step by step etching process of a SiC off cut surface.

From the previous discussion of growth and etching described by Figure 1.9 and Figure 1.11, we deduce the ideal conditions for homogeneous, step flow growth as following.

1. Step flow growth cannot be obstructed by any 3C nucleation or particle obstruction.
2. Absolutely no growth on c planes or terraces is ideal.
3. Etching should be optimized to such a point that 3C nucleation is completely etched away but the growth at the kink is preserved.

1.7 DEFECTS

There are three main dislocation widely discussed in SiC epitaxy. They are, threading screw dislocations (TSD), threading edge dislocations (TED) and the basal

plane dislocations (BPD). The discussion these dislocations are commonly found in many elementary books related to crystal defects (Johannes & Julia R., 1964; W. T. Read, 1953). These common defects are shown after KOH etching in Figure 1.12. Circular, or oval shapes are indicative of their directions in the crystal related to off cut.

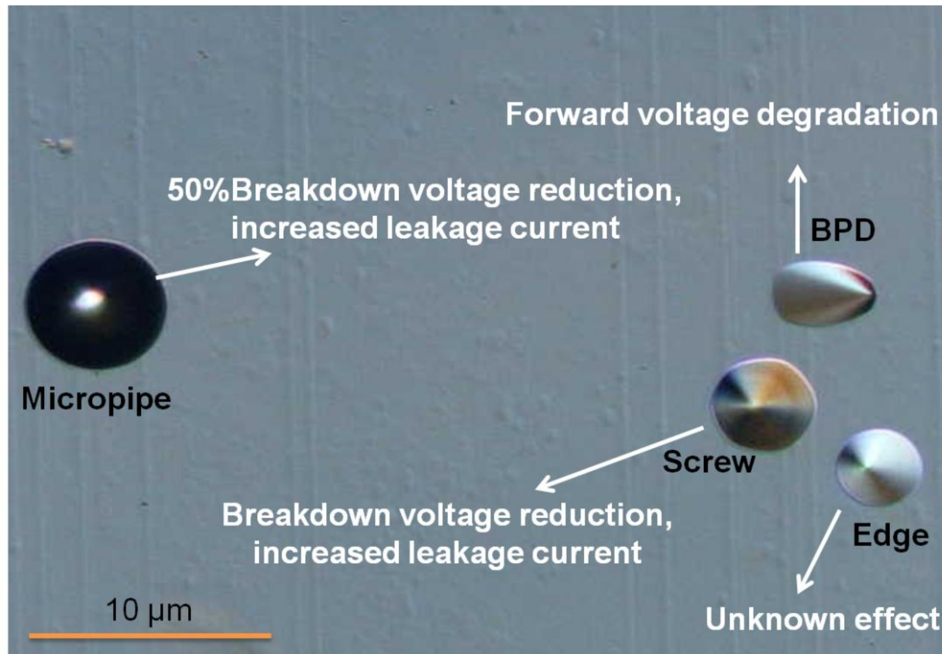

Figure 1.11 Various common SiC crystal defects delineated after KOH etching. Micropipe is a threading screw dislocation with a larger displacement.

Different crystal dislocations have different direction in the crystal. Dislocations are the results of stress stored in the crystal due to deformation. The stress has a line along which it exerts displacement force in the crystal resulting in the dislocation. When the stress line is perpendicular to the dislocation line, then the dislocation is called screw dislocation. On the other hand when the stress line is along with the dislocation line then it is called an edge dislocation. On the other hand, any dislocation which lies in the basal plane (0001) is called a basal plane dislocation or BPD.

As epilayer is grown on substrate, it has the tendency to replicate the structure of the bulk which includes crystal imperfections as well. So, defect sites in the bulk are the primary sources of defects in the epilayer. Both screw and threading edge dislocations propagate perfectly to the epilayer from substrate, though basal plane dislocation mostly converts into threading edge dislocation (Ha et al., 2002; Ohno et al., 2004). Lower elastic energy of threading edge dislocation per unit area along the growth thickness is more preferable to form during the growth than forming the basal plane dislocation of higher elastic energy (Ha et al., 2002). That is why it is assumed that most of the BPDs convert in TED during epitaxial growth.

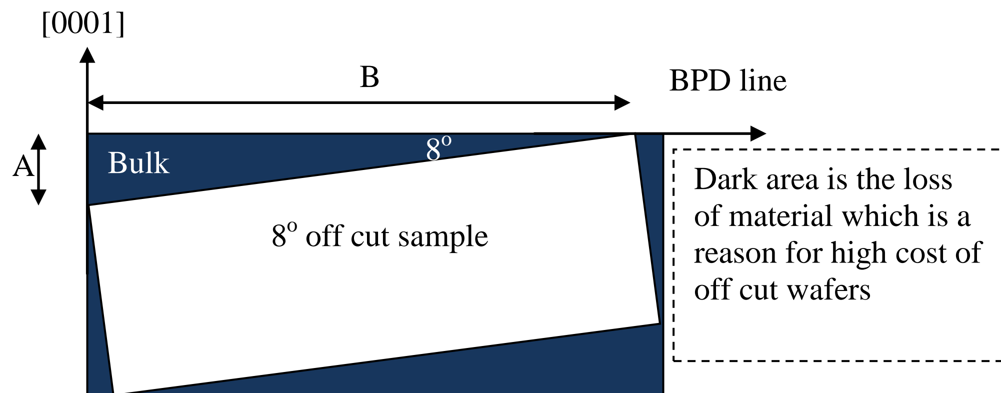

Figure 1.12 Wastage of SiC material due to cutting at an angle towards $[11\bar{2}0]$ direction.

Epilayer grown on on-axis substrate is prone to nucleation of different polytypes. As discussed earlier, this problem was solved by introducing step controlled epitaxial growth (Matsunami & Kimoto, 1997). It is easily understood from Figure 1.13 that higher the off cut angle, higher the amount of material will be wasted due to the cut. This is undesirable from manufacturers' point of view since it will increase the cost of the material. Lower off cut angle as much as 2° off cut is often preferred by the manufacturer to keep the price low.

1.8 FORMATION AND CONVERSION OF BPD

BPD is a device killing defect in epitaxial growth which is found to propagate in higher number from substrate to the epilayer for higher off cut angle. It was found that for off axis samples, few of the BPDs are able to propagate through the epilayer and emerge on the surface and the rest of them convert into TED. A to B ratio in Figure1.13 plays an important role to determine how the BPDs will propagate into the surface of epilayer. For a lower A to B ratio (lower off cut angle) it is energetically more favorable for BPDs to convert into TEDs (Ha et al., 2002). To the contrary, for a higher A to B ratio (or higher off cut angle) more BPDs can propagate into the surface. So, lower off cut angle is preferable over higher off cut angle in many ways. However higher density of some other defects as like as triangular defect, inverted pyramid and step bunching are observed on the epilayer grown on lower off cut angle substrate. So, there might be two ways to eliminate BPD in SiC epitaxial growth. One might be to move to lower off cut angle by solving its related defects; this will solve both material wastage and BPD issues. The other solution might be to find an effective method to convert all the BPDs to TEDs during the epitaxial growth on higher off cut substrate. However material wastage cannot be prevented by the second.

The dislocation lines of BPDs lie on the (0001) plane. For homoepitaxial growth, the wafer is often cut into 4° or 8° off cut angle towards $[11\bar{2}0]$ direction. Due to this off cut, BPD lines intersect and emerge on the surface of the wafer (Figure 1.14). BPDs are propagated to the epilayers from these intersection points during the epilayer growth.

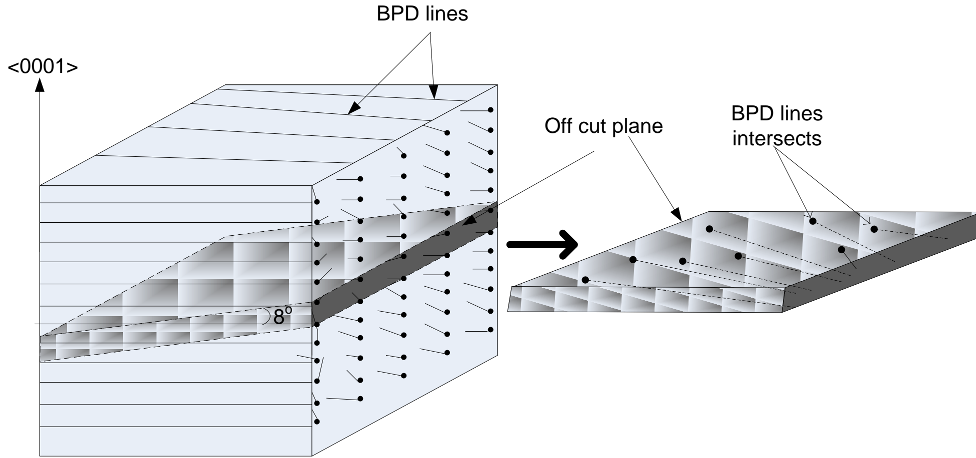

Figure 1.13 BPD lines intersects the surface due to the off cut angle

In SiC PiN diodes, a BPD is split into two under the stress due to the current flow and Shockley type stacking faults (SSF) are generated at basal point dislocation sites in forward bias which greatly impairs the device performance. Most of the BPDs (70% to 90%) convert into threading edge dislocations (BPD) during epilayer growth. This can be explained by Klapper and Küpper theory (Zhang & Sudarshan, 2005). The elastic energy per unit growth length for the defects propagating into the epilayer is given by

$$W = \frac{E}{\cos\alpha}$$

Fig-13: Defect propagation and growth direction.

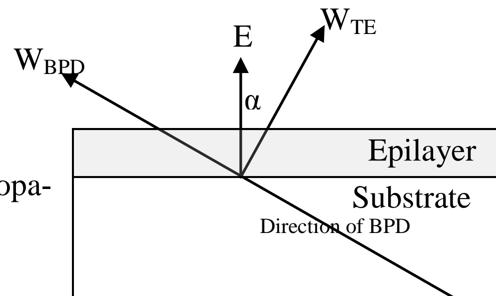

Figure 1.14 Propagation and conversion of Basal Plane Dislocation (Zhang & Sudarshan, 2005)

Energetically it is more favorable for BPDs to propagate as a TED along with the epilayer growth direction (E direction in Figure 1.15). So, for 8° off cut substrates 70% to 90% of the BPDs convert to TEDs following this energetically easier direction.

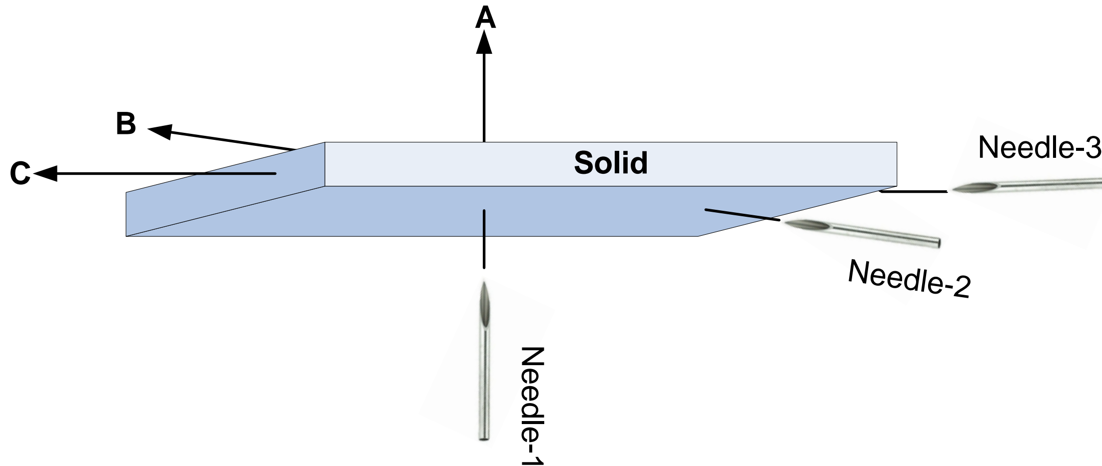

Figure 1.15 A simple analogy to BPD propagation and conversion.

The above is illustrated by a simple example shown in Figure 1.16. It is easily understood that it will be the easiest to pierce the solid by needle-1 towards direction A whereas it will be the hardest to penetrate it by needle-3 in direction C. Difficulty to pierce the material by needle-2 will be intermediate. They are equivalent to BPD direction in 90° off cut, 0° off cut (or on axis) and 8° off cut respectively. However for a perfect on axis (0° off cut) the issue of conversion or propagation is irrelevant since no BPD line intersects the surface in this case.

Until now, in this discussion, the direction of a BPD was considered in one-dimensional perspective for simplicity but in reality their direction varies on a two dimensional plane (Figure 1.17).

If we consider the real scenario in epitaxial growth in the light of above example, then

1. Highest number of BPDs should propagate into the surface for 90° off cut substrate (needle-1).
2. No BPD should emerge on the surface in case of a ‘perfect’ on axis or 0° off cut substrates (needle-3).

3. Most of the BPDs should convert into TEDs for 8° off cut (needle-2) however some BPDs will just be able to propagate. Their ratio (propagation to conversion) will depend on the off cut angle.

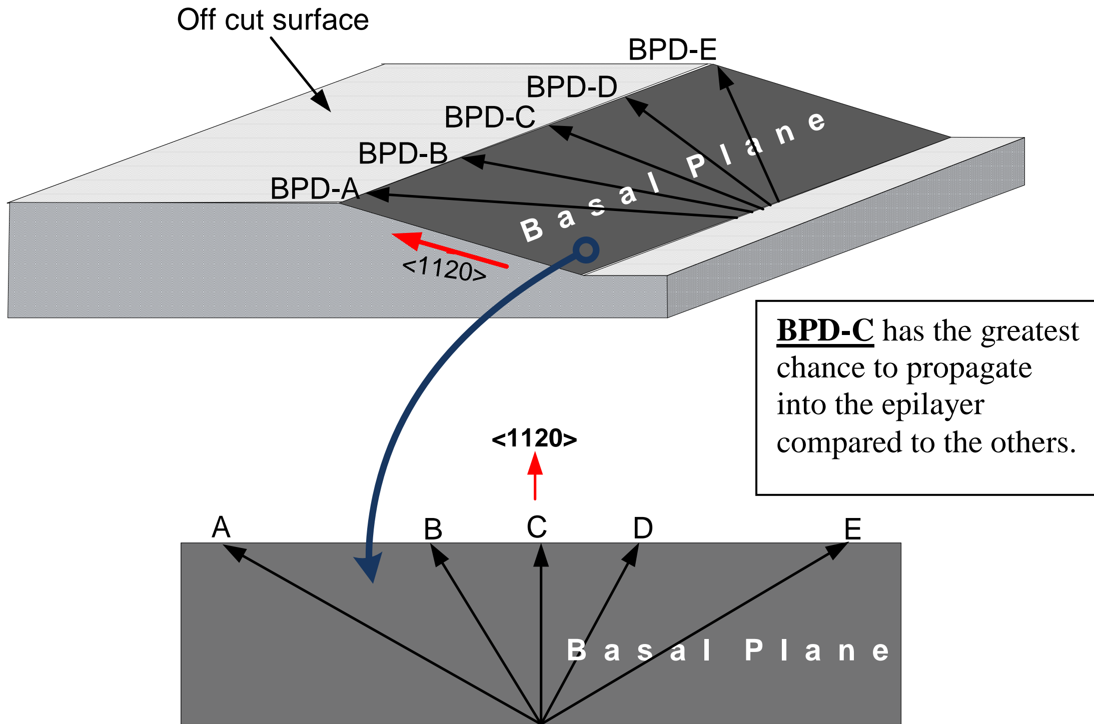

Figure 1.16 BPD propagation and conversion due to the variation of their directions.

Now, let us analyze Fig 17. A basal plane has been shown on the off cut substrate. BPD directions lying on the basal planes can be different. Five BPD lines have been shown in this Figure in different directions. It can be easily understood that BPD-C has the highest chance to propagate as it is over the rest due to the shortest distance it needs to travel across the epilayer. So, it can be inferred that the BPDs having the direction most closely aligned to the $< 11\bar{2}0 >$ direction will have greater chance to propagate into the epilayer without any conversion (fig-16). It was found from different

experiments that around 20 to 30 percent of the BPDs propagate into the epilayer during the growth on 8° off cut substrates. The rest convert into TEDs.

1.9 MORPHOLOGICAL DEFECTS

Morphological defects in the epilayers are comet, triangular defects, inverted pyramids, step bunching, pits, bumps etc. Some of these defects are shown in Figure 1.18. Lower off cut angle is desirable to prevent material wastage, however lower off cut angle generates some additional morphological defects during the epilayer growth. Triangular defect and inverted pyramids are observed in much higher number for lower off cut substrates. Many of the morphological defects are generated from the particulates hampering the step flow during growth.

Effect of particulates on the epilayer growth is investigated by introducing silicon particles artificially on the substrate before growth (Rana, Song, Chandrashekhar, & Sudarshan, 2012a). The sizes of the particles or cluster of particles showed in Figure 1.19a vary from ~1µm to 10µm. Epitaxial films are grown with ~3-4µm thickness on this substrate. After the growth, pits/bumps, stacking faults, screw dislocations were observed at the corresponding locations where particles were present (Figure 1.19a and Figure 1.19b for comparison).

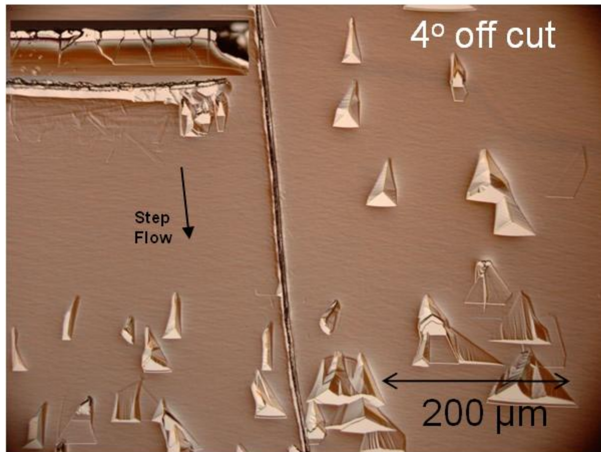

Triangular and pyramid defects

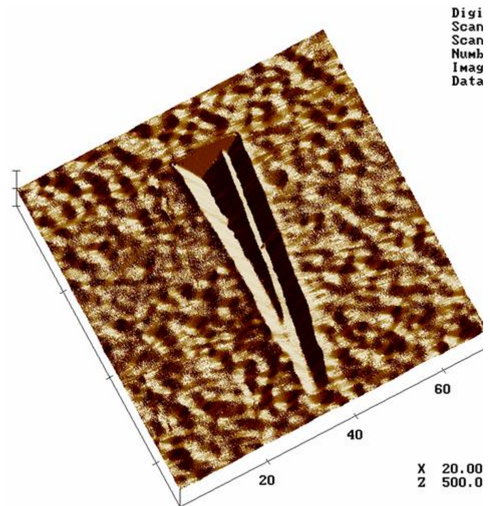

AFM of an **inverted pyramid defect**

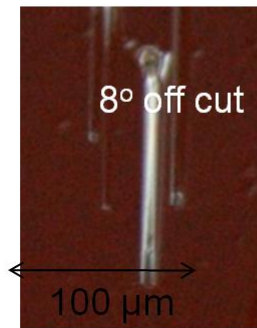

Comet defect

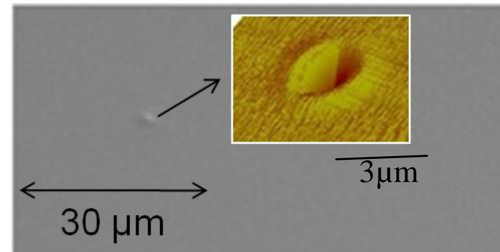

Growth pit

Figure 1.17 Triangular defects and inverted pyramids on 4°, 4H-SiC epitaxial growth.

During this particle experiment, it was found that new crystal and morphological defects are generated due to the intentionally introduced particles with different shapes and sizes. The density of newly generated defects in the epi will depend on the particle density in the substrate. Even though these defects were generated due to artificially introduced particles, a similar condition can also exist for regular epi growth. Firstly, due to the particles introduced by the exfoliation of the parasitic deposition (i.e. deposition taking place on the reactor wall) in the reactor and carried to the growth surface by the high gas

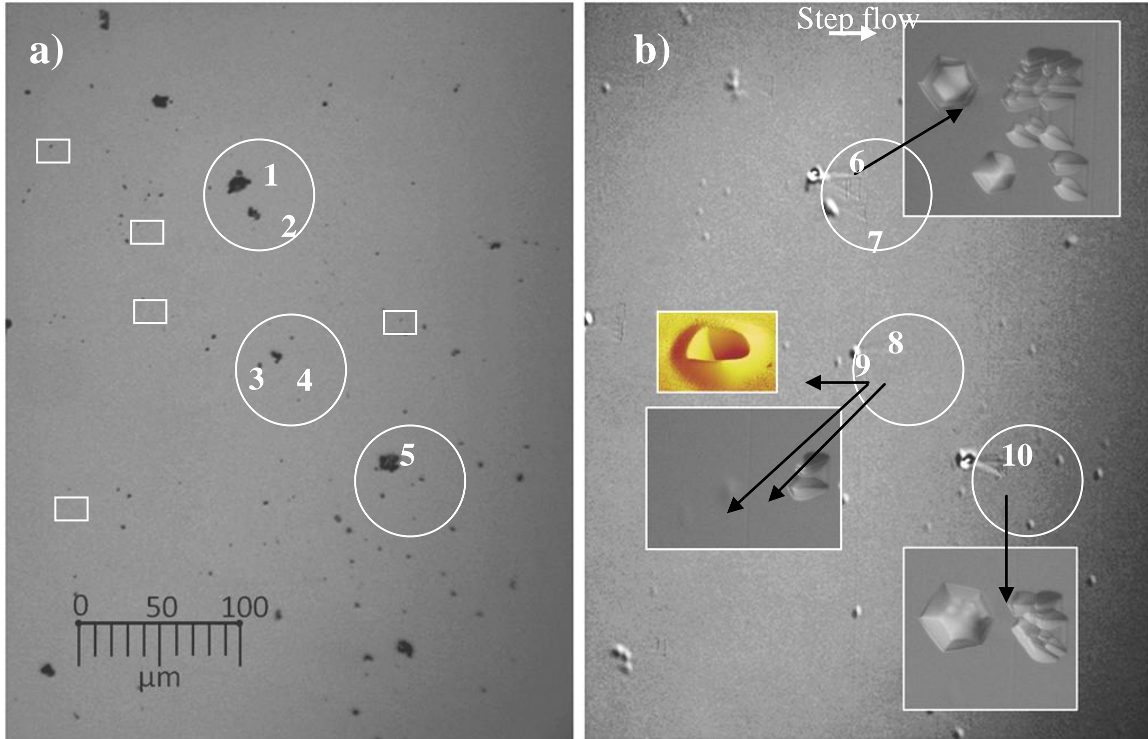

Figure 1.18 a) Nomarsky images of Si particles on a 4H-SiC wafer. b) Nomarsky image of the epilaery grown for the same place and magnified images of the positions corresponding the the circles (insets) after etching. AFM image is shown for a pit (#9) found in the epilayer.

flow. Secondly, particles may also be generated by the formation of clusters in the gas phase due to supersaturation (especially severe at high growth rate, i.e. high precursor concentration). These in-grown particles can also generate new defects during epi growth similar to the artificially introduced particles discussed earlier.

In summary, various important aspects of SiC epitaxial growth are explained in this chapter with new visual representations. This chapter will be a good supplementary reading to understand SiC fundamentals in conjunction to various literatures, e.g. (Matsunami & Kimoto, 1997; Neudeck, 2006). In this chapter we discussed important terms for SiC growth which will be frequently used in the later chapters. In next chapters we will present the results and discussion of actual epitaxial growth process using

chemical vapor deposition (CVD) process in order to solve some of the important challenges currently associated with SiC epitaxial growth.

CHAPTER 2

STUDY OF SiC EPITAXIAL GROWTH USING SILANE AND DICHLOROSILANE GASES

2.1 INTRODUCTION

Homoepitaxial growth of SiC is one of the most important processes in the fabrication of SiC devices. Although various methods such as molecular-beam epitaxy, liquid phase epitaxy, sublimation epitaxy and vapor-liquid-solid method are attempted in SiC epitaxial growth, chemical vapor deposition (CVD) is still the leading and the most attractive technique to grow thick and high quality epitaxial SiC layers (Henry, Hassan, Bergman, Hallin, & Janzen, 2006; Palisaitis & Vasiliauskas, 2008). [25] With development of the SiC-CVD technique, modeling and simulation become important for reactor design, growth optimization, prediction, and better understanding of the growth process, particularly to achieve high growth rate, high quality thick epi for electrical power applications (Danielsson, Henry, & Janzen, 2002; Iftekher, M.V.S.Chandrasekhar, Klein, Caldwell, & Sudarshan, 2011; Nishizawa & Pons, 2006). To understand the benefits of growth using halogenated silanes, it is essential to understand growths using both silane and chlorosilane chemistries. The theoretical and experimental knowledge gain from the comparative study between silane and dichlorosilane mediated growths presented in this chapter will lay the foundation of the next chapters where fluorinated silane is introduced as a novel precursor fog SiC epitaxial growth.

The conventional SiC-CVD process uses silane as the Si-precursor, light hydrocarbons e.g. propane (C_3H_8) or ethylene (C_2H_4) as the C-precursor, and hydrogen as the carrier gas. In recent years, chloride precursors such as $SiCl_4$ and/or HCl addition are induced to achieve high growth rate and to reduce Si-droplet formation in 4H and 6H SiC-CVD process (F. La, Galvagno, Roccaforte, et al., 2006; Pedersen, 2008; Pedersen et al., 2007; Wang & Ma, 2007). Numerical simulations have been carried out for traditional precursors (Danielsson et al., 2002; Nishizawa & Pons, 2006) and some chloride precursors (A Veneroni & Masi, 2006; Wang & Ma, 2008)for growth rate prediction.

An accurate growth rate calculation or model prediction is not possible without precise calculation of precursor losses due to gas phase nucleation and parasitic deposition. Calculation of gas phase nucleation requires prediction of the number of molecular collisions, the nucleated particle size estimation and their dynamics, which are very complex and different for different chemistries, and under different growth conditions with the variability of reactor geometry etc. A complete modeling tool, which considers all of the aforesaid issues to predict the growth rate correctly for various chemistries and growth conditions, does not currently exist. Nevertheless, despite the limitations, simulation is still a very important tool to understand the CVD growth process, to design experiments and to optimize growth conditions. On the other hand, simulation can also be improved and supplemented by analyzing experimental data, comparing them with the simulation results and optimizing the simulation for accurate predictability. Thus, comparisons of simulation with experiments in relation to various

growth conditions and gas chemistries are essential to improve the simulation as well as to optimize the experiment.

Dichlorosilane (SiH_2Cl_2, DCS) is a well-known precursor in the silicon industry which was first reported for thick silicon epitaxial growth in 1974 by P. H. Robinson and N. Goldsmith (P. H. Robinson & Goldsmith, 1975)and patented by them in 1976 (P. H. Robinson, 1976). The low boiling point (8.3^{o}C) of DCS ensures efficient and convenient reactant delivery at room temperature, which is an advantage over $SiCl_4$. Recently, use of DCS in 4H-SiC epitaxial growth was reported by the author's group for high growth rates (Iftekher et al., 2011). Growth rate up to 100 μm/h was obtained from the SiH_2Cl_2-C_3H_8-H_2 system. In depth research of the behavior of DCS in the SiC-CVD process is necessary for further optimization of the growth conditions to obtain high quality SiC epilayers, which is one of the main objectives of the research presented in this chapter.

Si contributing to SiC epi growth can be depleted due to gas phase nucleation, parasitic deposition on the reactor walls and other losses. This is called Si-limited growth where the growth is restricted by Si depletion. To overcome this restriction, chlorinated species are used by either HCl addition or by using some chlorinated silanes as such as $SiCl_4$, $SiHCl_3$, or SiH_2Cl_2. With the addition of Cl, the amount of Si available for SiC growth increases due to suppression of gas phase nucleation, thus increasing the growth rate proportionately, provided that the C-precursor flow is also increased. However, an increment in C-precursor flow may or may not increase the growth rate, due to the losses of carbon in various forms. In this situation, the growth is C-limited. Silicon carbide CVD epitaxy is primarily found to be Si-transport limited as per the results by various

researchers (Ellison, Zhang, Henry, & Janzen, 2002; Iftekher et al., 2011; Vorob'ev et al., 2000).

Kimoto et al. reported the activation energy for vicinal step controlled epitaxy, common for SiC film growth, to be very low (~3 kcal/mol compared to ~20 kcal/mol for terrace nucleated growth on on-axis SiC substrate). For typical temperatures (1100-1500°C), growth was not found to be limited by surface reactions, but rather by mass transport. In step-controlled epitaxy, at typical temperatures, the growth is mainly limited by the diffusion of growth species into the boundary layer at the growth surface (Kimoto et al., 1993). Increased growth rate at increased temperatures is shown to be due to the increased diffusivity of the gas molecules in the boundary layer at elevated temperatures, and not due to increased surface reaction (Kimoto et al., 1993). Similar discussions are available in (Matsunami & Kimoto, 1997). Transport limited growth in a similar type CVD reactor was also reported by Chowdhury et al. (Iftekher et al., 2011).

In a low growth rate environment with low inlet mass flow rate, gas phase nucleation is insignificant and hence does not reduce the growth rate considerably. A lower concentration of gas molecules due to lower precursor flow rate inherently reduces super saturation and gas phase nucleation. A carbon-limited growth might not be noticeable at low growth rate conditions due to the insignificant gas phase nucleation caused by reduced super saturation. However, later we will present evidence of C-depletion, even for the low growth rates, from the results of doping concentration variation with growth pressure.

This chapter is divided into two parts. In the first part, analytical calculation of diffusivity and growth rate is carried out in silane-C_3H_8-H_2 and DCS-C_3H_8-H_2 systems

for understanding the transport process. This general 1-D analytical model provides a valuable tool for reactor design in CVD.

In the second part, Virtual Reactor (VR), a commercial modeling software, is then employed to simulate the SiC-CVD process in both systems. Clear indication of gas-phase nucleation is obtained from the VR simulation results. In this study, parasitic deposition on gas injector wall is studied for both precursors. Combining the simulation and experimental results with respect to growth rate, doping, and morphology, the SiC-CVD process in DCS-C_3H_8-H_2 system is analyzed and compared with the traditional silane-C_3H_8-H_2 precursor system. Further, in this part, we provide clear evidence of carbon depletion which, in turn, influences the doping concentration of the epitaxial films.

PART I: ANALYTICAL MODEL

In this section we calculate the growth rate using the mass transport phenomenon. In essence, first the amount of Si and C atoms entering the boundary layer and participating the growth are calculated in this section, and then, the growth rate is found from the thickness calculation for 1 hour of mass deposition from these Si and C atoms.

2.2 DIFFUSIVITY

The diffusivity of precursor gas molecules plays a very important role in the diffusional mass transfer process during CVD epitaxial growth. Diffusivity of dilute gas A in carrier gas B can be found from the Reid and Sherwood (1966) expression which is valid below 20 atm (Skelland, 1985)

$$D_{AB} = 0.0018583 \frac{T^{\frac{3}{2}}}{P(\sigma_{AB})^2 \Omega_{D.AB}} \left(\frac{1}{M_A} + \frac{1}{M_B}\right) \tag{2.1}$$

Where P is in atmospheric pressure (atm), T is temperature in Kelvin, M_A and M_B are molecular masses of gas A and gas B, σ_{AB} is the collision diameter, which is the average of the diameters of two colliding molecules in Angstrom. A so called collision integral $\Omega_{D.AB}$ includes the dynamics of molecular interaction due to their speeds, masses and angles of collisions (Spencer, Toguri, & Kurtis, 1969). Collision integrals for gas molecules based on Lennard-Jones potentials can be found from the $k_B.\frac{T}{\varepsilon_{AB}}$ vs. $\Omega_{D.AB}$ Table reported by J.O. Hirschfelder et al. (1954) (Hirschfelder, Curtiss, & Bird, 1954; Skelland, 1985), where k_B is Boltzmann's constant and ε_{AB} is a Lenneard-Jones force constant in joules. Lennard-Jones force constants are found in the Lennard-Jones potential function, which estimates the electric potential between molecules A and B. The

diffusivities of silane and propane in hydrogen gas at 1 atm and 273K is calculated to be 0.51 and 0.37cm^2/s, respectively from Equation-1,. However, relevant data for DCS are not available to directly apply in Equation-1 to find the diffusivity of DCS.

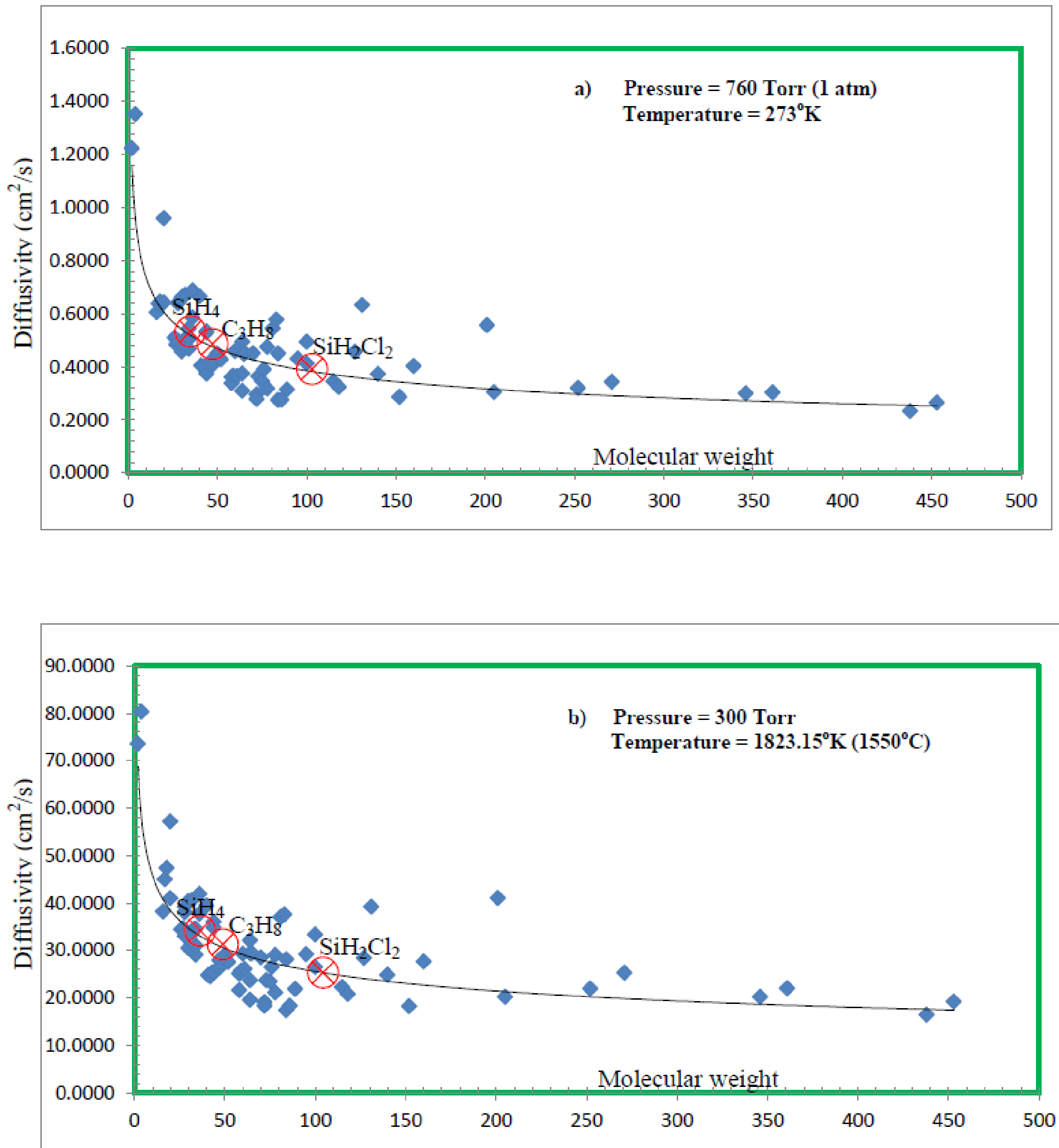

Figure 2.1 Theoretically calculated (a) diffusivity versus molecular weight plot calculated for various gases at 1 atm (760 torr) and 273°K, (b) diffusivity versus molecular weight plot for various gases at 300 torr and 1823°K (1550°C)

As a general rule, diffusivity of molecules decreases for heavier gases (Putte, Gilling, & Bloem, 1975). Lower diffusivity ensures lower activity of the associated gas molecules in terms of their participation in growth. Diffusivity of a gas molecule can be extrapolated from the empirical molecular weight versus diffusivity relation (Shephered, 1965). This is especially useful to estimate the diffusivity of gases for which the required data are not readily available to apply in Equation 1.1. We calculate the diffusivities of 72 gases found in (Skelland, 1985)using Equation 1.1 and estimate the diffusivity of DCS (molecular weight 100) in hydrogen at 1 atm and 273K, to be 0.38 from the power law trend line in Figure 2.1a.

The species primarily participating in growth depend on the gas decomposition at growth conditions. Decomposition of silane, chloro-silane, and propane in a SiC-CVD process has been extensively studied in previous publications (Kolke & Gardlner, 1980; Nishizawa & Pons, 2006; Swihart & Carr, 1998). Table 2.1 lists the main relevant molecules for growth in silane and DCS systems and their diffusivities at 273K and 1 atm extrapolated from Figure 2.1a. We extrapolated diffusivities of these molecules from the empirical molecular weight versus diffusivity relation from (Shephered, 1965) and listed them as well in Table 2.1 for comparison. The difference between them can be attributed to the inherent average (%) error of the Equation 1.1 (Reid and Sherwood, 1966) which is approximately 7.5% (Skelland, 1985).

Table 2.1 Experimental and theoretical values of the diffusivities of various gas molecules in the silane-propane and DCS-propane CVD chemistries at STP.

Molecule	**Molecular weight**	**Diffusivity, D_o (cm^2/sec) Calculated (Figure 2.1a)**	**Diffusivity, D_o (cm^2/sec) [23]**
SiH_4	32	0.51	0.62
SiH_2	30	0.54	0.64
SiH	29	0.54	0.65
Si	28	0.55	0.66
SiH_2Cl_2	100	0.38	0.25
$SiCl_2$	98	0.39	0.26
SiHCl	64	0.44	0.38
SiCl	63	0.44	0.40
HCl	36	0.51	0.58
C_3H_8	44	0.37	0.52
C_2H_5	29	0.55	0.65
C_2H_4	28	0.55	0.66
C_2H_2	26	0.56	0.68
CH_4	16	0.64	0.75
CH_3	15	0.66	0.77

It is seen in Table 2.1 that the different decomposed species from silane have similar diffusivities because stripping off the hydrogen does not change the molecular mass significantly. In the same way, for DCS, diffusivity of the DCS gas molecule (SiH_2Cl_2) does not vary much compared to $SiCl_2$, which has been shown to be stable, and to be the main growth- participating species decomposed from DCS (Valente, Cavallotti, Masi, & Carra, 2001). Using this consideration, later, we calculate the growth rate by using the diffusivity of SiH_4 molecule for silane and that of SiH_2Cl_2 molecule for DCS assuming that this calculation will not vary considerably from those of the other growth participating species for these chemistries.

The diffusivity of a gas molecules at temperature T_2 can be calculated from the diffusivity at temperature T_1 by applying the following relationship (Skelland, 1985).

$$D_{T_2} = D_{T_1}(\frac{T_2}{T_1})^{\frac{3}{2}}.\frac{P_1}{P_2}.\frac{\Omega_{D.AB.T_1}}{\Omega_{D.AB.T_2}} \qquad (2.2)$$

The diffusivity of silane at the regular growth condition (300 torr and 1550°C in this chapter) is analytically calculated to be 33.6 cm^2/s by using Equation 2.2. Since the collision integrals of the DCS molecule are not readily available, we extrapolate the diffusivity of DCS to growth conditions from the fitted curve (Figure 2.1b). We estimate the diffusivity of DCS to be ~25 cm^2/s from this graph at the growth condition (300 torr and 1550°C).

2.3 GROWTH RATE CALCULATION

In order to predict growth rate by analytical calculation, the growth process is analyzed in a simple reactor geometry as shown in Figure 2.2.

Initially, Hydrogen (6000 sccm) flows into the reactor. The silane flow (1 sccm) is initiated at 1550°C. A stagnant layer forms near the growth surface in the boundary layer (Figure 2.2b). The very first few adhered molecules start participating in the growth kinetics and a concentration gradient forms. The concentration of gas molecules at the solid-gas interface is reduced due to the gas molecules being incorporated into the solid surface, assumed the surface to be a perfect sink, and diffusional mass transfer sets in due to the difference in concentrations. It is assumed that there is always one carbon atom present (from propane) for each silicon atom (from the Si precursor) in the boundary layer during growth.

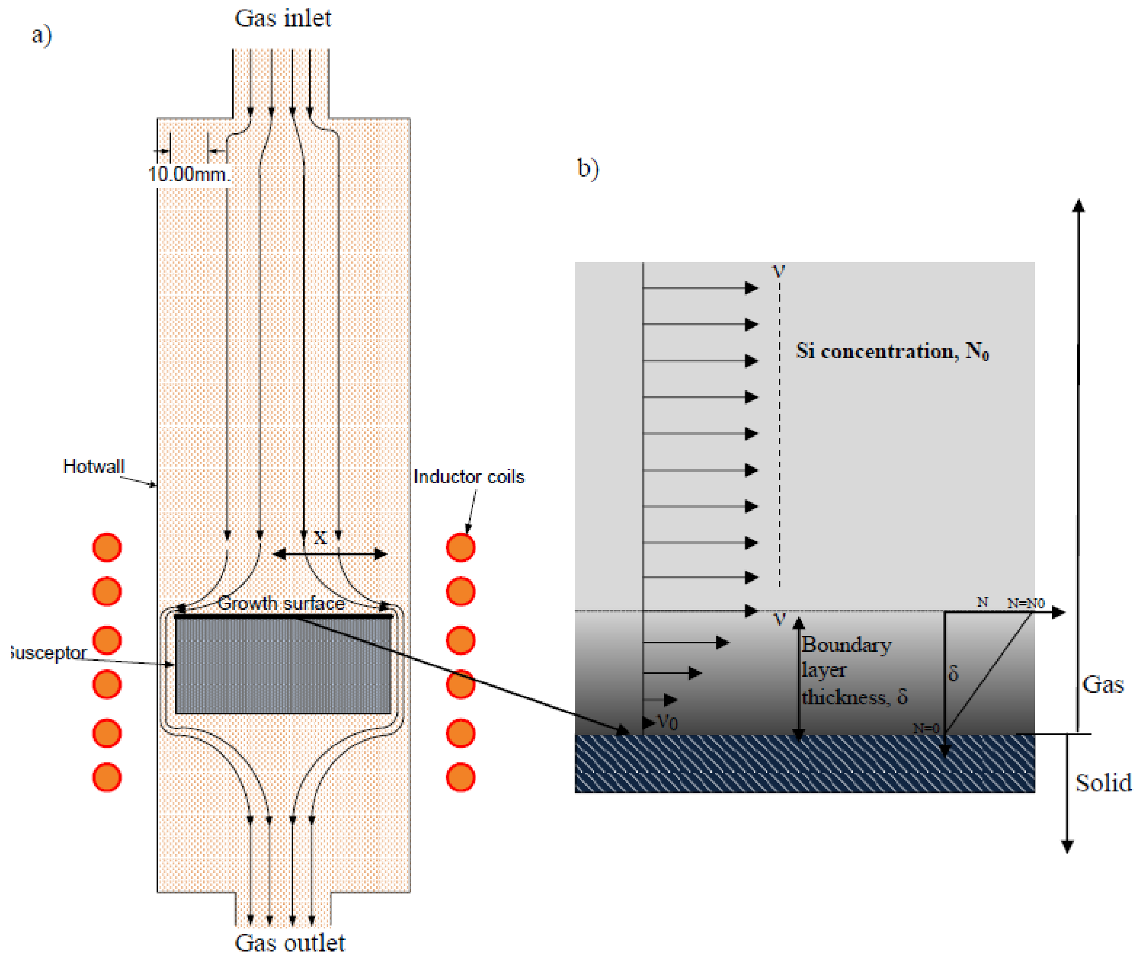

Figure 2.2 a) Schematic of the CVD reactor used for growth calculation. b) Boundary layer at the solid-gas interface.

The calculation can be divided into three parts. They are: calculation of diffusivity of silicon precursors in the hydrogen, calculation of the boundary layer thickness, and finally calculation of growth rate using Fick's law of diffusion. This provides a general first order 1-D estimation of growth rate for a given system. Since this calculation does not include gas phase nucleation or aerosol formation, *a lower growth rate is expected* compared to the actual experimental growth. The difference between experimental and calculated growth is an indication of precursor losses in the reactor and should be minimal for ideal growth conditions.

The Si flux ($cm^{-2}s^{-1}$) near the growth surface in the reactor geometry shown in Figure 2.2 can be found from (Ghandhi & Field, 1984)

$$J_D = \frac{-DN_0}{\delta} \tag{2.3}$$

N_o is the inlet reactant concentration (cm^{-3}) and δ is the boundary layer thickness (cm).

The inlet reactant concentration of Si, $C_{Si} = N_0 = \frac{P_{si}}{RT} = 2.6 \times 10^{20} cm^{-3}$ (Where P_{Si} is inlet Si partial pressure at a growth pressure of 300 torr and a temperature of 1550°C).

The thickness of the boundary layer is found from (Ghandhi & Field, 1984)

$$\delta_D = \sqrt{\pi . D . \frac{x}{V}} \tag{2.4}$$

Where x = 33 mm in our case in (Figure 2.2a) from (Ghandhi & Field, 1984).

The free velocity of gas in the tube beyond the boundary layer region is 4.5 m/s from Equation 2.5.

$$v = \frac{M}{S} . \frac{P_0}{P} \tag{2.5}$$

Here, the gas flow rate M= 6000 sccm, the cross section area of the hotwall S= 34 cm^2, P_o=Atmospheric pressure in torr, P= growth pressure in torr.

The boundary layer thickness is found using Equation 2.4 to be ~9 mm (diffusivity of silane D=33 cm^2/s by calculation from section 2.1).

Using the above values, the number of Si atoms diffusing into the boundary layer per second is calculated from Equation 2.3 to be, $J_D = 1 . 10^{20}\ cm^{-2}s^{-1}$

The total Si mass transfer in t seconds is,

$$m_{(Si)} = \left(\frac{J_D . t}{N_A}\right) M_{(Si)} \tag{2.6}$$

Here N_A is Avogadro's number, M is the molar mass. It is assumed that the propane flow rate is adjusted in such a way that there is no deficiency of carbon atoms in the boundary layer for each incoming silicon atom as discussed in the introduction.

The total C mass transfer in t second is,

$$m_{(C)} = \left(\frac{J_D.t}{N_A}\right) M_{(C)} \qquad (2.7)$$

The average growth rate for the hot wall cross sectional area (A) at the growth surface is,

$$R_G = \frac{m_{(Si)}+m_{(C)}}{\rho} \cdot \frac{1}{A} \qquad (2.8)$$

Here ρ, the density of SiC, is 3220 Kg/m^3.

Using Equation 2.8, the growth rate for the silane precursor was found to be ~7.5 μm/hr.

Using the diffusivity of DCS (SiH_2Cl_2) as 25.6 cm^2/s (estimated from Figure 2.1b for the growth conditions), the growth rate is found to be ~6.5 μm/hr for the DCS precursor.

Comparison of growth rates using silane and DCS precursor gases, based on the above 1-D calculations, is shown in Table 2.2. For silane, the growth rate calculated by the VR simulation software (details of VR are provided in the experimental section), is found to be ~6 um/hr for the geometry in Figure 2.2a. Experiments are conducted using the same reactor arrangement (Figure 2.2a) to compare simulation and analytical calculation results giving a growth rate of ~5 um/hr. This growth rate is lower than the analytical calculation and simulation results as expected. The difference is attributed to precursor losses due to gas phase nucleation and parasitic deposition. We will provide evidence of parasitic deposition later, while gas phase nucleation has already been reported in the literature to be an issue in CVD growth. While the analytical model is simple but incomplete, it provides a convenient starting point to study the growth of SiC.

Table 2.2 Comparison of analytical calculation of diffusivity, boundary layer thickness and growth rate for Silane and DCS.

Gas	Diffusivity, D (cm^2/sec)	Boundary layer thickness (mm)	Analytical growth rate (μm/hr)
Silane (SiH_4)	33.6	8.8	7.5 um/hr
Dichlorosilane (SiH_2Cl_2)	25.6	7.7	6.5 um/hr

PART II: SIMULATION AND EXPERIMENTAL STUDY

2.4 INFLUENCE OF GROWTH PRESSURE

In this section epitaxial growth using silane and DCS is compared at various growth pressures in terms of growth rates (found from experiment and simulation) doping and surface morphology. These are explained on the basis of different decomposition behavior of the precursor gases obtained from simulation.

In order to understand the influence of pressure on epitaxial growth, a brief discussion of the pressure control mechanism in the CVD reactor, which eventually controls the residence time, gas phase nucleation, parasitic deposition, and epitaxial growth for a given gas flow rate and reactor geometry is provided below.

In CVD growth, gases flow in the chamber at certain flow rates into the reactor and the pressure is maintained by an adjustable valve. This valve controls the aperture of the gas exit path in the reactor to maintain a certain pressure while gases flow constantly during the growth. A higher amount of gas is pumped away per unit time to maintain lower pressures and vice versa. A lower pressure shortens the residence time of the gas molecules in the reactor proportionately. At any instance during growth, the number of gas molecules per cc in the chamber is lower for lower growth pressures than that at higher growth pressures for fixed flow rates of precursor gases.

However, the total number of gas molecules flowing through the chamber cross section per unit time (molecules/cm^2/sec) remains constant at a certain gas flow rate irrespective of the growth pressure. Considering only the amount of mass passing through the reactor cross section, the pressure thus should not have any effect on the growth rate. It is important to consider the interaction of these gas molecules among themselves in the

gas and with the reactor furniture parts in order to estimate the correct growth rate at various pressures.

Obviously, a longer residence time at a higher pressure will allow these molecules to absorb more energy from the heating element as well as to interact among themselves for a longer period with shorter mean free path. This will increase both gas phase nucleation and parasitic deposition on the reactor walls and thus depletes the source elements from the intended crystal growth. These losses deplete the precursors, change the effective C/S and/or induce particulates on the growth surface and hence can affect growth rate, doping concentration and morphology. It is noteworthy that different reactors may behave differently and growth related results may not be comparable even at same growth pressures since volume and geometry of the reactor, which determines the residence time of the gas molecules in the reactor, might vary for different reactors. However, the trend of growth rates is expected to be the same despite different furnace geometries.

2.5 EXPERIMENTAL SETUP

Epitaxial growth of SiC is carried out using an inverted chimney type vertical hot-wall CVD reactor (Figure 2.3). This arrangement consists of a hotwall, a gas injector and a substrate holding susceptor. The system is inductively heated by a 20kW generator at 9090 Hz. Silane/ DCS and propane are used as precursor gases. Propane, silane/DCS and hydrogen gas flow are kept fixed at 1.5 sccm, 3.28 sccm and 6000 sccm respectively while the growth temperature is fixed at 1550°C. The distance between the injector end and the SiC substrate sample is 33 mm and the growth pressure is varied from 30 to 600 torr. Commercially available 4H-SiC wafers (8 degree off cut towards $[11\bar{2}0]$, optically

polished) are used as the substrate for all of the experiments. The epilayer thickness is measured using Fourier transform infrared (FTIR) spectroscopy. Atomic force microscopy (AFM) is used to measure the roughness of the samples. Capacitance-voltage (C-V) mercury probe measurement is performed to determine the doping concentration of the epilayers.

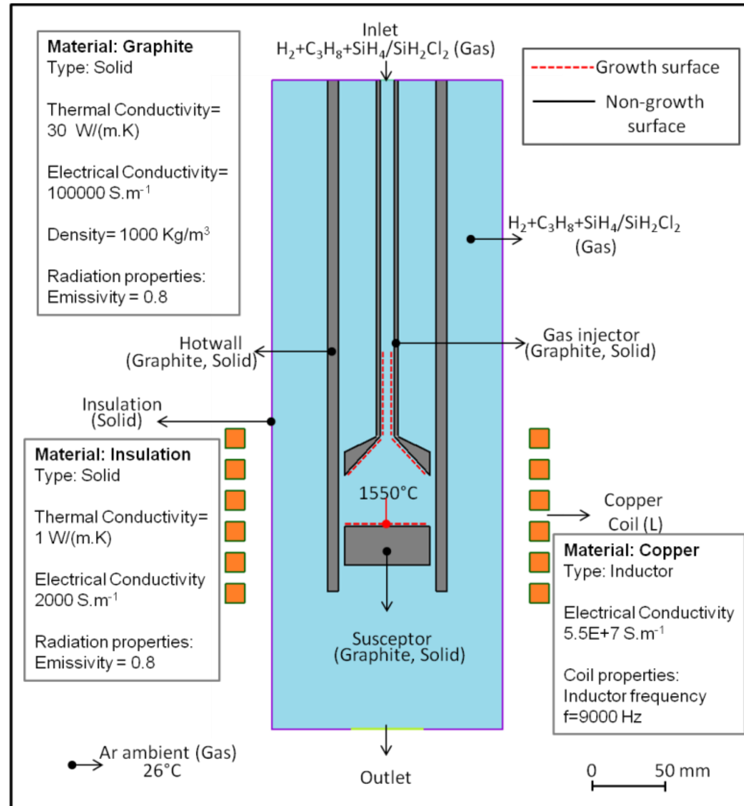

Figure 2.3 Schematic diagram and boundary conditions of the CVD furnace used in simulation. The sticking coefficient for the growth surface is assumed to be 1, i.e., growth species adsorbed on the substrate surface will participate in growth.

VR, developed by Semiconductor Technology Research Inc. is employed for simulation of the growth process in our reactor geometry shown in Figure 2.3. The boundary conditions and material properties are also provided in Figure 2.3. A complete discussion of the thermal field calculation using the VR can be found in (Bogdanov et al.,

2001). Parasitic deposition is included in the simulation by defining 'catalytic' or reactive growth surfaces in the furnace based on our observation of actual parasitic deposition taking place on the injector tube during growth. Catalytic surfaces are indicated by dashed lines in Figure 2.3. Silane or DCS chemistries can be used in the simulation for calculation of the partial pressures of the different decomposed species and growth rate at various pressures (30 torr to 300 torr). The simulation of gas decomposition in VR offers an important tool to compare DCS and silane chemistries at various growth conditions.

2.6 DECOMPOSITION OF SILANE AND DCS INTO ELEMENTAL SILICON

First, the decomposition of silane and DCS into elemental Si is analyzed at the same experiment growth conditions by VR. A higher dissociation bonding energy per mole for a molecular bond requires a relatively longer residence time (function of pressure) to dissociate into constituent species at a fixed temperature (1550°C in our case). The dissociation bonding energy of relevant bonds in silicon carbide CVD is shown in Table 2.3 (Huheey, 1972). The bond energy of Si-Cl is 381 KJ/mol compared to that of Si-H (318 KJ/mol), which implies that for a given system, when heat energy is applied, the Si-Cl bond should take a longer time to dissociate compared to the Si-H bond.

The VR simulation of the decomposition of DCS and silane into elemental Si at various growth pressures is shown in Figure 2.4 for different growth pressures. From Figure 2.4 it is evident that silane decomposes in a higher proportion into elemental Si at a low pressure (30 Torr) compared to DCS. However, at higher pressures (> 300 Torr)

Table 2.3 Dissociation bonding energies (Huheey, 1972) for various bonds related to silicon carbide growth.

Bond	KJ/mol
H-Cl	428.02
C-H	411
Si-Cl	381
C-C	345.6
Si-C	318
Si-H	318
Si-Si	222
C=C	602
C≡C	835.1

even DCS dissociates to form an increased amount of elemental Si. At 30 torr, the gas molecules pass through the chamber with a velocity of ~4.5 m/s (from simulation and analytical calculation) for the hotwall cross sectional area. At this velocity, the residence time of the gas molecules in the hot zone of the furnace is long enough for the silane (SiH_4) molecules to absorb adequate energy to dissociate into elemental Si in a notable amount as presented visually and quantitatively in Figure 2.4b (30 torr, silane). On the other hand, in DCS, elemental Si does not form in a considerable amount as DCS (SiH_2Cl_2) molecules posses higher dissociation bonding energy as seen in Figure 2.4b (30 torr, DCS). This is the key difference between DCS and silane in terms of their dissociation behavior, as evidenced by the VR simulation, which is the primary reason for the suppressed gas phase nucleation and parasitic deposition in DCS compared to silane.

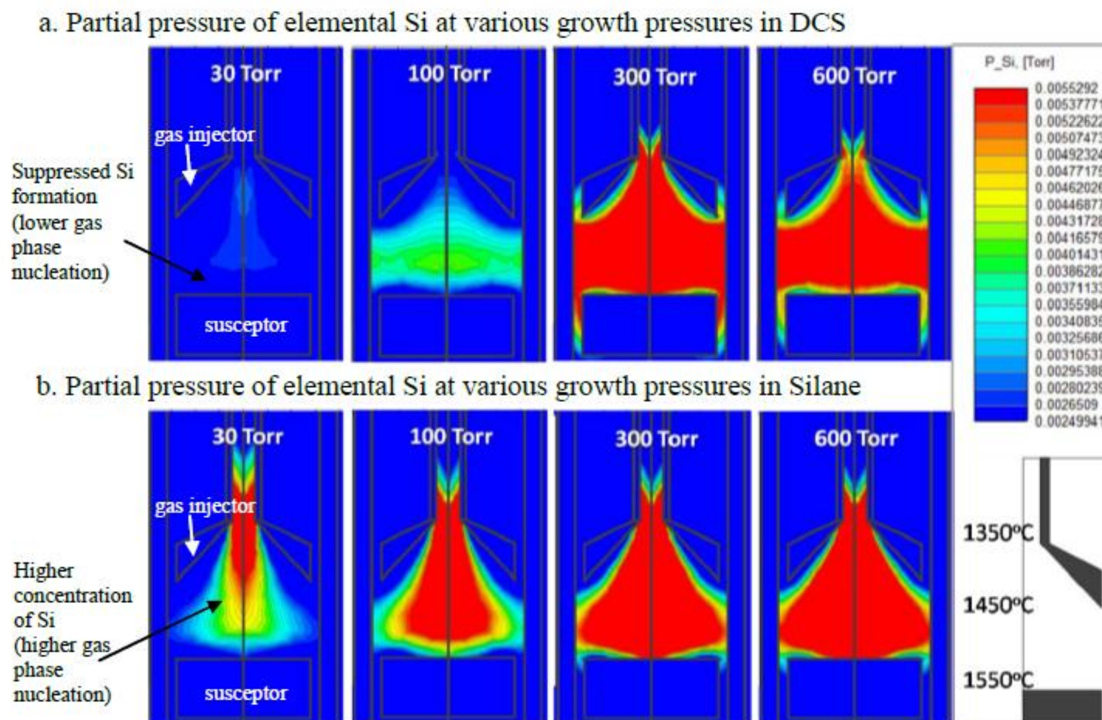

Figure 2.4 Simulation of Si partial pressure at various growth pressures. Suppression of Si formation in DCS is clearly seen at 30 torr. Temperatures at specific locations in the reactor are shown.

Change of gas velocity at various growth pressures influences the temperature profile. The variation of temperature profile at different pressures also influences the gas decomposition behavior (i.e. amount of different decomposed species) in the reactor. However our discussion is only limited to the comparison of the decomposition behavior of DCS and silane gases at a given growth pressure. Change of temperature profile due to change of gas velocity is applicable to both of the chemistries, and hence ignoring this effect does not affect our chemical decomposition comparisons of two gases presented in this section. Experimentally, we find that the RF power consumed at a given growth temperature and pressure is the same for both precursors, indicating that the temperature profile is similar.

2.7 GROWTH RATE VERSUS PRESSURE

The growth rates for various growth pressures are plotted in Figure 2.5 using simulation and experiments for silane-propane and DCS-propane precursor systems. The experimentally obtained growth rate for the DCS precursor is found to be higher compared to growth from silane at all growth pressures. This difference is found to be more significant at a lower growth pressure (30 torr). This is consistent with simulation shown in Figure 2.4. Expectedly, the simulation results *without the consideration of the gas phase nucleation* predicted a higher growth rate for silane than the DCS at the same conditions. We explain this behavior below.

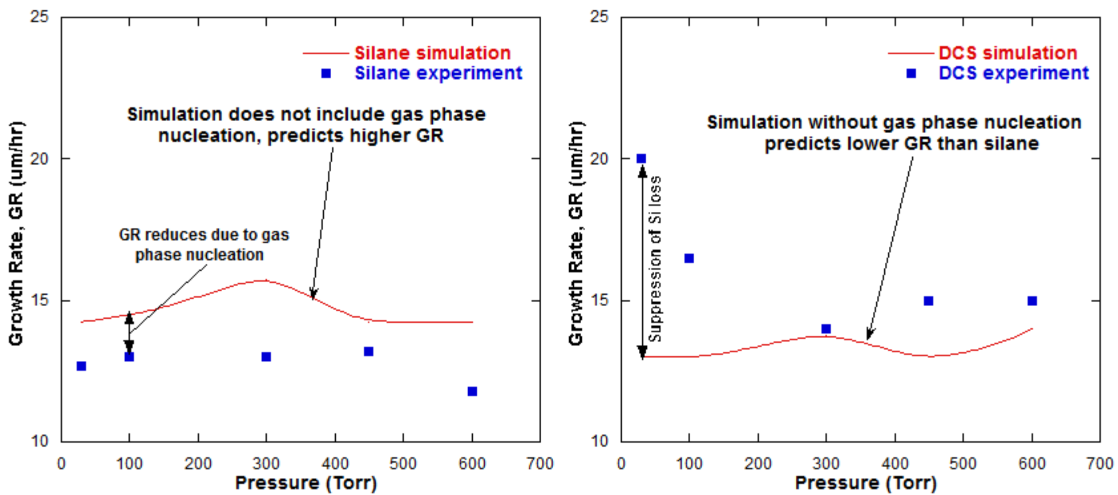

Figure 2.5 Growth rate versus pressure for a) silane and b) DCS precursors: simulation and experiments

Silicon and carbon growth species (supplied from precursor gas dissociation) which do not participate in the epitaxial growth can be considered as a loss mechanism. These losses in the SiC-CVD process are mainly due to silicon gas phase nucleation and parasitic silicon and parasitic Si_xC_y deposition on the injector or reactor walls.

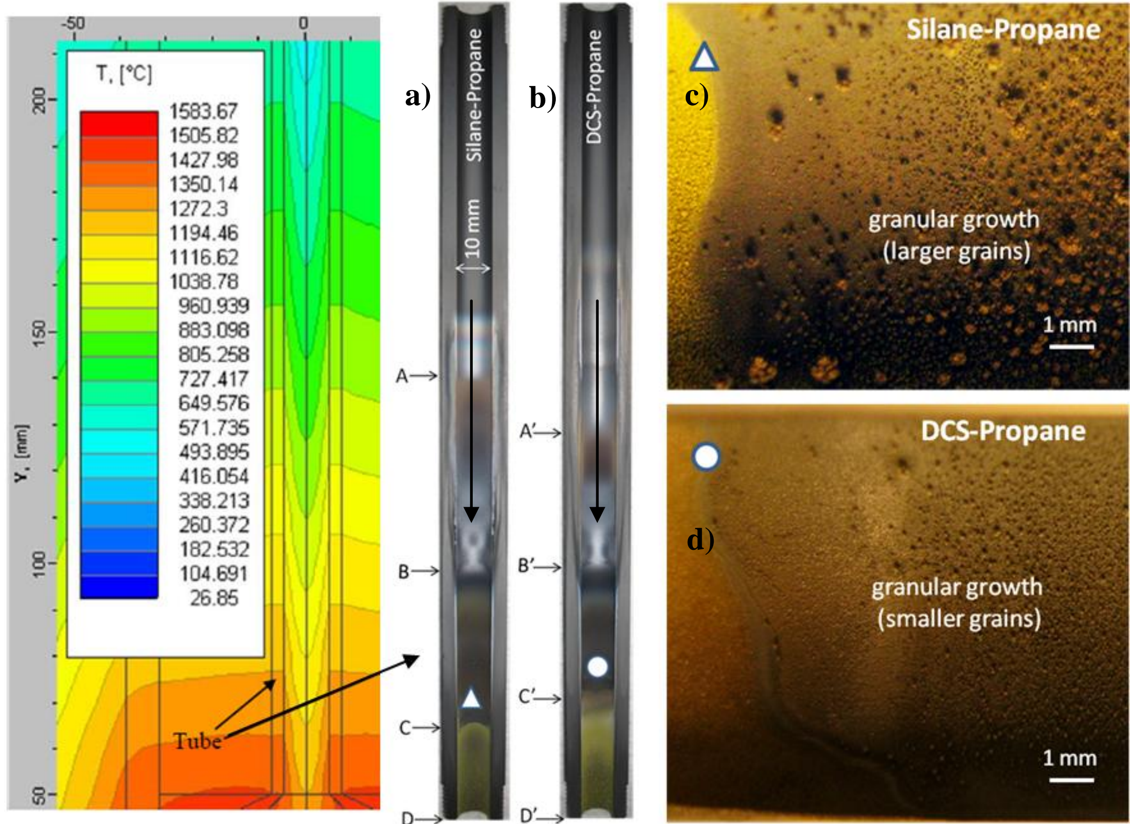

Figure 2.6 Comparison of parasitic deposition for DCS and silane in the gas injector tube shown as PQ in Figure2.1

The parasitic depositions on the injector tube wall after several growth runs is shown by the split tube image in Figure 6 with the associated temperature profile The deposition starts from points 'A' and 'A´' for silane and DCS gases respectively (Figure 2.6). Position 'A´' is about 15mm downshifted compared to position 'A' for the case of DCS which indicates that the parasitic deposition region is reduced for DCS. A reduced parasitic deposition will increase epi growth rate by reducing the precursor loss. Comparison of these regions indicates that: AB>A´B´, BC>B´C´ and BD=B´D´, and C´D´>CD (Figure 2.6a and 6b). A detailed study of the composition of these regions is beyond of the scope of this paper. Regions CD and C´D´ are to be the regions where SiC

growth take place on the tube wall. Elongated C´D´ is a sign of enhanced SiC growth using DCS growth compared to silane (CD). A close look at the positions corresponding to the triangle and circle marks (Figure 2.6a and 2.6b) reveal large, loosely bound granular growths in the tube for silane (Figure 2.6c). Growth with this condition is found to be deteriorated with particles on the epi surface, probably due to the exfoliation of these grains from the tube. Parasitic deposition using DCS was found to be smoother at the same position (Figure 2.6d). An improved epi surface was observed for this condition. Thus we can deduce that the smoother parasitic deposition in DCS is indicative of improved epi quality due to prevention of particle droplets from the tube wall being delivered on to the growing epi surface. These elemental assignments were confirmed using EDX (Energy Dispersive X-ray spectroscopy). The composition and span of this region depends on the growth conditions such as temperature and pressure for a given gas flow rate.

The total mass associated with parasitic depositions is measured to confirm that DCS increases the growth rate by suppressing losses (reduced gas phase nucleation and parasitic deposition). The mass of the parasitic depositions are measured by weighing the gas delivery system where parasitic deposition takes place, before and after Si precursor flow. Precursor flow rate is kept at 5sccm for silane and DCS experiments and other growth conditions are kept the same. The total deposited mass (Si) in the gas delivery system was found to be ~370mg for silane compared to ~323mg using DCS, indicating that less Si is lost to parasitic deposition using DCS. The above results support the experimentally observed increase of growth rate in DCS compared to silane (Figure 2.5).

Thus the DCS system increases the availability of growth species for the epi growth boundary layer by reducing Si losses in the gas stream and reactor walls.

It is to be expected that, unlike the experimental results, the simulation (and calculation in section-1) gives a higher growth rate for silane precursor than DCS. The higher diffusivity and more efficient decomposition of silane (Figure 2.4b) into elemental Si, suggesting a higher growth rate for silane compared to DCS for the simulation (Figure 2.5) without including gas phase nucleation (which exists during the actual growth). We attribute the difference between the growth rates found using simulation and experiment (Figure 2.5) is an indication of the suppression of gas phase nucleation and parasitic deposition using DCS compared to silane. Hence, an ideal simulation tool must incorporate the respective precursor losses in its model to predict the growth rate accurately for a given condition.

According to the collision theory of chemical reaction, elemental silicon has the highest probability to take part in the reaction, in the gas phase, to form Si particles since it has a higher number of dangling bonds to form Si-Si bonding. From the analysis of simulation results, the degree of formation of elemental Si for a certain growth condition is an indication of the severity of silicon gas phase nucleation in the reactor. Combining simulation and experimental results (Figure 2.4, 2.5), it can be concluded that growth at 30 Torr in DCS is mostly due to participation of $SiCl_x$ or SiH_xCl_x species in growth, due to the smaller amount of decomposed Si in this condition (Figure 2.4). Thus, DCS provides an environment with reduced Si gas phase nucleation, consistent with the assumption that collisions among $SiCl_x$ or SiH_xCl_x have lower probability to form Si droplets or silicon aerosol. On the other hand, Figure 2.4 shows that silane decomposes

much more easily to form elemental Si even at a lower pressure (30 torr) resulting in higher gas phase nucleation and lower growth rate. However, at higher pressures (>300Torr), simulation shows that even DCS decomposes significantly to produce increased amounts of elemental Si (Figure 2.4a) leading to increased Si aerosol formation (or gas phase nucleation) and reduced growth rate. However, the increased Si formation in DCS at higher pressures is still less than silane, consistent with the experimental results (Figure 2.5). Increased HCl formation (which will be discussed later) and related etching (Nakamura et al., 2000) may also be a reason for lower growth rate found at higher pressures using DCS.

2.8 VARIATION OF DOPING CONCENTRATION WITH PRESSURE

Experimental results demonstrate that n-type doping concentration of the epitaxial layer increases with increasing growth pressure (Figure 2.7) for both precursors; this result is consistent with the previously published results for silane (Forsberg, Danielsson, Henry, Linnarsson, & Janzen, 2002). The *effective* C/Si ratio is the carbon to silicon ratio at the growth surface rather than C/Si ratio at the inlet. The *effective* C/Si ratio depends on the relative losses of silicon and carbon precursors (or the relative availabilities of them for epi growth) mainly as a result of parasitic deposition and gas phase nucleation (or aerosol formation) prior to reaching the growth surface. Si-aerosol can be considered to be a “pseudo-gas” with much heavier particles, with considerably lower diffusivity (Vorob'ev et al., 2000). Lower diffusivity restricts the molecules participating in growth by diffusional mass transport. According to this picture, a higher gas phase nucleation rate at higher growth pressures should result in higher effective C/Si ratio (due to depletion of Si) and lower nitrogen incorporation by the site competition

principle (Larkin, Neudeck, Powell, & Matus, 1994). However, this is in contradiction with our experimental results where net n-type doping increased at higher pressures (Figure 2.7). This discrepancy can be explained if depletion of carbon is considered as well. If depletion of C is considered, then the relative depletion of carbon to the depletion of silicon (already discussed) will govern the *effective* C/Si ratio.

The details of carbon deposition from the hydrocarbon precursor are disscussed elsewhere (Feron, Langlais, Naslain, & Thebault, 1999), and summerized below to provide rationale for carbon depletion during growth due to carbon depositions on the reactor walls.

Carbon produced by the thermal decomposition of hydrocarbon gases such as methane, and propane is called pyrocarbon. Pyrocarbon is deposited for various applications such as carbon resistors, microphonic materials, nuclear material coatings, etc. Pyrocarbon deposition is a complex process which is believed to be the result of simultaneous gas phase and surface reaction of hydrocarbons (Feron et al., 1999). Removing hydrogen from the hydrocarbon molecules by applying heat initiates the process of carbon deposition. Interaction amongst these dehydrogenated molecules and their further dehydrogenation and collisions may form complex and heavier carbon enriched molecules or polymers (Grisdale, 1953). These are carbon particles of different sizes and shapes, which deposit on the reactor parts. The shape and size of these depositions is reported to vary at different temperatures (1000 to 2400˚C) (Feron et al., 1999; Grisdale, 1953). Formation of heavier carbon rich molecules or polymers in the gas can be considered as gas phase nucleation of carbon (Grisdale, 1953). The deposition rate of pyrocarbon from propane is a function of temperature, pressure, flow rate, etc. which

is well studied (Feron et al., 1999). In silicon carbide CVD, the presence of the hydrocarbon propane provides a favorable condition for carbon deposition on the furnace parts similar to the pyrocarbon CVD described in (Feron et al., 1999).

With respect to SiC epitaxy, the pyrocarbon deposition on the reactor walls and carbon gas phase nucleation are termed as carbon losses since they deplete the carbon precursor. These carbon losses will vary depending growth temperature and pressure since pyrocarbon deposition is influenced by temperature and pressure. We believe that carbon losses may affect growth in terms of growth rate, epi film doping concentration and crystal quality. However, due to the presence of silicon in the SiC CVD environment, carbon depositions in the reactor may take much more complex forms than the ordinary pyrocarbon depositions.

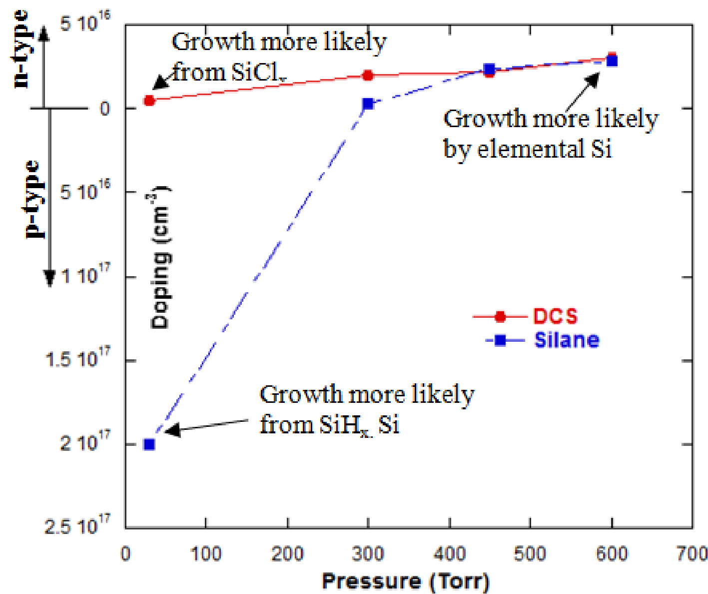

Figure 2.7 Doping concentration versus growth pressure.

As discussed earlier, parasitic depositions occur mainly in the injector tube and the hotwall. There are three possibilities for parasitic deposition on these walls:

pyrocarbon, silicon, and silicon carbide. The deposition of SiC (1C and 1Si) should not have any effect on the effective C/Si ratio at the growth surface and hence is not expected to affect the doping at the growth surface. On the other hand, the relative amounts of pyrocarbon and parasitic silicon deposition on the tube wall will play a dominant role in determining the *effective* carbon to silicon ratio at the epitaxial growth surface. The behavior of doping versus pressure in Figure 2.7 can be explained if we consider a higher amount of carbon depletion compared to silicon, reducing the effective C/Si ratio. This increased reduction of carbon can be attributed to the increased carbon losses at higher pressures due to increased pyrocarbon deposition on the reactor materials and formation of heavier carbon enriched molecules in the gas. We consider this loss of carbon to be the reason for the reduced *effective C/Si ratio* at higher pressures. This increases the net n-type doping according to the site competition rule (Larkin et al., 1994), a result consistent with our experimental observations in Figure 2.7. A detailed study is required to determine the relative depletion of carbon versus silicon in the reactor under different growth conditions.

It is observed that at higher pressures above 300 torr, both DCS and silane yield similar doping concentrations (Figure 2.7). We can conclude that at higher pressures, both precursors have similar precursor losses. Simulation results demonstrated a higher amount of elemental Si formation at higher pressures for both of the precursors (Figure 2.4) which indicates similar precursor losses for both chemistries. Growth with DCS at this condition is due to the participation of elemental Si in the growth unlike $SiCl_2$ at low pressures. Therefore at higher pressures, DCS growth is similar to silane growth. We therefore infer that at high pressures (>300 torr), both precursors result in a similar

effective C/Si ratio. The overall relatively higher n-doping for DCS compared to silane (Figure 2.7) can be explained by the mass measurement of the gas delivery tube discussed earlier. The lower parasitic deposition in DCS indicates a Si rich growth condition (lower C/Si ratio) which is consistent with higher n-doping as per site-competition epitaxy. A sharp change of doping is observed for silane at lower growth pressures compared to that of using DCS. Difference between the doping found by DCS growth and silane growth is particularly very high at 30 torr (Figure 2.7). This large difference indicates that at 30 torr, effective C/Si ratio using silane is much higher compared to that of using DCS, i.e. at lower pressures growth is much more carbon rich for the case of silane than DCS. Further study is required to explain this behavior and might be the subject of a future publication.

2.9 VARIATION OF SURFACE MORPHOLOGY WITH GROWTH PRESSURES

Even though a smoother surface is obtained using DCS at a low pressure (30 Torr), the surface quality degrades significantly at higher pressures (above 450 Torr, Figure 2.8b). A severely degraded wavy surface morphology, with increased roughness, is observed by AFM analysis for epilayers grown at higher pressures. However, no significant variation of surface morphology is observed for silane growths at various pressures (Figure 2.8c). Increased formation of HCl due to dissociated Cl from DCS at high pressures is responsible for surface waviness (degradation) because of excessive HCl etching (Nakamura et al., 2000) during growth. This assertion is supported by VR simulation as shown in Figure 2.8a, which shows ~20 times increased amount of HCl at 600 torr than at 30 torr, demonstrated by the larger red area.

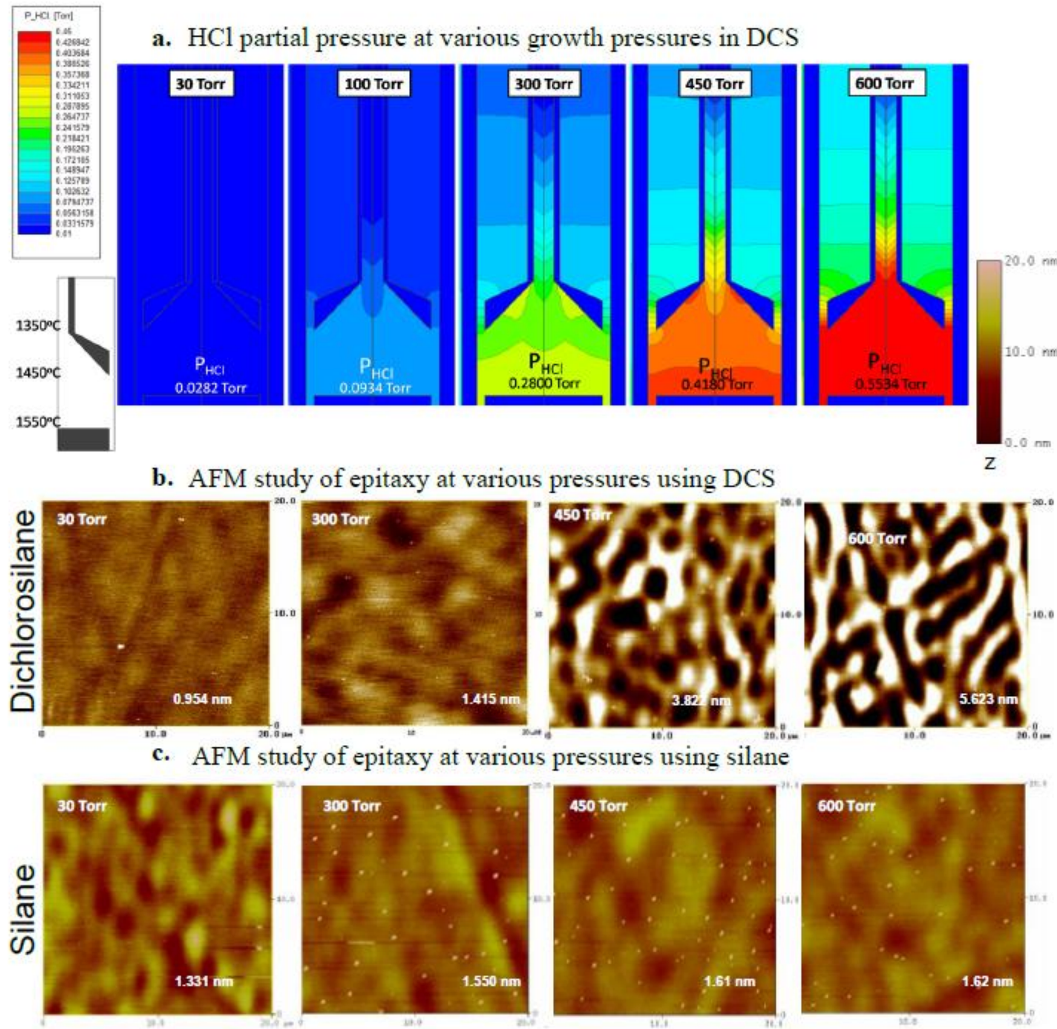

Figure 2.8 (a) Simulated HCl partial pressure for various growth pressures for DCS. Temperatures at specific locations in the reactor are shown. (b) AFM surface roughness at various growth pressures for DCS precursor. (c) AFM images for epitaxy grown by silane precursor at various growth pressures.

In summary, diffusivities of silane and DCS gases in hydrogen are calculated using Reid and Sherwood's formula and growth rates are calculated using diffusional mass transport. Experimentally, a higher growth rate is observed for DCS compared to silane chemistry despite DCS's larger molecular mass. This higher growth rate is due to reduced loss of the silicon precursor attributed to suppressed gas phase nucleation and parasitic deposition in DCS environment. The reduction of parasitic deposition using DCS is

confirmed by mass measurements of parasitic deposition. Further comparison is provided for growth rates obtained in silane and DCS using analytical calculation and by simulation.

Comparison of growth rates at various growth pressures for these chemistries demonstrate that DCS growth rate increases noticeably at low pressures (e.g., 30 Torr). With the support of simulation results, it is demonstrated that growth with DCS at this low pressure is mostly due to (mediated by) SiH_xCl_x species which creates the condition for reduced gas phase nucleation. At higher pressures even DCS decomposes into elemental Si, which reduces growth rate by increasing silicon loss.

The dependence of doping concentration on pressure is examined for both precursors and explained by consideration of *effective* C/Si ratio, the carbon to silicon ratio at the growth surface rather than the C/Si ratio at the inlet. Carbon depletion is considered for the first time in SiC CVD to explain the higher net n-type doping found at higher growth pressures. We infer that the relative losses of carbon and silicon growth species cause a variation in the *effective* C/Si ratio, which governs the doping concentrations at various growth pressures.

A wavy, degraded surface was observed using DCS at high pressures in contrast with growth by silane. Excessive etching due to the presence of higher amounts of HCl in DCS at higher pressures is believed to be the reason for the observed degradation in surface morphology.

In this chapter we discussed how growth can be improved by using a chlorinated silane gas instead of pure silane. Similarly, fluorosilane gases can also be used for the

growth. The extremely strong Si-F bond in fluorosilane gas gives some advantages over chlorosilane gases and will be discussed in the next chapter.

CHAPTER 3

EPITAXIAL GROWTH USING FLUORINATED SILANE (SiF_4)

3.1 INTRODUCTION

In the previous chapter we discussed the benefits of using a chlorinated silane (DCS) over using pure silane gas as Si precursor. Using the same reason for using DCS instead of silane, in this chapter we will argue that a higher bond strength gas SiF_4 will specifically suitable for high temperature SiC CVD.

High quality, thick (~100µm), low doped and low defect density SiC epitaxial films are essential for high voltage (blocking voltage >10kV), light, compact and reliable next generation power devices. These devices find application in efficient electric vehicles, power supplies and smart grids. One of the significant challenges in obtaining high quality thick SiC epitaxial films is to restrict/eliminate the Si gas-phase nucleation or aerosol formation during growth. The generated aerosol particles adversely influence growth by reducing the growth rate due to precursor losses, and also affect crystal quality (Vorob'ev et al., 2000), since the Si droplets are carried to the crystal growth surface. Moreover, liquid aerosol particles adhere to the various reactor parts (parasitic deposition), and contribute to their severe degradation during epitaxial growth. These parasitic depositions are generally loosely bound, and can be carried to the growth surface during growth as particulates, resulting in degradation of crystal quality by

introducing defects in the growing epitaxial layers (Rana, Song, et al., 2012a). The aforesaid condition is specifically severe at higher precursor gas flow rates or in long duration growth required to achieve high quality thick epitaxy since parasitic deposition and related particulate formation are also increased at these growth conditions. At this parasitic deposition enhanced condition, the cost of growth is also expected to increase due to frequent replacement of degraded reactor parts. Silane is commonly known to cause silicon supersaturation, limiting high growth rates (F. La, Galvagno, Foti, et al., 2006; Lu et al., 2005; Pedersen et al., 2007). Using silane, gas decomposition and parasitic deposition start very early in the gas delivery system and impede achieving good growth by impinging particulates to the growth surface (Leone et al., 2010; Rana, Song, et al., 2012a; A. Veneroni, Omarini, & Masi, 2005). In spite of the above limitations, high growth rate (growth rates of 32um/hr (Myers, Shishkin, Kordina, & Saddow, 2005), 50um/hr (Hori, Danno, & Kimoto, 2007), and even 250um/hr (Ito, Storasta, & Tsuchida, 2008)), good quality (good crystallinity and surface morphology), thick epitaxy has been reported using silane. However, it is to be noted that the above reported high growth rates require very high hydrogen flow rates and low pressure conditions in order to suppress Si droplet formation, rendering such a process impractical. Consequently extreme parasitic deposition and degradation of reactor parts is expected.

No systematic study of parasitic deposition is present in the current literature. One of the challenges associated with the study and understanding of parasitic deposition is the difficulty to quantify and characterize the deposited parasitic materials in the reactor. The reactor gas delivery system consists of a closed tube which is difficult to observe or measure for parasitic deposition. Efforts have been made to suppress parasitic deposition.

Parasitic deposition and related particle formation is considered to be the reason for lower process yield for device fabrication. Parasitic deposition and related issues might not be an important consideration for small quantity production. For quantity production changing reactor parts after few runs does not increase the cost dramatically and possibly over looked by various research groups. However, in industries, where bulk amount of epilayers are grown, parasitic deposition related issues cannot be ignored in order to reduce the cost. Parasitic deposition was suppressed (U.S. PATENT 7,118,781 B1), where a special arrangement is used to prevent the deposition of parasitic material on the wall. In this arrangement an inert gas is also flown along with the precursor gases. The purpose of the flowing of this inert gas is to create a buffer gas layer or a shield between the precursor gases and the surfaces of the reactor parts so that the precursor gases do not come into contact to the reactor wall. This is a technical process where parasitic deposition is reduced by reducing the number of gas molecules reaching the reactor walls. Despite claim of improvement, no quantitative analysis is provided in this patent for the parasitic deposition using this technique. This technique adds a layer of complication in the process. A special arrangement of gas delivery system is required for this method. Further, parasitic deposition is still expected since it is not possible to completely separate the precursor gas from reaching the reactor surface in this process; i.e precursor gases will diffuse into the buffer layer and will deposit on the walls. Moreover, this process is only beneficial for suppressing parasitic deposition, but it cannot suppress Si gas phase nucleation or aerosol formation. On the other hand in our proposed method described in this chapter, the suppression of parasitic deposition as well as gas phase nucleation is achieved by exploiting the chemical property of a gas

appropriate for high temperature SiC CVD instead of controlling the gas dynamics as in Figure 3.1.

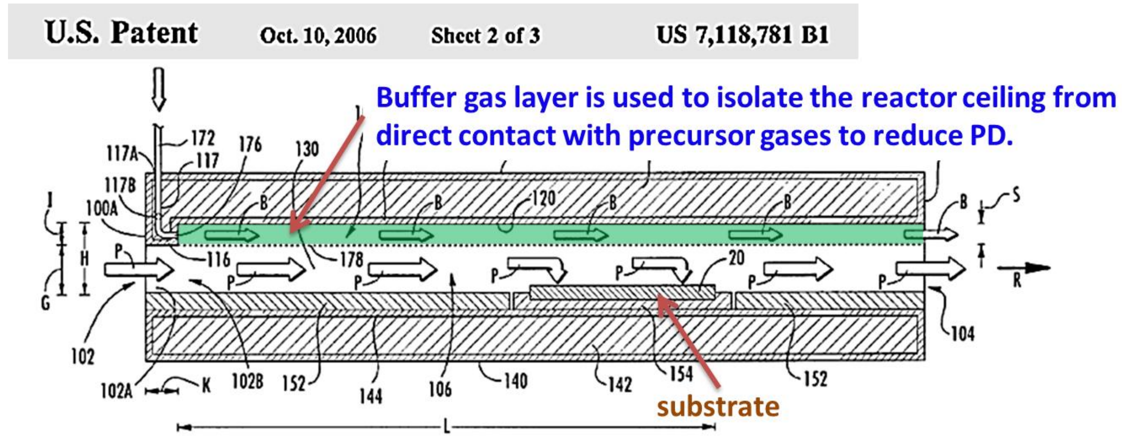

Figure 3.1 Patented technology to suppress parasitic deposition by creating a buffer gas layer.

To understand how gas chemistry can prevent the parasitic deposition or gas phase nucleation during growth we need to first understand how Si droplets start forming. To understand the gas phase nucleation mechanism let us consider that SiH_4 gas is flowing into the inlet of a container at a certain flow rates and exiting the outlet at a fixed pressure and at room temperature. From the basic law of gases, SiH_4 molecules are moving in the container with random motion, colliding to each other. Here the number of collisions and the mean free path of gas molecules depend on the concentration, molecular size, container pressure etc. At lower temperatures (e.g. room temperature), even though the gas molecules collide to each other but they do not react and do not form complex Si molecules or Si clusters. As an example, SiH_4 gas is stored in the cylinder at room temperature, where the gas remains intact (no chemical change) even at higher pressures (~1E6 torr) with a shelf life of 2 years. This is possible because SiH_4 does not

decompose at lower temperatures. However, if the temperature is increased then the decomposition and chemical reaction in the chamber will take place.

Whether gas molecules in the stream will react and stick to each other and form Si clusters at a certain temperature will depend on inertness at that temperature. Here inertness of gas molecules is its resistance against the heat energy preventing them being decomposed. In molecules atoms are bonded together with certain strength or bonding force. These bonds can be broken by applying external energy, i.e. heat. The energy required to break a bond is called dissociation bonding energy (energy/mole). For the case of SiH_4, when temperature is increased to point (starting from ~600C), there should be enough heat energy (318kJ/mol) to break Si-H bonds. At this temperature the original form of SiH_4 is lost and SiH_4 transforms into some free Si radicals with free or dangling bonds. These radicals (e.g. SiH_3, SiH_2, SiH or Si) are much more reactive than their parent molecules (e.g. SiH_4) due to the free bonds. At this condition, when these Si containing free radicals collide to each other then they easily react to each other and form heavier Si clusters unlike at room temperature condition. Temperatures at which a silicon source gas is decomposed, becomes reactive and starts forming Si clusters are different for different silicon precursors. A gas chemistry which decomposes at a higher temperature will produce less Si cluster (or aerosol) compared to the gases decompose at lower temperatures. Similarly, these high temperature gases will also suppress parasitic deposition more effectively.

Silicon droplet formation and reactor degradation (parasitic deposition and particulates) can be improved compared to pure silane by adding HCl (Crippa et al., 2005; R. L. Myers et al., 2005) into silane. The gas chemistry during this HCl mediated

growth is as following. At higher temperature (~600C), hydrogen is detached from silane and free radicals with dangling bonds are formed. These free radicals have at least one (or maximum four) dangling bonds. Now, collisions will occur due to the random movement of the decomposed free radicals. While previously, without HCl, these Si free radicals collided to other Si free radicals, now Cl is also present in the system. Hence a Si radical also have the possibility to collide with a Cl present in the reactor in addition to Si atoms. If a Si radical has probability to create bond either to a Si or a Cl then Si has the higher probability to form a bond with Cl leading to SiClx type radicals since Si bonds stronger with a Cl than to itself (Pedersen et al., 2007). Hence in this condition Si containing free radicals are mainly SiClx species. Now formation of Si-Si bonds and eventually Si clusters are less likely (than pure silane condition) since the free bonds of Si are now occupied by Cl by the formation of $SiCl_x$. Eventually, this mechanism of occupying free dangling bonds by a Cl by HCl addition suppresses the Si gas phase nucleation compared to using just pure Silane.

In another process instead of adding HCl into Silane a chlorinated silicon gas source is used. High growth rates (>100um/hr) were demonstrated in a condition of suppressed Si droplets using chlorinated silane precursors such as methyltrichlorosilane (Lu et al., 2005; Pedersen et al., 2007), trichlorosilane (F. La et al., 2008), tetrachlorosilane (M. A. Fanton, Weiland, & Redwing, 2008), methyle chloride (Kotamraju, Krishnan, & Koshka, 2009) and dichlorosilane (Iftekher et al., 2011). The advantage of using a chlorinated silane unlike HCl addition into SiH_4 described previously is that for chlorosilanes SiClx molecules are already present in the precursor gas which does not need any additional reaction to form. These SiClx molecules prevent

Si-Si bond and consequent Si cluster formation in a similar manner described earlier. Further, using for chlorosilanes the temperature can be increased without breaking Si-Cl bonds compared to the Si-H in silane since Si-Cl bond is stronger than Si-H. Thus chlorosilanes suppresses Si droplet formation and also parasitic deposition compared to Silane at higher temperatures.

As noted in the above reports, use of chlorinated precursors represents an improvement over the use of conventional silane. Yet, many challenges still remain for commercial production of thick SiC epitaxial films. Increased visible morphological defects due to particulate downfall on the substrate caused by parasitic deposition is reported to be a limiting issue in achieving thick epitaxial layers (Burk et al., 2012). Particulate related defects were also pointed out to be reason for low yield of device quality material in thick epilayers grown by hot wall CVD (O'Loughlin et al., 2008). Hence, increased parasitic deposition and related particulates, which are directly related to various growth parameters (e.g. type of Si precursor (Rana, Song, Chandrashekhar, & Sudarshan, 2012b), temperature, pressure, gas flow rates and growth duration), are a crucial limiting factor preventing thick epilayers for commercial production. A systematic comparative study of parasitic deposition for various precursors in the reactor is essential to improve the epitaxial growth but does not exist in the literature. In this paper, we demonstrate that the growth condition in SiC epitaxy in terms of parasitic deposition and particulate formation can be improved much further using a fluorinated silane.

Efficient decomposition of gases with stronger bonds requires higher temperature, although the likelihood of Si-cluster formation is also increased. Reaching higher growth

temperature without initiating parasitic nucleation is advantageous if a certain crystal requires higher surface diffusivity for efficient migration of atoms to their respective sites in the crystal. Thus different crystals may need different suitable gas chemistries for good growth. In *silicon* CVD epitaxy, a higher growth temperature (900°C-1200°C) (Grovenor, 1994), essential for single crystal growth, can be reached by using $SiCl_4$ instead of SiH_4 without early dissociation and Si cluster formation. Here, the optimal Si-dissociation/cluster formation balance discussed above is achieved by replacing SiH_4 with $SiCl_4$. However, *silicon carbide* polytypes (e.g. 4H and 6H) require much higher growth temperatures (>1550°C) compared to the *silicon* CVD epitaxy. At these higher temperatures, with chlorinated species, decomposition of Si_xCl_y is significantly enhanced, leading to greater gas-phase nucleation, thus reducing the benefits obtained for lower temperature *silicon* growth and preventing achievement of high quality, thick *silicon carbide* epitaxy. Hence, it is essential to find a suitable halogenated silicon precursor with stronger Si-X bond strength than Si-Cl for the high temperature *silicon carbide* epitaxy, beyond the conventional *silicon* CVD regime. This leaves only SiH_xF_y (x= 0, 1, 2, 3 and y =4-x) gases as the remaining choices.

It is to be noted that tetrafluorosilane (SiF_4) was used to grow polycrystalline silicon carbide films deposited by low power radio frequency plasma decomposition (Cicala, Capezzuto, Bruno, Schiavulli, & Amato, 1996; Ganguly, De, Ray, & Barua, 1991)**.** SiF_4 has also been used for growing micro-crystalline 3C-SiC on a Si substrate (Kida et al., 2008). However, high quality, homoepitaxial growth of 4H-SiC by high temperature CVD has not been reported. In this paper we report silicon carbide homoepitaxial (4H-SiC) growth using SiF_4 with elimination of Si gas phase nucleation

and significant suppression of overall parasitic deposition and subsequent particulate downfall on the growth surface.

3.2 EXPERIMENTAL SETUP

Experiments were conducted in a homebuilt vertical hot wall CVD reactor. SiF_4 was used as the silicon precursor. Conventional precursor gases SiH_4 and DCS were also used for comparison. Propane was used as the carbon source while hydrogen was used as the carrier gas. Purity of the precursor gases was 99.999% whereas purity of the carrier gas was 99.9999%. Growths were carried out at a temperature of 1550°C and a pressure of 300 torr for all three Si precursors. The C/Si ratio was maintained at 1. Commercially available 8mm x 8mm, 4H-SiC (Si face, 8° off cut towards $11\bar{2}0$ direction) substrates were used. Samples were cleaned following the standard RCA cleaning method. Simulation of temperature profile (Figure 3.2b) in the reactor was performed using Virtual Reactor, a commercial simulation tool (Bogdanov et al., 2001). The temperature was ramped up to 1000°C at 50°C/min. Propane was added at 1000°C (to mitigate excess substrate etching and consequent Si droplet formation (A.A. Burk & Rowland, 1996) and the temperature was ramped up to 1550°C in 20 minutes. Hydrogen etching was performed for 5 minutes while stopping the flow of propane at 1550°C. Epitaxial growth was then initiated by flowing propane and the silicon precursor gases. The hydrogen flow rate was kept fixed at 6 slm and the pressure was maintained at 300 torr for the whole process. The thicknesses of the epilayers were measured using the Fourier transform infra red reflectance (FTIR). The mercury-probe C-V technique was used for measuring the

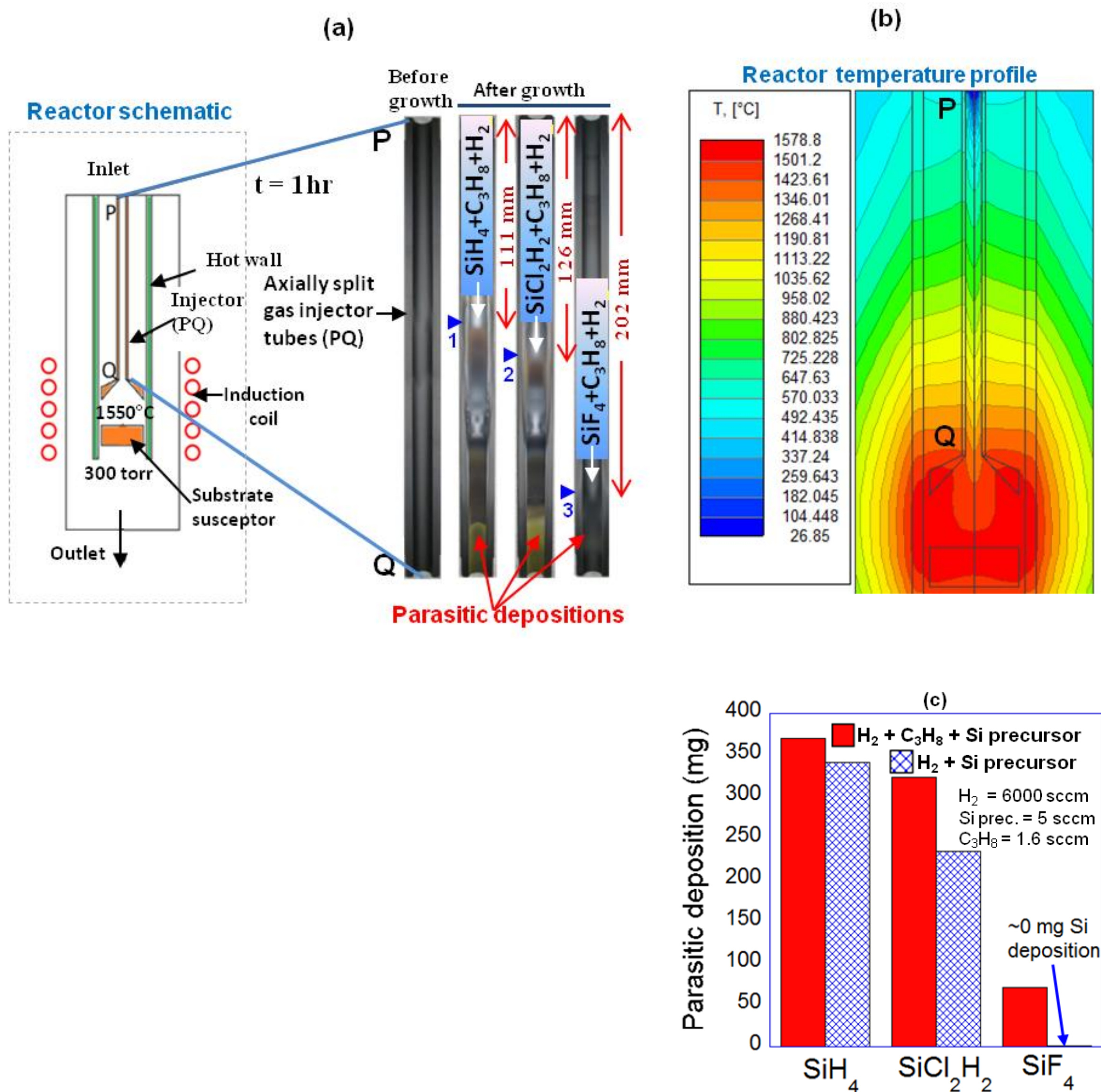

Figure 3.2 (a) Reactor geometry showing the position of the split gas-injector tube (left). Split tube before growth and parasitic depositions after growth are shown for different silicon precursor gases with propane and hydrogen. The locations from where the parasitic deposition starts are marked as 1, 2 and 3 for silane, DCS and SiF_4 respectively. (b) Temperature profile in the reactor obtained using a simulation tool is shown. (c) Bar graph showing the masses of parasitic depositions on gas injector walls using silane, DCS and SiF_4 precursor gases *with* and *without* propane addition. An ~80% reduction of parasitic depositions for SiF_4 *with propane* and a ~100% reduction *without propane* was found. (T= 1550°C, P= 300 torr, H_2 flow rate = 6 slm, propane flow rate = 1.6 sccm, Si precursor flow rates = 5 sccm and duration = 1hr).

doping concentration of the epilayers. Fixed C/Si ratios were maintained throughout the experiments for various gases and the doping (background) was achieved without introducing any intentional dopant. KOH etching was performed to determine the defect density in the epilayer. X-ray diffraction rocking curve and Raman-spectroscopy were employed to determine the crystallinity of the epilayers.One of the difficulties using fluorinated chemistry is that they may easily react with the glass container and corrode them. However, SiF_4 is one of the few fluorinated chemistries which is glass safe (Margrave & Wilson, 1971). It is to be noted that in the use of a fluorinated precursor, an important safety concern exists regarding the HF etching of the quartz glass enclosure] (Pedersen et al., 2012), assuming that HF is formed as a byproduct of the fluorinated CVD process. However, even though HF is produced, anhydrous HF does not etch glass since the basic principle of glass (SiO_2) etching by HF is that HF ionizes in water, and reacts with glass according to the following chemical reactions (Musket, Yoshiyama, & Contolini, 2002).

$$2HF + H_2O \Leftrightarrow H_3O^+ + HF_2^-$$

$$SiO_2 + 3H_3O^+ + 3HF_2^- \Leftrightarrow 2H_3O^+ + SiF_6^{--} + 3H_2O$$

As in the case of using chlorinated or other silanes, the reactor must be hermetically leak-tight and properly degassed (~$1x10^{-7}$ torr) before the growth. Pre-baking of the furnace was performed before growth to remove any residual water vapor introduced into the growth chamber during sample transfer. Further, a graphite liner was used to shield the glass from direct contact with the hot gas as an additional precaution. An in line gas trap was used in the exhaust system to trap any HF produced during the growth. An HF

gas detector was used to ensure safety. Similar precautions were taken for HCl produced during growth using dichlorosilane.

A split gas delivery tube system (gas injector made of SiC coated high purity graphite) was used to visualize parasitic deposition in the tube (Rana, Song, et al., 2012a). This design is an effective tool to identify the location at which the gases start decomposing in the injector tube by the observation of parasitic deposition. In this scheme, the gas delivery tube was axially split into two halves, which was then reassembled for growth. The scheme is shown in Figure 3.2a where the split part of the gas delivery tube can be seen as PQ in the CVD reactor. The split halves were assembled together to form a complete tube before growth, and was separated again after the growth for post examination. The inside image of one half of the split tube before and after growth is shown in Figure 3.2a. Here it can be seen that the tube is clean before the growth. However, after growth, parasitic deposition, composed of different Si and C compounds, can be clearly seen. The location where gas decomposition begins prior to reaching the growth surface is estimated from the locations of parasitic deposition regions in the tubes. This technique is proven to be beneficial especially for comparing the extent of parasitic deposition for different gas chemistries in a CVD reactor.

3.3 THERMO-CHEMICAL STUDY OF SiH_4, SiH_2Cl_2 AND SiF_4

SiF_4 is one the most stable gas molecules (Yershov, Orlov, Petrov, & Prokhorov, 1993). The Si-F bond is the strongest among all silicon precursors with the highest dissociation bonding energy (Si-F: 565kJ/mol vs, Si-Cl: 381kJ/mol; Si-H: 318 kJ/mol; Si-C: 318 kJ/mol, Si-Br: 309 kJ/mol and Si-I: 234 kJ/mol) (Gutmann, 1967; Huheey, 1972). The higher dissociation bonding energy of a gas molecule requires a higher temperature

for thermal decomposition. In the case of chlorinated silanes with a weak Si-Cl bond, hydrogen reacts and reduces chlorosilanes starting at 1000°C for tetrachlorosilane ($SiCl_4$) or even at lower temperatures for silicon chlorohydrides ($SiHCl_3$, SiH_2Cl_2). On the other hand, SiF_4, with the strongest Si-F bond is reduced by hydrogen at much higher temperatures- starting only above 2000°C (Collins, 2000). This ability of SiF_4 among all Si precursors to remain inert in hydrogen environment even until 2000°C is the reason for the effective elimination of liquid Si droplet formation and Si parasitic deposition observed at SiC growth temperatures. This highly stable chemically inert SiF_4 gas in H_2 environment has the least possibility of forming Si aerosol from molecular collision due to lack of reactive free radicals in the gas.

The Gibbs free formation energies of the thermal decomposition reactions of SiF_4 compared to that of SiH_4 and SiH_2Cl_2 are shown in Figure 3.3. Three main thermal decomposition reactions are considered for their free formation energies for 0 to 2000°C calculated from thermo-chemical data [JANAF] (kinetics.nist.gov/janaf/).

Thermal decomposition reactions are:

$$SiH_4 \rightarrow Si\ (g) + 2H_2 \qquad (1)$$

$$SiH_2Cl_2 \rightarrow Si\ (g) + 2HCl \qquad (2)$$

$$SiF_4 \rightarrow Si\ (g) + 2F_2 \qquad (3)$$

In these reactions Si gas precursors are completely decomposed into elemental Si liberating four of its occupying bonds in Si. Gibbs energies of these reactions are shown in a graph (Figure 3.3). For a certain temperature, higher Gibbs free energy indicates less favorable reaction compared to the reaction with lower free energy. In Figure 3.3, it is

clearly shown that the thermal decomposition of SiF_4 and formation of elemental Si is extremely difficult compared to SiH_4 and SiH_2Cl_2. From the graph in Figure 3.3 it is understood that even partial decomposition of SiF_4 and formation of SiF, SiF_2, SiF_3 radicals are highly unlikely at the temperatures shown in Figure3.3. Thus SiF_4 eliminates Si gas phase nucleation than any other Si precursor gases due to its very high stability at high temperature conditions.

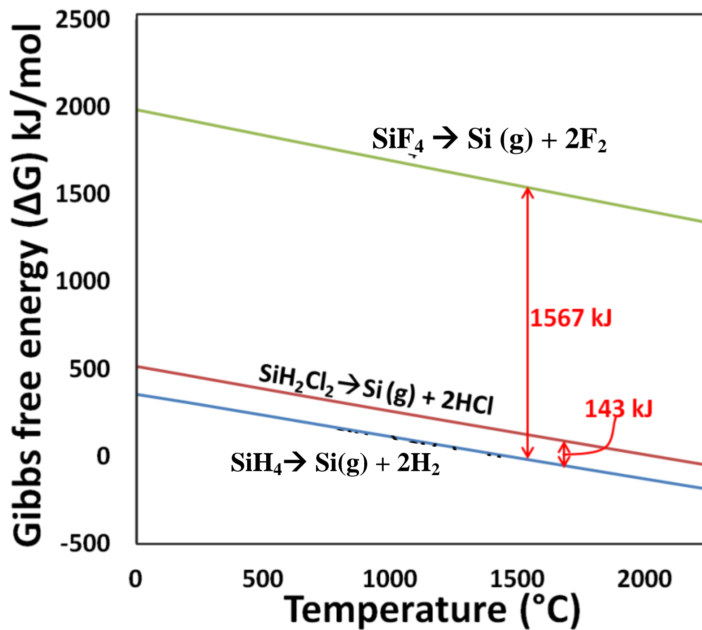

Figure 3.3Temperature versus Gibbs free energy of thermal decomposition reactions of SiH_4, SiH_2Cl_2 and SiF_4 showing very less favorable thermal decomposition reaction for SiF_4.

From the above discussion we find that there should be less Si gas phase nucleation if the gas is more stable (less reactive). Here the chemical reaction in the gas is suppressed due to the higher stability of the gas. The same argument is applied for the epitaxial growth. For epitaxial growth, chemical reaction at the surface should also be suppressed due to inertness of the high temperature gas. If the molecule is more stable (or less reactive) then the crystal growth rate should also reduce. Now, the question arises

that if the stable, less reactive Si precursor gases reduce the crystal growth rate then how it can be beneficial for epitaxial growth.

If the gas is highly unstable, e.g. SiH_4, ideally, it should increase the epitaxial growth provided that there are no Si precursor losses. However, practically SiH_4 starts faster reaction in the gas to each other very early in its flow path and in fact depletes Si source by excessive parasitic deposition and gas phase nucleation related precursor losses. As a result, higher reactivity of SiH_4 reduces the growth rate by increasing the Si losses due to gas phase nucleation and parasitic deposition. This condition not only reduce the growth rate but also degrades the crystal quality since particles produced in this process is carried to the growth surface.

On the other hand, when a stable gas is used (i.e. halogenated silanes), the growth rate should decrease due to the higher stability of the gas. However, even though the growth rate at the crystal surface should be reduced due to less reactive, stable gas molecules but suppression Si cluster formation and parasitic deposition increases the availability of Si precursor and increases the growth rate at the growth surface. At this condition, growth rate is compensated and increased by the increased availability of Si source gas at the surface.

It may appear that too strong Si-F bonds in SiF_4 would prohibit SiC epitaxial growths since reactive Si containing free radicals with dangling bonds are assumed to be absent in the gas stream. Previously (Pedersen et al., 2007) considered fluorinated gases not to be a choice of SiC CVD epitaxial growth due to too strong Si-F bond. We have observed experimentally that when no propane was added, a mixture of SiF_4 and hydrogen indeed results in no ***silicon*** deposition in the gas injector wall (Figure 3.2c) and

on the substrate. This result leads us to believe that there should be no epitaxial growth of SiC using SiF_4 as well. However, deposition on the reactor walls and epitaxial SiC growth took place when propane was added (Figure 3.2c). This deposition possible with presence of a hydrocarbon gas indicates that the hydrocarbon plays an important role in SiC growth by SiF_4 even though SiF_4 itself is much stable in a hydrogen environment.

Another reason for which growth is possible even using highly stable SiF_4 gas is because the surface reaction is considerably different than reactions in the gas. A gas, which is extremely difficult to be decomposed, still may participate in the growth at the surface of the crystal. As an example, nitrogen triple bond is one of the strongest bonds in the nature with a dissociation bonding energy of 945 kJ/mole. This bond is extremely unlikely to be decomposed at regular growth temperatures. However nitrogen is widely used for n-type dopant indicating even strongest nitrogen triple bond is broken at the surface where surface works as a catalyst to initiate the reaction. In a similar process it is also possible that SiF_4 molecule is broken at the surface of the substrate and takes part at the surface reaction and enables crystal growth.

In this chapter, we report the first homoeptixial growth of SiC films in a Si droplet free, parasitic deposition suppressed growth condition. The chemical route and surface reaction for the growth mechanism using SiF_4 is the subject for future detailed investigation.

Silicon CVD techniques are often used as guidance for silicon carbide CVD (Pedersen et al., 2011). The reason for which a fluorinated silane is not a suitable gas for *silicon* CVD is because the Si-F bond strength is too high and the growth temperatures are low, which must remain <1400°C, i.e. the melting temperature of silicon.

Furthermore, SiF_4 is an etchant for silicon at above 1150°C since ***SiF_4 (g) + Si (s) → $2SiF_2$ (g)*** (Timms, Kent, Ehlert, & Margave, 1965) and obviously cannot not be a choice of silicon growth by typical CVD methods. The aspect of Si etching by SiF_4 will be discussed in details in Chapter 4. However, *silicon carbide CVD* is considerably different than *silicon CVD*. Unlike the *silicon CVD*, typically, much higher temperature is needed for *silicon carbide CVD* (melting temperature of SiC is ~2700°C). The chemistry of *silicon carbide CVD* is fundamentally different from *silicon CVD* due to the presence of a hydrocarbon gas. At these high temperatures and with hydrocarbon addition needed for *silicon carbide epitaxy*, even SiF_4 with strong bonds participates in silicon carbide epitaxial growth as described in the later sections.

3.4. STUDY OF PARASITIC DEPOSITION USING SIH_4, SIH_2CL_2 AND SIF_4

To study parasitic deposition, which also indicates how early the gas decomposes in the reactor, the split gas injector tube as described in the experimental section is utilized. The photographs in Figure 3.2a qualitatively show the degree of parasitic deposition and the approximate location where the parasitic deposition begins taking place in the gas delivery tube for SiF_4 in comparison with conventional gases. In Figure 3.2a, three split gas injector tubes (their location shown in the reactor geometry) are shown after the epitaxial growths with different gases using the same growth conditions. A gas mixture of a silicon precursor gas (SiH_4 / DCS/ SiF_4) *with* or *without* propane, along with hydrogen, enters the cold end of the tube, and exits the hot end towards the growing crystal. During this travel, silicon/carbon compounds deposit on the tube wall starting at ~700°C, ~950°C and ~1200°C for SiH_4, DCS and SiF_4 precursors respectively (estimated from Figure 3.2b). Clearly, from Figure 3.2a, for similar growth conditions in the reactor, SiF_4 begins

parasitic deposition in the presence of propane much later in the gas stream (202mm from inlet) producing the least amount of parasitic deposition compared to SiH_4 (111mm) and DCS (126mm) due to the highest Si-F bond energy (565 kJ/mol) of SiF_4. The measured weight of these depositions from the weight difference of the injector tube measured before and after growth is shown in a bar graph in Figure3.2c.

For SiF_4, approximately ~0mg of Si deposition (compared to 341mg for SiH_4 and 235mg for DCS) was measured for the case *without propane* indicating *Si deposition-free* condition in the reactor- essential for high quality growth in a clean reactor environment (implying no Si pyrolysis and elimination of Si gas phase nucleation due to strong bonds). On the other hand, using SiF_4, parasitic deposition began *with propane* addition. With this propane addition, only 71mg of parasitic deposition took place on the gas injector tube for SiF_4 compared to 370mg and 323mg respectively for SiH_4 and DCS. A ~80% suppression of parasitic deposition was achieved using SiF_4, whereas no significant difference was observed for DCS and SiH_4 gases. This significant suppression of parasitic deposition obtained using SiF_4 is an important consideration for achieving high quality thick epitaxy by long duration growths (Burk et al., 2012). Suppression of parasitic deposition using SiF_4 does not only improve the crystal quality by minimizing parasitic particles originating from the reactor parts but also increases the re-usability of the reactor parts, which is an important factor to reduce the growth cost.

3.5. COMPARISON OF EPITAXIAL GROWTHS USING SIH_4, SIH_2CL_2AND SIF_4

A large number of particulate related defects (Figure 3.4) were observed for the growth using SiH_4 at 5sccm for one hour growth at a growth rate of ~7µm/hr. These large particles were directly related to the degradation of the reactor parts due to severe

parasitic deposition and their consequent particle downfall on the growth surface. Long duration growth with good morphology was not possible in this case. The density of particle related defects is shown in Table 3.1. Growth using DCS exhibited somewhat

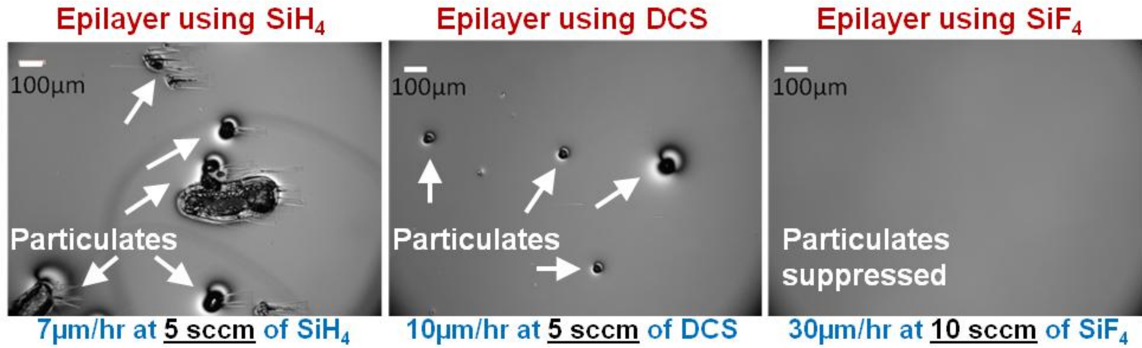

Figure 3.4 Particles on epilayer surface grown using various gas precursors at similar growth condition. No large particle related defects are observed for the epilayer grown using SiF_4 even at higher flow rates. (T= 1550°C, P= 300 torr, H_2 flow rate = 6 slm and duration = 1hr).

Table 3.1 Comparison of epilayer quality using various precursors for (T= 1550°C, P= 300 torr, H_2 flow rate = 6 slm, C/Si =~1 and growth duration = 1hr; substrate E_2(TO)/E_1(TO) or 4H/3C peak ratio = ~32, substrate doping = ~1x10^{19}-N-type and substrate XRD FWHM = ~20 arcsec).

CHAPTEI i precurs- or	CHAPTEI i gas flow rate (sccm) [a]	CHAPTEI rowth rate (µm/hr)	CHAPTEI aman E_2 to E_1 (4H/3C) peak	CHAPTER ! oping CHAPTER !	CHAPTER urface roughness R.M.S. (nm)	CHAPTEI RD CHAPTEI	CHAPTER 13 P article density 100- 400µm	CHAPTER article density 30-100µm (cm^{-2})	CHAPTER article density 10-30µm (cm^{-2})	CHAPTER it density 1µm-3µm (cm^{-2})
SiH_4	5	7	~30	1x10^{17} p	~0.5nm	~20	20	~50	~200	~3x10^{5}
DCS	5	10	~50	5x10^{16} p	~0.4nm	~12	0	~45	~100	~2x10^{3}
SiF_4	10	30	~60	1x10^{15} n	~0.3nm	~7.5	0	0	~5	~50

[a] epilayer surface significantly degrades with particulates at these flow rates (5 sccm) for silane and DCS. However, growth is improved due to suppression of particulate using SiF_4 even for higher flow rates (10 sccm). Figure 3.4. represents the growth surfaces at these flow rates.

[b] excluding the particulates in the epilayers

lower density of particles (due to lower parasitic deposition). Long run growths with good quality epilayers were still not possible even at this growth condition due to these particles. On the other hand SiF_4 suppressed parasitic deposition and gas-phase nucleation significantly and a much higher growth rate (30µm/hr) was achieved by increasing the mass transport to 10sccm. In this cleaner growth environment achieved using SiF_4, long duration growth (4 hours) with good quality epitaxy was possible and films up to 120µm thicknesses were grown at a growth rate of 30µm/h. A comparison of particulates generated during growth using three different Si precursors is shown in Table 3.1. Large particles on the epitaxial layer, mostly generated from loosely bound particles formed due to parasitic deposition in the gas delivery pathway were eliminated using SiF_4 gas by suppressing parasitic deposition as described earlier.

For SiF_4, a lower density (~ 5 cm^{-2}) of smaller sized particles (10µm-30µm) compared to silane and DCS mediated growths were observed (Table 3.1). Also, pits of 1µm -3µm size were significantly reduced using SiF_4 compared to silane and DCS (Table 3.1). We believe that these morphological defects were not growth related and mostly appeared because of downfall of particles during the loading of substrate in the reactor (located in a non-cleanroom environment). To confirm particle downfall during sample loading, the sample was loaded in the reactor, evacuated, and kept for 12 hours typical to reach high vacuum. The substrates were then unloaded without growth and particles were indeed observed on the surface by Nomarski microscope.

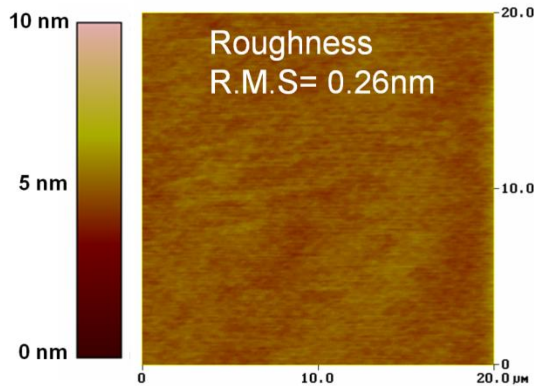

Figure 3.5 AFM image of a 60um thick epilayer with excellent surface morphology grown using SiF_4.

Morphologically, a very smooth surface (RMS roughness ~0.3nm) was observed for a ~60um thick epilayer grown at 30µm/hr for 2 hours using SiF_4 (Figure 3.5). The surface roughness does not increase much for thicker (~120um grown over 4 hours) epilayers (RMS roughness ~0.5nm vs. ~0.3nm) using SiF_4.

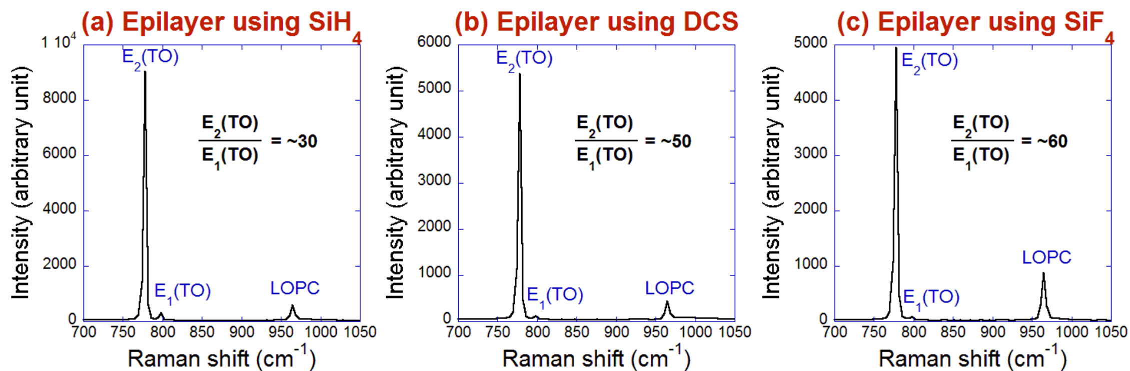

Figure 3.6 Raman analysis for epilayers grown using (a) silane, (b) DCS and (c) SiF_4. A higher E_2(TO)/E_1(TO) peak ratio for the epilayer grown using SiF_4 (c) indicates improved polytype uniformity compared to growths using silane (a) and DCS (b). High LOPC mode peak intensity for SiF_4 grown epilayer (c) is indicative of lower dopant incorporation compared to epilayers using silane (a) and DCS (b).

The ratio of the 4H peak (E_2 transverse optic or TO mode at 776cm^{-1}) and 3C peak (E_1 transverse optic or TO mode at 796cm^{-1}) (Iftekher et al., 2011; Nakashima & Harima,

1997) of a Raman scattering spectrum provides indication of the polytype uniformity. The higher peak ratio of the E_2 (TO) and E_1 (TO) demonstrates lower formation of 3C polytype in the epilayer (Iftekher et al., 2011). Typical E_2(TO)/E_1(TO) peak ratio (4H/3C) was found to be ~60 for the epilayers grown using SiF_4, indicating improved 4H polytype uniformity (Table 3.1), whereas ratios for the epilayers grown using silane and DCS were found to be ~30 and ~50 respectively. Here it is noteworthy that the typical E_2(TO)/E_1(TO) peak ratio of the original substrates used for these growths was ~32.

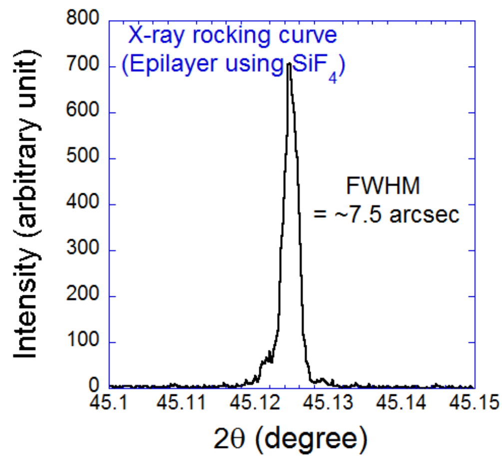

Figure 3.7 X-ray rocking curve of a epilayer grown using SiF_4 gas with a FWHM of ~7.5 arcsecond.

The increased height of the LOPC (longitudinal optical phonon-plasmon coupled) mode peak found at ~964 cm^{-1} for SiF_4 (Figure 3.6c) denotes lower free carrier densities (Nakashima & Harima, 1997) or lower doping concentration compared to silane (Figure 3.6a), and DCS (Figure 3.6b) mediated epilayer growths for the same inlet C/Si ratios. The doping concentrations for the epilayers are shown in Table 3.1. N-type epilayers (background doping) were found for SiF_4 mediated epilayers, whereas SiH_4 and DCS resulted in p-type epilayers for the same inlet C/Si (Table 3.1). According to site competition epitaxy (A.A. Burk & Rowland, 1996)**,** the growth performed in SiF_4 takes

place in a lower effective C/Si ratio or Si rich condition, which is possibly a consequence of increased Si species at the growth surface compared to SiH_4 and DCS growths, i.e. SiF_4 suppresses Si losses (due to parasitic deposition and gas phase nucleation) more efficiently than SiH_4 and DCS. Fluorine might have an influence on dopant incorporation and cause of lower doping using SiF_4 and will be subject for further investigation.

X-ray rocking curves were obtained to measure the crystalline quality of the epilayers grown using SiF_4. The X-ray rocking curve full width half maxima (FWHM) of various epilayers, indicating good crystal quality, were reported to be 7.8 (Iftekher et al., 2011), 10 (Pedersen et al., 2007), 11 (R.L. Myers et al., 2005), 18 (Lu et al., 2005) and 22-25 (M. Fanton et al., 2004) arcseconds. The typical (FWHM) of a 60um thick sample using SiF_4 was ~7.5 arcsecond (Figure 3.7), which is an indication of good structural quality comparable to the published literature. The lower value of FWHM epitaxial layers grown using SiF_4 compared to silane and DCS indicates superior crystal structure (Table 3.1).

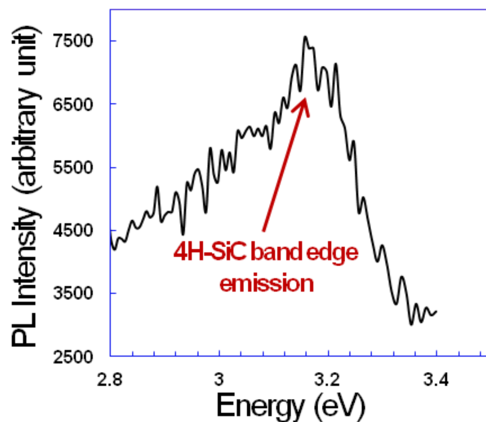

Figure 3.8 Room temperature PL spectrum of a SiC epilayer grown using SiF_4 demonstrates peak at 3.17eV.

The room temperature photoluminescence (PL) spectra (Figure 3.8) shows the typical exciton/band edge peak for 4H SiC at 3.17eV (391nm) (Klein et al., 2006), indicating no change of bandgap of the SiC epilayer grown using fluorine chemistry. Finally, thick (~100um) epilayers were etched using molten KOH solution for defect delineation. Typically, very low basal plane dislocation (BPD) density ~20/cm^2 was observed for the epilayers grown using SiF_4. The density of threading screw dislocations (TSD) was found to be similar to that in the substrate. Carrot defect was found to be typically ~0 cm^{-2}, further confirming good quality epitaxy using SiF_4.

CHAPTER 4

SiC SURFACE PREPERATION (ETCHING) BY SiF_4

4.1 INTRODUCTION

Silicon carbide is a promising material for next generation high voltage (>10kV), low weight, compact power electronics due to its various outstanding properties such as wide bandgap, high breakdown electric field, lower intrinsic carrier concentration, high saturation velocity, high mobility and high thermal conductivity (Neudeck, 2006). Demand for high quality, thick epitaxial growth of SiC is growing rapidly for high voltage or high power electronics. To achieve high quality thick epitaxy, it is essential to suppress silicon gas phase nucleation or cluster formation by HCl addition or using chlorinated precursors such as Methyltrichlorosilane ($SiCH_3Cl_3$), tetrachlorosilane ($SiCl_4$), trichlorosilane ($SiHCl_3$), or dichlorosilane (SiH_2Cl_2) (Crippa et al., 2005; F. La, Galvagno, Roccaforte, et al., 2006; F. La et al., 2008; M. A. Fanton et al., 2008; Iftekher et al., 2011; R. L. Myers et al., 2005; Pedersen et al., 2007).

Recently, the authors' group reported on tetrafluorosilane (TFS or SiF_4) precursor gas for high quality homoepitaxial growth (Rana, Chandrashekhar, & Sudarshan, 2012), and demonstrated superior abilities in reducing, and even eliminating gas phase nucleation and parasitic deposition. Parasitic deposition, while a severe problem, is rarely explicitly treated in the literature, as it is difficult to quantify. Parasitic deposition on reactor parts leads to loose particles in the system which deposit on the growing epitaxial

layer, leading to in-grown defects that degrade the epitaxial layers (Rana, Chandrashekhar, et al., 2012). TFS is expected prominence in future as a Si precursor due to its ability to eliminate Si gas phase nucleation and suppress parasitic deposition and related particulates significantly in the reactor (Rana, Chandrashekhar, et al., 2012). A study of SiC substrate etching using TFS in comparison to the other precursor gases is essential in order to understand and optimize the growth using TFS since the competition between growth and etch determines the net growth rate during epitaxy (VanMil et al., 2009).

Importantly, it will be an added advantage if the growth species can also be used as an etchant of the SiC substrate during the CVD process. Using the same Si growth precursor as an effective etchant of the substrate will minimize engineering challenges associated with gas switching transients as the process shifts from etching to growth initiation.

4.1.1 EX-SITU PRETREATMENT OF THE SURFACE: LAPPING, MECHANICAL POLISHING AND CMP

After slicing the boules into wafers using diamond wire saw, SiC surface is opaque and heavily marked with wire saw cutting scratches. The surface is not flat at this point. The first step to prepare the surface for further processing is lapping. Here the surface is constantly lapped using some very large grains of B_4C particles (20um-100um) with an applied pressure of 50-200gm/cm^2 by using an iron plate. The surface after the lapping process is extremely rough with a roughness of over 100nm (RMS). During this time high numbers of pits are generated on the surface and FWHM of the surface is around 122.4 arcsec (compared to ~7 arcsec for the best quality surface). Surface of these wafers after lapping is then polished using micron size (~1um diameter) diamond

polishing compound mixed in water. The surface is repetitively polished by a pad at room temperature until it becomes mirror-like. This process is called mechanical polishing since the granular diamonds interact with the surface only mechanically and no chemical reactions takes place between the diamond and the SiC surface since both of them are chemically inactive at room temperature. The surface roughness achieved by this process is usually around 1nm-3nm (RMS). Though mechanical polishing improves the surface quality dramatically compared to the surface found after lapping process but deep scratch marks are left on the surface due to movement of micrometer size large diamond particles on the surface under applied force. The surface smoothness can be improved further by using finer diamond particles (submicron size). However, the surface damages cannot be completely eliminated (X. Chen et al., 2006). As a result, after the mechanical process, residual surface and subsurface damages remain at the surface. While the subsurface damages after the mechanical polishing are buried under the surface and not visible from the top, the surface damages are easily observable by an AFM. These damages are also barely observable at higher magnifications by Nomarski microscopy. So, at the end of this process two types of surface imperfections remains. They are i) visible surface scratch marks and ii) invisible sub surface damages. Newly generated defects (dislocation loops) in the epilayer along with the polishing related scratch marks are reported (Grim, Benamara, Skowronski, Everson, & Heydemann, 2006). No study has been conducted yet for the influence on the subsurface damages on epilayer growths.

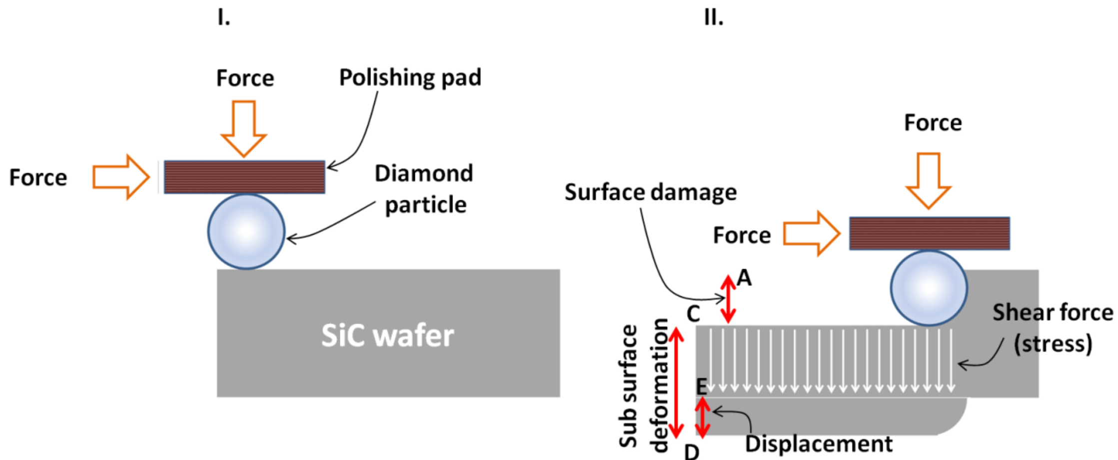

Figure 4.1 Surface and subsurface damages are shown I. Initial state II. Force is applied on the diamond particle and SiC crystal is deformed, initiating surface and subsurface damages.

Sub surface damages takes place mainly due to the plastic deformation of the crystal due to the shear force exerted on the surface through the abrasive particles (diamond) by the polishing pad. Surface damage and subsurface damages are shown in Figure 4.1. Initially lateral and vertical forces are applied on a diamond particle by a polishing pad shown in Figure 4.1(I). Since diamond is harder than SiC an impression of the movement of the diamond particle is created on the surface as AC in Figure 4.1 (II) depending on the size of the diamond particle. This impression AC can be seen from the top using microscope. Due to the shear force applied, also plastic deformation takes place in the crystal The visible scratch marks after the mechanical polishing are flattened by a chemical-mechanical polishing process. Here some finer (~50nm diameter) abrasive particles are used (e.g. Cr_2O_3, SiO_2, NaOH etc.) at an elevated temperature. In this chemo-mechanical polishing process, instead of mechanical interaction, the abrasive particles react chemically with the surface of the SiC, oxidize it and then the oxidized surface is removed mechanically by a rotating pad. Unlike the lapping or mechanical polishing, chemo-mechanical polishing is much slower.

Now, here it is important to note that the surface damage can be completely removed by the removal of the top layer with a thickness of AB (Figure 4.1). At this stage, very smooth, atomically flat surface is found; however subsurface damage (BC in Figure A1) will still be present and buried under the surface. It is important to note that even though in Figure 4.1 only subsurface damage due to the mechanical polishing by diamond particle is shown, in reality subsurface damage will be present due to slicing and lapping processes. Hence the thickness of the layer on top with subsurface damage might actually be much thicker.

These subsurface damages can be made visible by some electro-chemical technique where bias is applied on the CMP substrate immersed in electrolytic $CuSO_4$ solution for 15 minutes at 30V (Figure 4.2a). After this process the subsurface damages are decorated (Figure 4.2b). This experiment proves that despite smooth surface after CMP, the electrical behavior of the subsurface damage related stress points are different from the rest of the surface. Though no detailed study on the effect of these subsurface damages on epilayer growth are done yet, but it can be assumed that ideally they should not be present for good growth since these stress regions will propagate in the epilayer and may generate defects. The subsurface damage related issues are still not quantified and no specification is provided from the manufacturer's side. Hence despite atomically flat surface is achieved after CMP, it is still essential to treat the surface further (in situ) before the epitaxial growth by some dry etching technique to remove a certain amount of material from top without further degrading the surface.

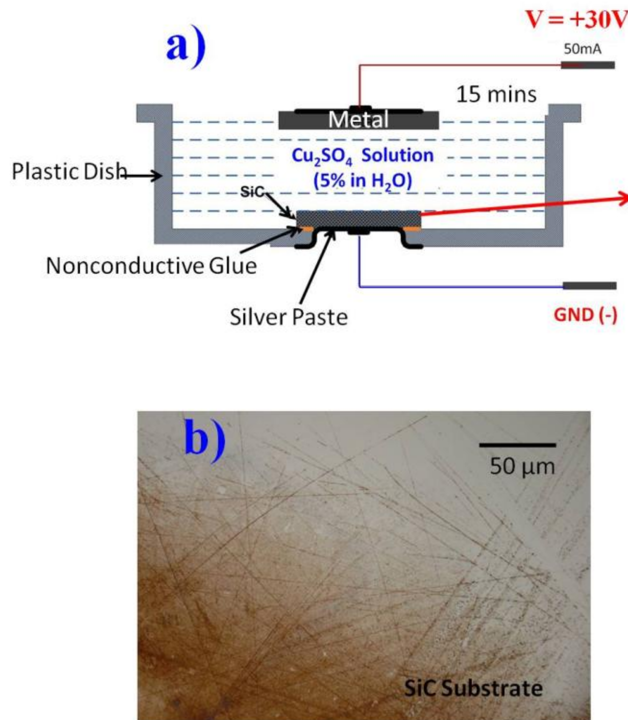

Figure 4.2. a) Electrochemical setup. b) Decoration of subsurface damages after electrochemical treatment of SiC wafers in $CuSO_4$ solution.

5.1.2. IN SITU DRY ETCHING TECHNIQUES

In situ dry etching is an important step performed before the initiation of epitaxial growth, where various polishing related surface and sub-surface damage (Sanchez et al.), and contaminants on the surface are removed in order to expose the dangling bonds on the SiC substrate for growth. This is done to minimize the potential for in-grown defects in the epitaxial layer originating from the substrate/epilayer interface, as sub-surface polishing damage induces dislocations and defects extending below the substrate surface (Sanchez et al.). Thus, if the etching process is too slow, it will not be effective in removing this damage. This process is typically done in a hydrogen ambient (Ramachandran, Brady, smith, & Greve, 1998) with or without C_3H_8 (VanMil et al., 2009) and/or HCl gases (Nakamura et al., 2000). Optimization of the surface by etching

is not only important for SiC epitaxial growth, but also for epitaxy of III-V materials (GaN) where SiC substrates are used.

It was reported that pure hydrogen etching induces excess Si and forms droplets on the surface which is undesirable for SiC surface preparation (A.A. Burk & Rowland, 1996). This excess Si and consequent liquid Si droplet formation on the surface can be prevented either by HCl or propane addition in hydrogen (Nakamura et al., 2000; VanMil et al., 2009). The mechanism of the Si droplet suppression by using HCl or propane will be discussed in a later section, where we will argue that Si-removal is the limiting factor or the bottleneck for etching of SiC.

It has been shown that pure hydrogen etching introduces morphological imperfections by delineating defects on the SiC surface (Bondokov, Tipirneni, & Sudarshan, 2004; Hassan, Bergman, Henry, & Janzen, 2008). These defects were reported to be reduced by introducing silane during the pre-growth etch, which improved the morphology of the pre-growth surface and consequent epitaxial growth (Fujihira, Kimoto, & Matsunami, 2003; Hassan et al., 2008). Silicon rich etching by silane (SiH_4) addition results in a different surface chemistry than etching in pure hydrogen (Leone et al., 2010), leading to an improved surface morphology. U. Starke et al. demonstrated that in a Si-rich condition, the SiC surface reconstruction changes, thereby changing the surface energetics (Starke, Schardt, Bernhardt, Franke, & Heinz, 1999) which is the reason for the improved epitaxial quality.

Etching under a Si-rich condition has been reported using SiH_4 addition. Halogenated silanes can also be added during hydrogen etching, but these studies have not been reported. The surface etching mechanism by addition of halogenated silanes is

much different than using just pure silane due to two reasons. Firstly, at similar conditions, silane, due to its weaker Si-H bond (Table 4.1) decomposes and forms elemental Si in a greater amount than halosilanes. Secondly, halosilane gas molecules contain halogen elements resulting in different chemistries compared to silane (A Veneroni & Masi, 2006).

Table 4.1 Dissociation bonding energies of various bonds found in Si precursors

Bond	Dissociation bonding energy kJ/mol
Si-F	565
Si-Cl	381
Si-Br	309
Si-I	234
Si-H	318
Si-Si	222
Si-C	318

In this chapter, we compare the etching of the SiC surface using TFS to that using chlorinated silicon precursor, dichlorosilane (SiH_2Cl_2, or DCS), and show TFS to be a superior etching agent for substrate pretreatment. These results are compared to that using propane. We argue that the same reasons that make TFS a superior growth precursor for SiC CVD (Rana, Chandrashekhar, et al., 2012) are the reasons that make it a superior pre-growth surface etchant.

4.2 EXPERIMENTAL

4.2.1 SETUP

Experiments were conducted in a vertical hot wall CVD reactor. 4H-SiC substrates with 8°, 4° and 0° off cut towards <$11\bar{2}0$> direction are used in a vertical hot

wall CVD reactor. Reactor pressure during etching (pre-treatment) was kept at 300 torr and the temperature was fixed at 1600°C. The temperature was ramped up to 1600°C from room temperature in 30 minutes in a pure hydrogen ambient.

For different experiments, the H_2 flow rates were varied while the precursor gas flow rates and various etching conditions (e.g. pressure, temperatures) were kept fixed. The etching was then performed for 1 hour for all experiments and then the temperature was ramped down in pure hydrogen. For these experiments, the susceptor or sample holder was made of TaC coated graphite and the gas injector was made of SiC coated graphite. The reactor reported in this paper is regularly used for SiC epitaxial growth (Rana, Chandrashekhar, et al., 2012) and hence new graphite parts without any parasitic deposition were used to avoid any unintentional growth caused by sublimation of deposited material on the reactor parts during etching. It is noteworthy that in these experiments only DCS generated severe liquid Si droplets on the reactor parts. To avoid Si contamination in subsequent experiments using H_2/TFS or C_3H_8, the DCS experiments were performed at the end and a separate set of reactor parts was used. SiC etch rates and Si deposition rates were determined by mass measurement of the substrates before and after the etching and they were correlated to the measurements using Fourier Transform Infrared (FTIR) spectroscopy with an error of +/-5%. Surface morphology was characterized using atomic force microscopy (AFM). Gibbs formation energies of the reactions were calculated for 1800K, 1900K and 2000K for different reactions using JANAF thermo-chemical data (kinetics.nist.gov/janaf/). Raman spectroscopy analysis was also performed on the etched epilayers to confirm Si deposition (Nakashima & Harima, 1997).

4.2.2. GIBBS FREE ENERGY CALCULATION

If P and Q are the reactants then at a certain temperature or pressure condition there are two possibilities for a chemical reaction:. i) they will react with each other spontaneously and **release energy** (exothermic reactions). ii) they will not react with each other until some **additional energy** is applied on them (endothermic reactions). In simple terms these energies related to chemical reactions are called **Gibbs energy** (kJ/mol or kcal/mol) or Gibbs free energy or free formation energy or free enthalpy.

By knowing the Gibbs energy it is possible to know whether the reaction is favorable or not at a certain condition. Also it is possible to know the phase of the reactants at the temperature or pressure condition from the Gibbs energy.

Gibbs energy can be calculated for a reaction by the following formula

$$Gibbs\ energy\ of\ a\ reaction = \sum Gibbs\ energy\ of\ products - \sum Gibbs\ energy\ of\ reactants$$

Or,

$$\Delta G_{Reaction} = \Delta G_{Products} - \Delta G_{Reactants}$$

If $\Delta G > 0$, the reaction is endothermic (additional energy required)

If $\Delta G < 0$, reaction is spontaneous (it will release energy)

If $\Delta G = 0$, reaction is in equilibrium.

If the Gibbs free energy of reaction A (say) is smaller than that of reaction B, then reaction A is more favorable to happen than reaction B. However, it is not correct to say

that reaction A will definitely occur instead of reaction B. By Gibbs energy, in general, the favorability of a reaction (over another) is only stated.

Gibbs energy of a reaction can be calculated from the known Gibbs energy of the reaction constituents of the reaction. These values are found from existing thermo-chemical data e.g. JANAF.

As an example let us calculate the Gibbs energy of the following reaction at 1900K and 1 atm pressure,

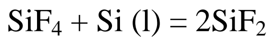

$SiF_4 + Si\ (l) = 2SiF_2$

From the JANAF thermo-chemical data, at 1900K, we find that

ΔG for SiF_4 = -319.26 kJ/mol

ΔG for SiF_2 = -151.67 kJ/mol

ΔG for Si(l) = 0 kJ/mol

Hence ΔG of the reaction

$= 2 \times (-151.67) - (-319.26) - 0$

$= 15.9$ kJ/mol

4.3 RESULTS AND DISCUSSION

4.3.1 ETCH RATES WITH VARIOUS GAS PRECURSORS (8° OFF CUT)

Etch rates using different precursor gases are shown in Figure 4.3, where H_2 gas flow is varied while keeping the precursor gas flow, pressure, temperature fixed. In other words, the dilution of the precursor gas is varied. The etch rates in pure H_2 at different flow rates in Figure 4.3 are considered to be the baseline reference for comparing etching

with different chemistries (DCS, TFS). When pure hydrogen is used, the etch rate of SiC decreases for lower hydrogen flow rates (Figure 1) and the SiC etching is limited by the slower Si removal process of thermal evaporation by reaction (5) in Table 4.2.

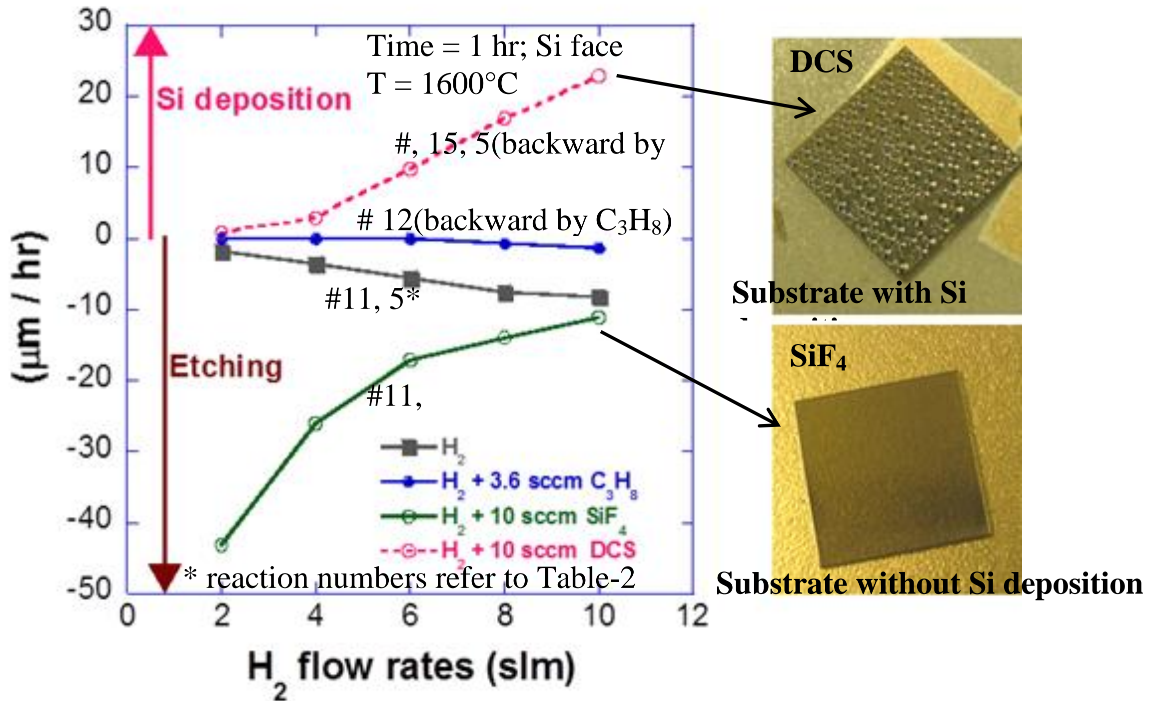

Figure 4.3 Etch rates using various precursor gases with various concentrations in H_2 gas with dominant reaction numbers found in Table 4.2. Both DCS and Propane mitigate the etching of hydrogen whereas TFS enhances the hydrogen etching. Etch rates using TFS increases at higher concentration.

Table 4.2 Free formation energy (kcal/mol) for various SiC etching reactions calculated from JANAF thermo-chemical data (kinetics.nist.gov/janaf/)

	Reaction	1800K	1900K	2000K
	Dissociation and evaporation reactions			
1	$SiC(s) \rightarrow Si(s) + C(s)$	13.72	13.53	13.344
2	$SiC(s) \rightarrow Si(l) + C(s)$	12.90	12.00	11.116
3	$SiC(s) \rightarrow Si(g) + C(s)$	58.19	54.60	51.183
4	$SiC(s) \rightarrow 1/2Si_2C(g) + 1/2C(s)$	36.99	34.69	32.4175
5	$Si(l) \rightarrow Si\ (g)$	45.29	42.59	39.904
	Hydrogen reactions			
6	$SiC(s) + 1/2H_2(g) \rightarrow Si(g) + 1/2C_2H_2(g)$	73.44	69.23	62.085
7	$Si(l) + 1/2H_2 \rightarrow SiH(g)$	44.81	43.12	41.44
8	$Si(l) + 2H_2(g) \rightarrow SiH_4(g)$	48.96	52.02	55.07
9	$C(s) + 3/2H_2(g) \rightarrow CH_3(g)$	42.86	43.47	44.08
10	$C(s) + 2H_2(g) \rightarrow CH_4(g)$	25.94	28.62	31.29
11	$2C(s) + H_2(g) \rightarrow C_2H_2\ (g)$	30.50	29.26	28.03
12	$2C(s) + 2H_2(g) \rightarrow C_2H_4(g)$	44.34	46.34	48.20
	Halogen reactions			
13	$SiF_4 \rightarrow Si\ (g) + 2F_2$	368.90	362.20	355.32
14	$Si\ (l) + SiF_4 \rightarrow 2SiF_2\ (g)$	19.69	15.93	12.22
15	$SiH_2Cl_2 \rightarrow Si\ (g) + 2HCl$	30.17	24.21	18.25
16	$Si(l) + 2HCl \rightarrow SiCl_2 + H_2$	-4.06	-3.79	-3.5
17	$C(s) + 1/4SiF_4 \rightarrow CF + 1/4Si(g)$	107.83	103.65	99.52
18	$C(s) + 1/2SiF_4 \rightarrow CF_2 + 1/2Si(g)$	128.23	124.16	120.19
19	$4C(s) + 3SiF_4 \rightarrow 4CF_3 + 3Si(g)$	184.63	180.62	176.69
20	$C(s) + SiF_4 \rightarrow CF_4 + Si\ (g)$	211.04	206.36	204.56
21	$2C(s) + 1/2SiF_4 \rightarrow C_2F_2 + 1/2Si\ (g)$	175.24	171.05	175.24

Contrary to etch rates found in pure hydrogen, when TFS is added to the hydrogen, the SiC etch rate increases significantly (Figure 4.3). The higher etch rates using TFS at lower H_2 flow rates (Figure 4.3) can be explained by the increased Si removal rate by increased rate of chemical reaction (14) in Table 4.2, as discussed earlier. At a lower H_2 flow rate, holding the TFS flow rate constant, the partial pressure, and hence, concentration of TFS is higher, driving the reaction (14), in Table 4.2 to the right. At a TFS/H_2 ratio of 0.05, a significantly higher etch rate of 43 μmh^{-1} was observed

compared to that without TFS addition, which gave an etch rate of only 1.8 μmh^{-1}. This significantly higher etch rate achieved by TFS addition shows that in an H_2 ambient (usually at high H_2 flow rates i.e. abundance of H_2), SiC etch rate is mainly limited and controlled by efficient removal of Si (in our case reaction 14 in Table 4.2) but not by C removal rate by H_2 by reactions (10, 11 in Table 4.2).

For the case of pure H_2, the surface is degraded by Si droplet like features as has been previously reported due to excess Si on the surface (A.A. Burk & Rowland, 1996; Hallin et al., 1997; Hassan et al., 2008), due to incomplete removal of surface Si by thermal evaporation (Table 4.2, reaction 5) . On the other hand, TFS addition at this condition resulted in an improved surface due to Si removal reaction-14 (Table 4.2). No silicon deposition is observed for the etched surfaces using TFS, which was confirmed by Raman analysis (Nakashima & Harima, 1997).

Prior to the discussion of the role of TFS and other precursor gases during hydrogen etching, it is essential to discuss the mechanism of hydrogen etching itself briefly. As described by Kumagawa et al. (Kumagawa & Yamada, 1969), the hydrogen etching mechanism has the following major reaction steps: I) SiC Dissociation, II) silicon removal, and III) carbon removal reactions. The major reactions associated with hydrogen etching and their Gibbs free formation energies (ΔG) are shown in Table 4.2 for 1800K, 1900K and 2000K, at atmospheric pressure, based on reactions found in (Kumagawa & Yamada, 1969). Considering the Gibbs free energies of formation, the dissociation of SiC and consequent liquid Si formation as per reactions (1) and (2) in Table 4.2, is expected on the surface. The other reactions, 6- 8 in Table 4.2, have higher free formation energy, and hence are less favorable.

In the case of H_2, it has the possibility to react with thermally dissociated Si or C on the surface. Carbon removal by hydrogen is more favorable since the free formation energy of C removal reactions by hydrogen (10-11, Table 4.2) are lower than the free formation energies of Si removal reactions by either thermal evaporation or hydrogen reactions (5-8, Table 4.2). Carbon removal by H_2 is possible by both reactions (10) and (11) in Table 4.2 at 1900K considering similar Gibbs free energies for the two reactions at this temperature. However, reaction (10) is more favorable at lower temperatures and (11) is more favorable at higher temperatures. Hence, when H_2 is introduced, the removal of C (difficult by only thermal dissociation, forming solid C without H_2) increases, leaving behind excess liquid Si (A.A. Burk & Rowland, 1996; Hallin et al., 1997), formed by reaction (2) on the surface. Even though H_2 initiates C removal from the surface, the overall SiC etching is still limited by the slower Si removal rate by (5-8, Table 4.2) since H_2 cannot react with the carbon efficiently until liquid Si is removed from the surface, as the excess Si on the surface drives the dissociation reaction (2) backward, slowing the etch rate down. Thus, the removal of Si is the limiting factor in the etch rate of SiC in a pure hydrogen ambient, supported by experiment and Gibbs free energy considerations. This excess Si on the surface can be removed efficiently by HCl addition (Nakamura et al., 2000) which increases the etch rate by increased Si removal rate (16, Table 4.2). In another method, by the hydrocarbon addition (e.g. C_3H_8), the hydrogen-carbon reaction is suppressed at the surface, driving the H_2 etching (10-11, Table 4.2) backward due to C overpressure. By this hydrocarbon addition it is ensured that C is not removed from the surface at a faster rate than Si, which removes the bottleneck for SiC etching due to reactions (1, 2, 10 and 11) and prevents the formation

of excess Si on the surface, and consequently lowers the SiC etch rate (A.A. Burk & Rowland, 1996).

Based on the hydrogen etching mechanism discussed above, the etching mechanism of TFS and other precursors in hydrogen ambient is described in the following. The mechanism of TFS mediated hydrogen etching is considerably different than that mediated by a chlorinated silicon precursor such as dichlorosilane due to the inertness of TFS. TFS is one the most stable gas molecules (Yershov et al., 1993) due to its strong Si-F bond, which is the strongest Si-halogen bond among available silicon precursors with the highest dissociation bonding energy (Table 4.1) (Gutmann, 1967; Huheey, 1972)**.** The higher dissociation bonding energy of a gas molecule requires a higher temperature for thermal decomposition. In the case of a chlorinated silane with a weaker Si-Cl bond, hydrogen reacts and decomposes chlorosilanes starting at 1000°C for tetrachlorosilane ($SiCl_4$) or even lower temperatures for silicon chlorohydrides ($SiHCl_3$, SiH_2Cl_2). The participating species for etching reactions are free Si radicals, H_2 and HCl at the typical SiC growth condition (~1600°C) (A Veneroni & Masi, 2006), leading to several reaction pathways, complicating the process.

On the other hand, TFS, with the strongest Si-F bond, is decomposed by H_2 at much higher temperatures, starting above 2000°C (Collins, 2000). There is only one participating etch species at typical temperatures, TFS itself, greatly simplifying the etch mechanism. This simplicity is also responsible for suppressing other parasitic reactions present for chlorosilanes, which lead to parasitic deposition during the *growth* of SiC (Rana, Chandrashekhar, et al., 2012). The unfavorable TFS decomposition is also apparent from reaction (13) in Table 4.2, where the free formation energy for complete

decomposition of TFS is very large. On the other hand the Gibbs free energy of formation of the decomposition reaction of DCS to form elemental Si is significantly lower (15, Table 4.2) indicating much easier thermal decomposition of DCS and consequent formation of free elemental Si.

TFS reacts with silicon according to the following reaction above 1150°C and forms gaseous SiF_2 (Timms et al., 1965). According to reactions (1) and (2) in Table 4.2, it is very favorable for Si to be liquid on the surface at typical conditions (1600°C) due to the decomposition of SiC to its constituent elements. Hence the most likely etching reaction using TFS (SiF_4) is

$$SiF_4\ (g) + Si\ (l) \rightarrow 2SiF_2\ (g) \qquad \text{(Table 2 reaction 13)}$$

as found experimentally using Si (Timms et al., 1965). The process of Si removal from the SiC surface by TFS is illustrated in Figure 4.4. During etching, each TFS molecule reacts with elemental Si formed by decomposition of SiC, thereby forming gaseous SiF_2 (14, Table 4.2) while hydrogen removes C (10, 11, Table 4.2). By this reaction, the Si removal is not the limiting step anymore for SiC etching since the free formation energy of reaction of Si removal by TFS (ΔG = 15.93 kcal/mol; T=1900K) is much lower than a) the free energy of the Si evaporation reaction (ΔG = 42.59 kcal/mol; T=1900K) and b) the C-removal reactions as shown in Table 4.2 (reactions 5,10,11,14). This mechanism of SiC etching using TFS in a H_2 ambient is illustrated in Figure 4.4.

The free formation energy of Si removal reaction by TFS by forming gaseous SiF_2 is 15.93 kcal/mol at 1900K (14, Table 4.2) is also considerably lower than that of C removal by H_2 by reacting with C and forming gaseous C_2H_2 with a free formation energy of 29.26 kcal/mol (11, Table 4.2). At this condition, according to (10, 11) and

(14) in Table 4.2, the Si removal rate by TFS is higher than the C removal rate by H_2 reaction-11 (Table 4.2). This enhanced Si removal using TFS prevents the formation of excess Si on the surface, and consequent Si droplet formation, further increasing the SiC etch rate which was previously limited by the slower Si removal rate in pure hydrogen ambient.

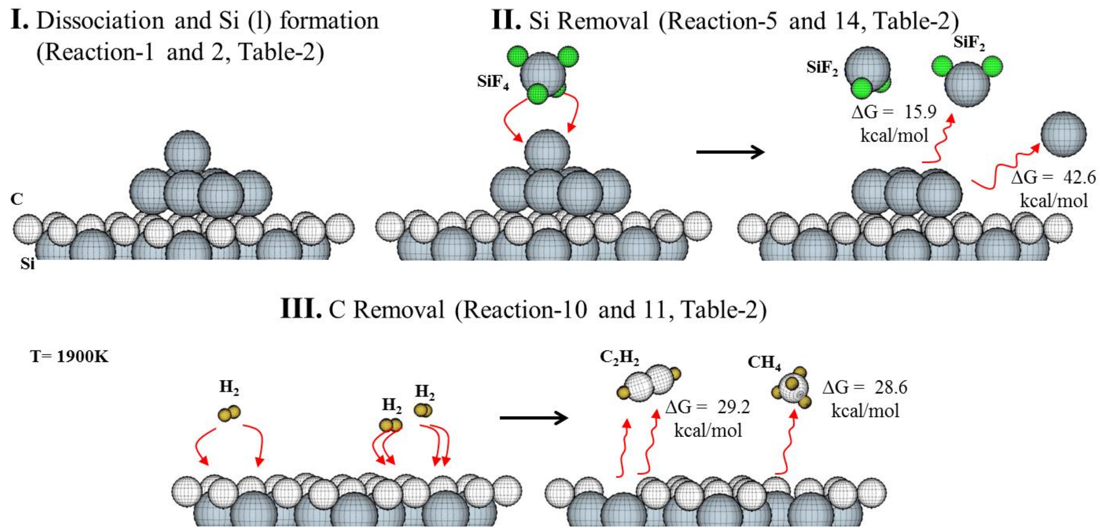

Figure 4.4 Mechanism of SiC etching using TFS and H_2. I. Si and C of SiC dissociate and form Si (l) on the surface according to reactions 1 and 2 in Table 4.2, II. Si on the surface is removed by TFS (reaction 14, Table 4.2). In the absence of TFS, the removal of silicon would be by thermal evaporation (reaction 5, Table 4.2), which is much less favorable, and III. Hydrogen reacts and removes C by forming either CH_4 or C_3H_8 gases (reactions 10 and 11, Table 4.2).

In this process, it may be thought that the surface should have excess carbon due to higher removal rate of Si. However, in practice, the hydrogen partial pressure significantly outweighs the TFS partial pressure, allowing unrestricted removal of the dissociated carbon (1, Table 4.2) leading to complete SiC etching, and removing the Si-removal bottleneck in reactions (5-8) in Table 4.2 . It is noteworthy that removal of C by TFS is unfavorable due to the much higher free formation energy found for carbon

reactions with TFS (Table4.2, reaction 17-21), which supports the reaction pathways proposed here.

To compare a chlorosilane for its influence on hydrogen etching, DCS is used in the reactor with the same flow rates and other conditions, as each DCS molecule has one Si atom, just like TFS. Contrary to the TFS chemistry, DCS decomposes thermally to elemental silicon much easier due to a low free formation energy of reaction (15) in Table 4.2. During this decomposition, HCl may be produced by reaction (15) and would be expected to increase the Si etching since the free formation energy of Si removal by (16) is exothermic and highly favorable. However, experimentally, we found that in fact DCS suppresses SiC etching in H_2 as shown in Figure 4.4. The above anomaly is explained as follows.

By reaction 15 in Table 4.2, any HCl partial pressure increase is caused by an increase in the partial pressure of elemental Si due to dissociation of Cl from DCS. This increase of the partial pressure of Si free radicals counteracts the potential effects of HCl etching of SiC by depositing Si(l) on the surface which eventually drives the reaction-5 (Table 4.2 and Figure 4.3) backwards and restricts overall SiC etch by H_2 and HCl [reaction 11 and 16 (Table 4.2)]. When the Si deposition rate (due to Si pyrolysis) is higher than the etching rate by H_2 and HCl, the net etching is lost (Figure 4.3). Severe liquid silicon deposition is observed at higher hydrogen flow rates (Fig 2) indicating an increased Si pyrolysis reaction rate at higher H_2 flow rates. These depositions are visible as large liquid silicon droplets on the surface after the experiment (Figure4.4).

Finally, hydrogen etching was performed with propane addition, as has been investigated by others (A.A. Burk & Rowland, 1996; Hassan et al., 2008; VanMil et al.,

2009). For the case of propane addition, the etch rate of SiC is also reduced (Figure4.4). However it was found that for similar atomic concentrations of C compared to Si concentration in the DCS experiments, the effect of propane on etching suppression is less severe, as there was no Si-deposition. The reduction of the etch rate is attributed to the addition of hydrocarbon species in the vapor, which drives reaction 11 in Table 4.2 backwards, suppressing the etch rate.

5.3.2 TFS ETCHING WITH VARIOUS OFF-CUTS

Similar to SiC growth by step-controlled epitaxy (Matsunami et al., 1997), etching of the SiC surface also occurs at the kink sites (Nakajima, Yokoya, Furukawa, & Yonezu, 2005). The density of kinks is higher for higher off-cut substrates. Although the differences are not large, a trend of higher etch rates were observed for higher offcut substrates (Figure 4.5). The higher etch rates for higher off-cuts are associated with the higher number of kinks for higher off-cut substrates since the etching occurs at the steps or kinks (Nakajima et al., 2005). A surface study using AFM is presented in Figure 4.5. Step bunching of the etched surfaces was observed for different etch conditions for 4° and ~0° off cut surfaces. Both etch rate and off cut dependences were observed for step bunching and are discussed below.

The fundamental reason for step bunching is the fact that the atoms landing on the surface (for growth or etching) have different probabilities of migration to, and reaction at, the kinks and steps, respectively (Schwoebel, 1966). As a result, the step flow rates (growth or etch) are different for the step and kink directions. The faster step flow direction catches up with the slower one,

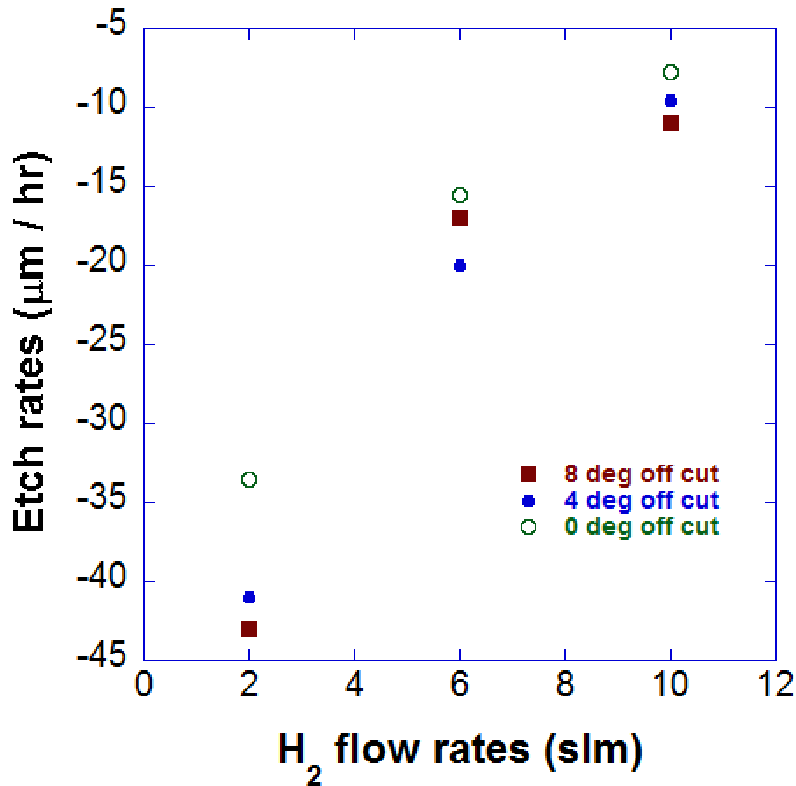

Figure 4.5 Etch rates as a function of TFS concentration in H_2 gas for various off cut SiC substrates. A trend of slightly higher etch rates were observed for higher off cut substrates.

leading to step bunching. Whether the steps will coalesce and form bunched steps depends not only on the different probability of the adatoms to migrate to the kinks but also on the crystallographic structure of the steps (e.g. off cut, polytype, stacking of the steps etc.) (Schwoebel, 1966). Step bunching also depends on the growth condition; e.g. temperature, pressure and duration. Once step bunching has been initiated, it increases over time (Sato & Uwaha, 2001). This is because, for longer time, the steps move longer distances and more steps coalesce to form macro steps, increasing step bunching. Similarly, increased step bunching results for higher etch rates (or growth rate) since at

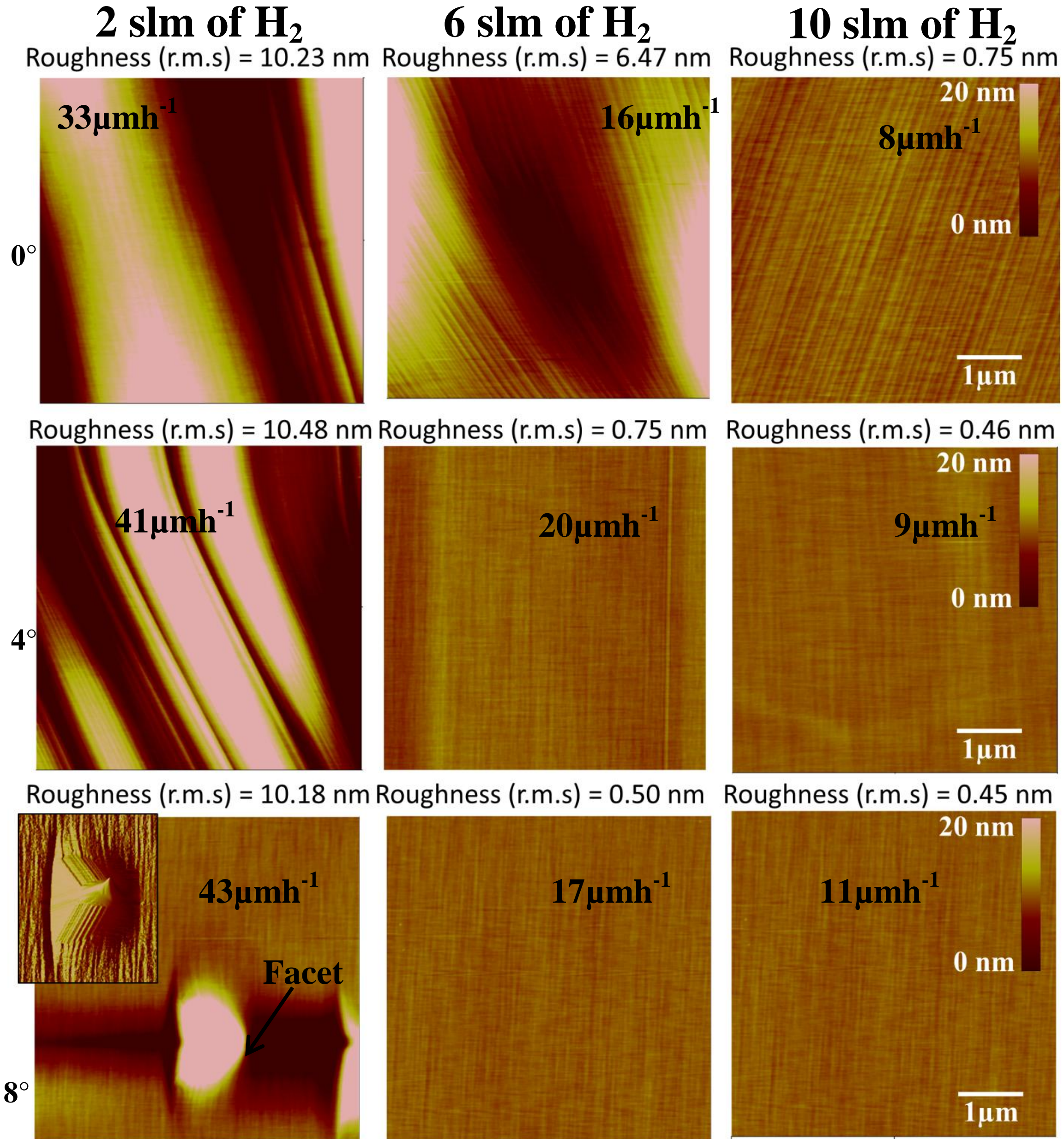

Figure 4.6 AFM surface morphology of SiC surfaces for 0°, 4° and 8° off cut substrates etched at various TFS gas concentrations in H_2.

this condition, steps move longer distances for a given time and hence, at higher etch rates, more steps coalesce, forming macro steps and increasing step bunching. Very rough, wavy surfaces are observed (Figure 4.6) at higher etch rates due to severe step bunching.

Greater step bunching was also observed for lower off-cut substrates for a given condition (Figure 4.6). From Figure 4.5, it can be observed that step bunching takes a severe form (roughness ~6.5 nm) at an etch rate of 16μmh^{-1} for on-axis substrates whereas this severity of step bunching is not observed for 4° off cut substrates even at etch rates of 20μmh^{-1}. On the other hand, for 8°offcut substrates, step bunching is not observed even at higher etch rates (43μmh^{-1}) (Figure 4.6). However, at this high etch rate for 8° off cut substrates, hillock structures are observed which are attributed to delineation of polishing related surface and sub-surface defects in the as received substrate (Figure 4.6) (Sanchez et al.).

M. Syvajarvi et al showed that step bunching is dependent on the difference between the lateral growth rates between $[1\bar{1}00]$ (step) and $[11\bar{2}0]$ (kink) directions (Syvajarvi, Yakimova, & Janzen, 2002). When the substrate is cut towards the $[11\bar{2}0]$ direction, unintentional miscut is also present creating steps towards the $[1\bar{1}00]$ direction. For higher off cut substrates, this miscut related step density towards $[1\bar{1}00]$ is negligible compared to the step density along the $[11\bar{2}0]$ direction due to the primary off-cut angle. Hence, for higher off-cut substrates, etching is mainly unidirectional or anisotropic, where the etch rates along $[11\bar{2}0]$ is much higher than the etch rates along $[1\bar{1}00]$ directions and the step bunching is minimized. However, for lower off-cut substrates (e.g., vicinal on axis), the miscut angle is not negligible towards $[1\bar{1}00]$ and step densities towards both $[1\bar{1}00]$ and $[11\bar{2}0]$ directions are comparable. Hence, with lower off-cut substrates, step flow due to etching is more isotropic which results in increased step bunching on lower off-cut substrates compared to higher off-cut substrates (Figure 4.6).

The trends presented in Figure 4.5 enable the identification of an ideal TFS partial pressure as a function of SiC substrate off-cut for optimized SiC surface preparation. This optimization is a balance of etch-rate, required to remove enough damage from the surface, with minimization of step-bunching, which otherwise degrades the surface prior to growth.

In summary, tetrafluorosilane (TFS) selectively reacts with Si on the SiC surface enhancing hydrogen etching by faster Si removal from the surface in the form of SiF_2 gas, relieving the Si-removal bottleneck. TFS is proposed to be an alternative choice for etching SiC compared to using HCl. TFS is reported to be a unique Si precursor gas which is also a strong SiC etchant in hydrogen environment. Dichlorosilane (DCS), a chlorisilane gas having weak Si-Cl bond (compared to the Si-F bond in TFS) decomposes easily at typical SiC CVD temperatures and prevents SiC etching due to Si deposition. Here, DCS mitigates the hydrogen etching to a higher degree than mitigation of hydrogen etching by the use of propane in hydrogen. On the other hand, very high etch rates can be obtained using TFS in hydrogen compared to the etch rates using only hydrogen gas. Greater step bunching was observed for higher etch rates and for lower off-cut substrates. Optimized etch conditions for pre-growth surface preparation can be obtained from the off-cut and partial pressure dependences presented in this paper. The elimination of the Si-removal bottleneck using TFS represents the development of a much more robust surface preparation technique for SiC epitaxy, critical for the continued improvement of material quality for high power SiC devices.

A detailed study of growth rates, doping, off cut dependency etc. using SiF_4 gas precursor will be provided in Chapter 5.

CHAPTER 5

EFFECT OF C/SI RATIOS ON EPILAYERS GROWN ON VARIOUS OFF CUT SUBSTRATES USING TETRAFLUOROSILANE GAS

5.1 INTRODUCTION

Silicon carbide is the choice for the next generation high power and high temperature electronic device applications due to its various extraordinary properties. Properties that make SiC a special material for high power and high temperatures devices are its lower intrinsic carrier concentration, higher bandgap, higher breakdown electric field, good mobility and high thermal conductivity (Neudeck, 2006). From theoretical calculations, for ideal material, SiC device should operate at a temperature up to 800°C compared to 300°C for the case of Si devices. Using SiC, theoretically, thickness of the voltage blocking region can be made 10 times thinner than Si and the doping concentration can be increased 10 times higher compared to Si (Neudeck, 2006). However, despite the enormous promises, SiC's true power is yet to be unleashed. High power, high temperature reliable devices are still not present in the market. One of the major issues for which the promise of SiC cannot be met despite high demand is the difficulty to achieve high quality SiC materials. SiC material is yet to be matured both for its bulk growth and epitaxial film growths. Substrate defect density is still significantly higher compared to the silicon technology. When SiC epitaxial films are grown on the

substrates, existing defects already present in the substrate mostly propagate to the epilayer either in the same form as the original or converted into a different defect (e.g. Basal plane dislocation to threading edge dislocation). While, from epitaxial growth perspective, nothing much can be done to completely prevent the propagation of defects from the substrate, the primary goal of SiC epitaxy is then preventing new crystal or morphological defects generated during growth due to process related issues.

Particle generation during the epitaxial growth is one of the leading issues for low yield of the epilayer on the wafer, as discussed in the Chapter 3. Particulate generation in SiC CVD is particularly much more severe compared to other semiconductor materials due to various reasons. The main reason is that SiC CVD requires much higher temperatures, typically ~1600°C or more. At this temperature condition, gas decomposes much earlier in the gas delivery system, rendering severe Si gas phase nucleation and a wider zone of region where parasitic deposition takes place and generate particles. Another reason for which particulate condition is particularly severe for SiC epitaxy is the thick epitaxy requirement for high voltage application. When thick epitaxy is required, growth rate must be increased and as well as the growth duration. When higher flow rate of gases are used for a prolonged period of time for thick epitaxy, particle generation is also proportionately increases and prohibit good growth. In Chapter 3 we have shown that using SiF_4 as the Si-precursor Si gas phase nucleation can be practically eliminated and parasitic deposition can be suppressed significantly. In this chapter we present some detailed results regarding the growth using SiF_4 gas. Before we further proceed presenting our results related to the growth using SiF_4 gas, it is essential to discuss briefly about the history of using various Si precursor gases in SiC epitaxy.

We start our discussion with silane (SiH_4), which is the simplest Si gas precursor. Despite difficulties in growing SiC epitaxy using silane described in Chapter 2 and 3, high growth rates and thick epitaxy are reported by various authors. O. Kordina et al demonstrated high growth rate (200um/hr) at high temperature using silane (Kordina et al., 1997). R. Myers et al. used silane for high quality epilayer growth and demonstrated 65 um thick epi at a growth rate of 32um/hr. X-ray rocking curve FWHM of ~11 was demonstrated and AFM surface roughness of 0.32nm was reported (R.L. Myers et al., 2005). High growth rate (50um/hr) with low BPD density (22/cm2) was demonstrated by Tsutomu et al (2007) (Hori et al., 2007) using silane. Epilayer with high growth rate as much as 250um/hr was reported by Masahiko et al. in 2007 by using silane as a precursor gas (Ito et al., 2008) with good uniformity of thickness and doping. Smooth surface with a roughness of 0.2nm was demonstrated for thick epilayers (>200um). Despite reports of aforesaid high growth rates using silane, it is not a practical gas for high temperature SiC CVD to achieve thick epitaxy due to the fact that such growth requires extreme conditions to suppress Si cluster formation (e.g. very high flow rate, 50-100 slm of H_2). Although growth at such extreme conditions can prevent gas phase nucleation near the SiC growth surface, Si parasitic deposition takes place on various reactor parts (e.g. hotwall) necessitating their frequent replacement in order to achieve good epitaxial growth. The detailed discussion of parasitic deposition and particulate related issues are provided in Chapter 3.

Chlorinated silicon precursor was introduced to suppress Si gas phase nucleation associated with the use of silane. Chlorine was first introduced with silane as HCl to suppress Si cluster formation and a growth rate of 20- 30 um/hr was demonstrated in

2005 by (Crippa et al., 2005; R. L. Myers et al., 2005). Roughness of these samples was reported to be ~0.25nm. During almost the same time, carbon and silicon containing chloro precursor methyl trichlorosilane (MTS) was used to demonstrate a growth rate up to 90um/hr by Peng Lu et al in 2005 (Lu et al., 2005). Later (2006) F La Via et al reported a high growth rate of 112um/hr using HCl/TCS with a surface roughness of 0.3nm (F. La, Galvagno, Foti, et al., 2006), where density of defects was reported to be 400-3000/cm^2, 3E4-7E4/cm^2, and 2000-6000/cm^2 of TSD, TED and BPD respectively. In 2007, H. Pedersen et al. reported a growth rate of 100µm/hr using methyltrichlorosilane (MTS) (Pedersen et al., 2007). Roughness of the epilayer was reported to be as good as 0.57nm. M. A. Fanton (2008) reported very high growth rate (200um/hr) using $SiCl_4$, though information about crystal quality was not provided (M. A. Fanton et al., 2008). Trichlorosilane ($SiHCl_3$) was used by F. Fla Via et al for growth in 2008 at a growth rate of 100um/hr (F. La et al., 2008). S. Leone and his group demonstrated a growth rate of 25um/hr on on-axis 6H and 4H SiC substrates (Leone, H.Pedersen, A.Henry, & O.Kordina, 2009). Mixture of methyl chloride (CH_3Cl) silicon tetrachloride ($SiCl_4$) was used to demonstrate epilayer growth at 100 um/hr by Siva Kotamraju (2009) (Kotamraju et al., 2009). Chowdhury et al reported DCS as precursor for high growth rate (2011) (Iftekher et al., 2011), demonstrating 100um/hr. X-ray rocking curve FWHM was reported to be 7.8 arcsec.

Thick epitaxy is utmost important for SiC growth since the main application of SiC is expected to be high power devices. One of the reasons for which enormous effort was made to achieve high growth rate in recent years by various research groups was to reduce the cost by reducing the production time of the long duration growth at low

growth rates to achieve thick epitaxy. However, the degradation of growth environment of the reactor (e.g. cleanliness, particle formation etc.) and its influence on the crystal growth were not addressed or discussed adequately (e.g. particulates on the epi and consecutive morphological defects etc.) in the literature. The requirement for achieving high growth rate is that precursor flow should also be increased to increase mass transport at the growth surface. At this high growth rate condition, high amount of parasitic deposition (especially Si parasitic deposition) also takes place in the reactor. The detail of these parasitic depositions was presented in ICSCRM 2011 conference by the authors' group (Rana, Song, et al., 2012a, 2012b). These depositions does not only degrade the epilayer but also cause frequent replacement of the expensive reactor parts and increase the cost of the growth counteracting one of the primary goal of achieving high growth rate.

Despite numerous reports of high growth rates (>100um/hr) - high voltage, reliable devices are still a challenge for commercial applications mainly due to unavailability of high quality thick epilayers in the current market. It can be found that, for commercial production a growth rate of only 20µm/hr is typical (Burk et al., 2012). Standard thickness for 3" and 4" epilayers as published in (www.cree.com) is still 50µm (Table 5.1) with exorbitant cost indicating the underlying difficulties in achieving thick epilayers (>100um). Hence, despite reports of thick epitaxy presented in the existing literatures, we believe that the need for finding a new gas chemistry to improve the CVD epitaxy has not been diminished yet.

Table 5.1 Current commercial specification of 3" and 4" diameter wafers

	Epi Thickness	**Tolerance**	**Epi Doping**		**Tolerance**	**Epi defects (Carrot, Particles, TD etc)**
			n type	**p-type**		
Si face	0.2-50um	10%	9E14-1E19	9E14-1E19	25%	25/cm2
C Face	0.2-10um	15%-25%	1E16-1E19		50%	

As a novel gas for SiC epitaxy, it is important to study the growth using SiF_4 on various off cut substrates. It is well known that the surface morphology improves for higher off cut substrates. Ideally the growth should take place at the kinks to preserve the polytype. Longer terrace width for lower off cut substrates is not preferable since longer terrace width of a substrate also indicates lower kink density, which will reduce the density of nucleation sites rendering lower growth rates. Also the probability of 3C formation on the terrace is higher. The details of off cut and its effect on growth rate and crystal quality were discussed in detail in Chapter 1. In recent days more attention has been paid to improve the epitaxy on lower off cut substrates especially on 4° off cut or even lower tending to on-axis substrates. The advantage of using lower off cut substrates is that they inherently suppresses BPD propagation as well as reduce the material wastage unlike associated with higher off cut substrates. The suppression of BPD propagation and material wastage using lower off cut substrates were discussed in detail in Chapter 1.

Effect of C/Si ratio on doping and surface morphology was studied by various groups for silane gas (W. Chen & Capano, 2005; Fujiwaraa, Dannoa, Kimotoa, Tojob, & Matsunami, 2005; Larkin et al., 1994). In the previous chapter we discussed the first homoepitaxial growth of SiC using novel tetrafluorosilane (SiF_4) gas. To utilize the growth using SiF_4 it is needed to study the growth in further details for C/Si ratio versus doping, growth rates, surface morphology and crystal quality. Here in this chapter we will provide the detailed experimental results of the epitaxial growths using tetrafluorosilane to discuss relation of C/Si ratios versus doping, dependence of growth rates on C/Si ratio and the surface morphology of epilayers grown on various off cut substrates.

The growths described in this chapter were conducted in a vertical hotwall CVD described in previous chapters. Tetrafluorosilane gas was used as a Si precursor whereas propane is used as the C precursor. SiF_4 flow rate was kept fixed at 10 sccm and the C/Si ratio was varied by changing the propane flow rate. Hydrogen gas was used as the carrier gas and the H_2 flow rate was fixed at 12 slm for all the growths. Growth pressure was fixed at 150 Torr and the temperature was fixed at 1600°C. Veeco Nanoscope III atomic force microscope is used for the AFM images. Mercury probe CV analyzer was used to measure the net doping concentration of the samples. Fourier transform infrared spectroscopy (FTIR) was used to measure the thickness of the epilayers.

5.2 RESULTS AND DISCUSSION

5.2.1 C/Si VERSUS DOPING

For the growth of compound semiconductor materials, when two or more precursor gases are used (e.g. C source and Si source gases for SiC epitaxy), the ratio of these gases

are extremely important since it defines the doping concentration and also influences surface morphology of the epilayers (e.g. step bunching, growth pits, carrot, triangular defects etc.). Effect of C/Si ratio on the doping concentration is described in (Larkin et al., 1994). It is well known that for the SiC growth, the n-type dopant (N) occupies C sites and the p-type dopant (B) occupies the Si sites. When there is a higher amount of Si present than C, there will be relatively more vacancy of the C sites present during the crystal growth. As a result, at lower C/Si ratios, with greater C vacancy sites, nitrogen has more probability of being incorporated in the crystal rendering higher n-type doping. On the other hand, at higher C/Si ratios or Si deficient condition, more Si sites will be available for p-type dopants to be incorporated in the crystal and more p-type doping is expected. Higher n-type doping was observed for lower C/Si ratios and higher p-type doping was observed for higher C/Si ratios as per the well-known site competition rule (Larkin et al., 1994) (Figure 5.1). Polarity crossing was observed at a C/Si ratio of around ~0.9. C/Si ratio of 0.8- 1.0 was found to be in the low doped region (this range is more apparent from Figure 5.2).

One of the most interesting aspects of using SiF_4 gas for the growth was its C/Si versus doping relation. The doping concentration of epilayers grown using SiF_4 is comparatively more insensitive to the variation of C/Si ratios compared to conventional Si precursors. A comparison is provided for the doping concentration versus C/Si ratio graph for DCS and SiF_4 mediated growths in Figure 5.2.

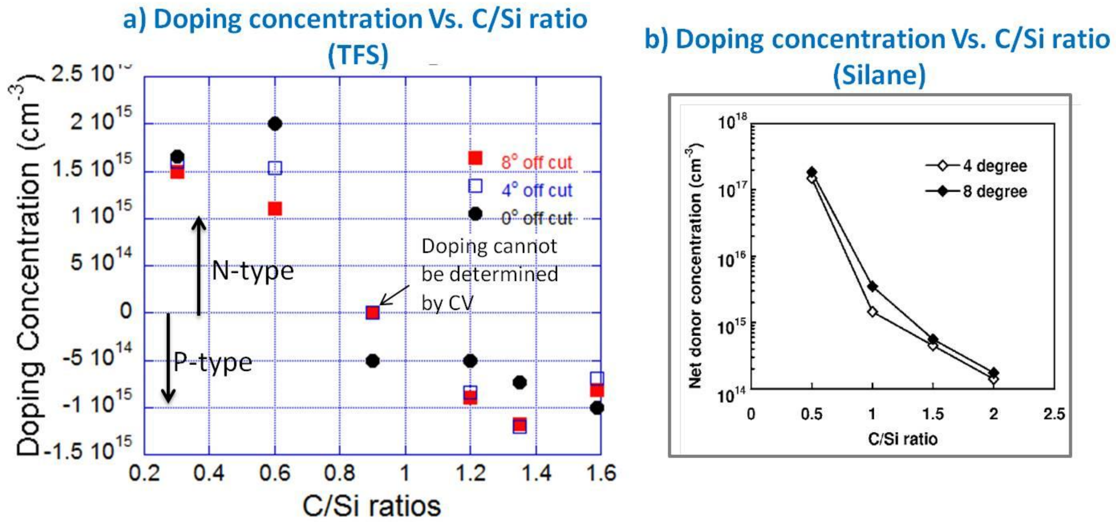

Figure 5.1a) C/Si ratio versus doping graph for various off cut substrates using SiF_4 and C_3H_8 as precursor gases; b) Doping concentration versus C/Si ratio for various off cut substrates using silane.

No obvious off cut dependency was observed for the doping at various C/Si ratios in our experiments. This is in contradiction to previously reported results using silane gas (W. Chen & Capano, 2005; Forsberg et al., 2002; Yamamoto, Kimito, & Matsunami, 1998). This off cut independent doping found for TFS will be explained later.

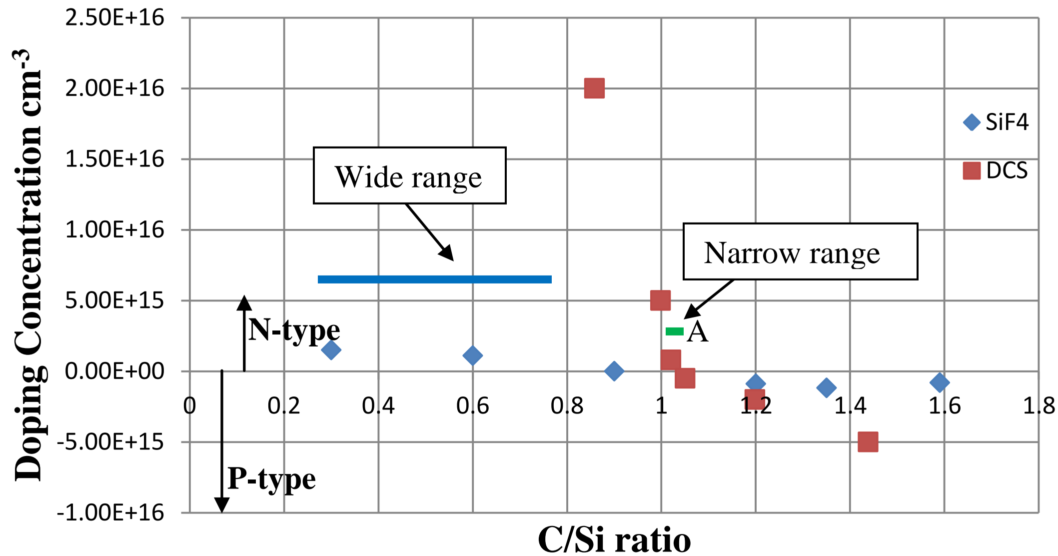

Figure 5.2 Comparison of C/Si ratio vs. doping for SiF_4 and DCS showing the doping change is less affected for SiF_4 compared to DCS (8° off cut).

Table 5.2 : Metric for doping $\Delta N = N_D - (-N_A) = N_D + N_A$ of epilayer using various gases.

Gas	Range of C/Si ratio	$\Delta N = N_D + N_A$	Reference
Silane	0.8 - 1.25	5×10^{16}	(R.L. Myers et al., 2005)
DCS	0.8 - 1.25	6×10^{15}	(Iftekher et al., 2011)
DCS	0.8 - 1.25	2×10^{16}	Reported in this dissertation
TFS	0.8 - 1.25	2×10^{15}	Reported in this dissertation

A significantly higher variation of doping (2×10^{16} n to 5×10^{15} p) was observed for C/Si ratio ranging ~0.8 to 1.4 for DCS. Similar sharp change of doping is also found for the growth using silane reported in (R.L. Myers et al., 2005) and using DCS reported in (Iftekher et al., 2011). On the other hand, variation of doping concentration due to the change of C/Si ratios are much flatter for SiF_4 compared to the curve found using DCS (Figure 5.2). Figure 5.2 indicates SiF_4 has a much larger window of C/Si ratios to achieve lower doped samples. Here we propose a metric for the C/Si variation versus doping concentrations found for different Si gas precursors Table 5.2, which might be useful to know the C/Si ratio sensitivity of doping concentration using various gases. For the similar C/Si ratios for various silicon precursors it can be found from Table 5.2 that SiF_4 has the lesser variation of doping changes.

The donor and acceptor impurities in Si epitaxy are also commonly used as donor and acceptor impurity atoms in SiC. Calculations performed by Chadi (Emtsev et al., 2009) demonstrated that substitutional F, Cl and Br behave like shallow single donors in Si crystal. On the other hand, due to their strong electro-negativity, these VII elements can also behave like acceptors when they are tetrahedral interstitials. However, only F

can be stable in interstitials due to their smaller size (Emtsev et al., 2009) and hence F will have more tendency to behave like an acceptor unlike Cl. It was reported that Cl implantation turns p-type Si into n-type semiconductor(Daas et al., 2012) proving Cl to be a n-dopant in Si(Emtsev et al., 2009). Experimentally, Cl found to be a more efficient n-type dopant than the F(J. A. Robinson et al., 2009).

Substitutional Cl (Cl_{Si} or Cl_C) was also reported be like a n-type dopant in SiC crystal (Oshima & Nagashima, 1997) as reported for Si (Emtsev et al., 2009). F incorporation in SiC has not been investigated yet. However, for SiC, the atomic arrangement is more closely packed (HCP) than cubic Si and hence Cl or F incorporation can be assumed to be considerably less for SiC. A detailed SIMS analysis is required to quantitatively analysis to investigate F incorporation (if any) in the epilayers grown using SiF_4.

The most expected application of SiC is high power devices, where high voltage (>10kV) is needed to be blocked at reverse bias. Breakdown voltage is related to critical electric field (or breakdown electric field) and doping concentration by the following formula.

$$V_B = \frac{\in_S E_{crit}^2}{2qN} - \phi_{bi} \qquad (5.1)$$

From the above equation it can be found that while $\in_S$ (relative permittivity), E_{crit} , ϕ_{bi} (barrier potential) and q are fixed, higher breakdown voltage can be achieved only by reducing the doping concentration. Hence, for high voltage applications (i.e. the primary goal of SiC), low doped sample is essential and hence convenience of growing low doped epitaxy using SiF_4 due to the larger window (Figure 5.2), is an advantage to meet the primary objective of SiC material.

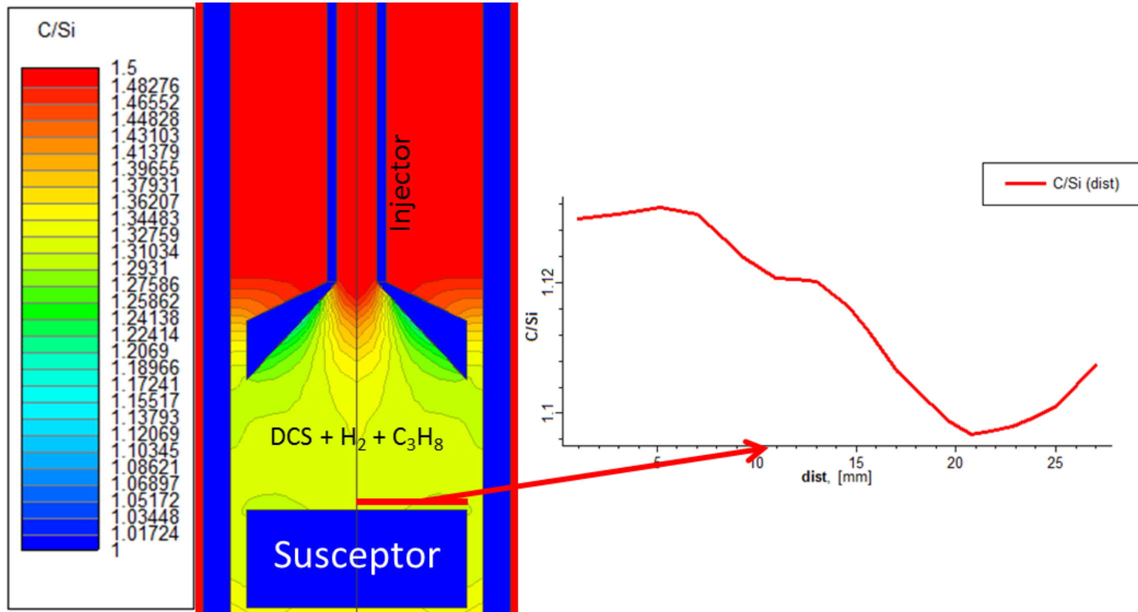

Figure 5.3 C/Si ratio distribution in the reactor (2D analysis) and distance versus C/Si ratio plot of the susceptor surface.

For the commercial production it is essential to grow multiple large diameter wafers in a single run to reduce manufacturing cost while maintaining doping uniformity. Current substrate technology is tending to 6” in diameter. While for silicon epitaxy main parameter to control the doping uniformity is the N_2 flow rates (flux uniformity over the substrate), on the other hand, during the silicon carbide epitaxial growth, both N_2 flux uniformity and the uniformity of C/Si on the surface area have to be precisely controlled. It was found using the virtual reactor simulation described in Chapter-2 that C/Si ratio varies over the surface of substrates depending on gas flow dynamics, temperature, pressure etc as shown in Fig. 5.3. While it is much easier to get doping uniformity on a smaller sample (usually 8mm x 8mm) placing it at the center of the susceptor where the flux concentration does not change very much, it is extremely difficult to maintain the same C/Si ratio for large diameter substrates. In modern SiC CVD system, it is needed to

grow multiple (6 or more) 150mm diameter substrates (Burk et al., 2012) where the geometry of the reactor and the gas flow dynamics are much more complex. Presumably, maintaining the uniformity of C/Si ratio and the doping will be much more difficult in those complex large diameter multi substrate systems. In Figure 5.2, there is a sharp change of doping from as C/Si ratio changes from 1.05 to ~1 in epitaxial growth using DCS. For this change of C/Si ratio of only 0.05 (from 1.05 to 1), the doping changes from ~5 x 10^{14} to $5x10^{15}$ cm^{-3} (shown by a green line- A in Figure 5.2). As an example, to achieve a doping of $1x10^{15}$ which is very typical for SiC epitaxy for high voltage applications, the C/Si ratio has to be very precisely controlled at 1.03 with a very high tolerance. This is extremely difficult due to non-idealities and run to run variations for flow rates, pressure, temperature etc. However, in epitaxial growth using TFS, since doping concentration is much insensitive to the variation of the C/Si ratio for a large range (e.g., the doping concentration will remain near to $1.0x10^{15}$ cm^{-3} (n-type) in the C/Si ratio range of 0.3 to 0.7 as shown in blue line in Figure 5.2), there will not be significant change of doping for the growth using SiF_4 compared to that of using DCS. From preliminary results, doping concentration was found varied considerably using DCS when samples were placed at the center and at the edge on the large diameter (55cm) susceptor because of the large variation of C/Si ratio over the substrate surface as shown in Fig. 5.3 and the high sensitivity of doping concentration versus C/Si ratio in epigrowth using DCS. On the contrary, when SiF_4 was used, variation of doping concentration was found to be considerably smaller compared to than that of DCS because in epigrowth using TFS, the doping concentration is much insensitive to the variation of the C/Si ratio. Larger variation was also observed for the growths using

silane. Hence we state that using SiF_4 significant improvement on doping uniformity over large diameter, multiple substrates can be achieved over silane and dichlorosilane gases even under the non-ideal condition leading to slight variation of C/Si ratios. We believe this will be very useful for commercial production with doping uniformity over the large substrates. A detailed study is necessary to investigate further to understand this behavior of doping concentration found using SiF_4.

5.2.2 C/SI VERSUS GROWTH RATES

Growth rate of SiC is strongly related to the C/Si ratios during the growth. When one element of SiC is abundant, the growth will be controlled by the amount of another and vice versa. When SiF_4 flow rate was fixed and C flow rate was increased, growth rate increases almost linearly up to a C/Si ratio of 1.6 as shown in Fig. 5.4. Growth rate saturates above a C/Si ratio of 1.6 and does not increase further and the C rich condition is reached. Similar behavior was also reported previously (W. Chen & Capano, 2005) for the growth using silane. Using halogenated gases, Si loss due to gas phase nucleation is suppressed (unlike silane) and the growth rate becomes C-supply dependent even at a higher flow rate of Si precursor. For the case of silane, higher flow rates of silane precursor will result in supersaturation and Si gas phase nucleation and growth rate cannot be increased further by the increase of C-precursor flow rate due to Si deficiency. Ideally, in C-supply dependent growth, the growth rate is increased as C-precursor flow rate is increased as the Si-source can be kept 'adequate' due to the suppression of Si-supersaturation. For growth in the C/Si range of 0.2~1.6, the growth rate was observed to be C-supply dependent (Figure 5.4) for TFS similar to a previous report using DCS[27]. However in SiC growth using silane, the growth rate becomes Si limited for C/Si >

0.4(Kimoto, Tamura, Chen, Fujihira, & Matsunami, 2001), > 0.7(R.L. Myers et al., 2005), or >1(W. Chen & Capano, 2005).

Off cut dependency on growth rates are discussed in details by (Matsunami & Kimoto, 1997). It is well known that, for homoepitaxy, the growth has to take place at kinks (discussed in details in Chapter-1). A higher off cut will render a higher growth rate due to higher density of kinks or nucleation sites. In our experimental results shown in Fig. 5.4, off cut independent growth rate was found.

Off cut independent growth rates and doping found using TFS needs further detailed study in future to explain. However, we speculate the following to explain the off cut independent growth and doping presented in this chapter.

As per the step controlled epitaxy (Matsunami & Kimoto, 1997), the growth rate can be found using following formula

$$R = v_{step}\tan\theta = \frac{2h\lambda_s}{n_0\lambda_0}\left(J - \frac{n_{s0}}{\tau_s}\right)\tanh\left(\frac{\lambda_0}{2\lambda_s}\right) \qquad (5.2)$$

Where v_{step} = step flow velocity

$\tan\theta = \frac{h}{\lambda_0}$, Where h = step height and λ_0 = terrace length

n_s = adatom concentration on surface

λ_s = average length for adsorbed species to migrate on a 'step free' surface before desorption.

τ_s = mean resident time of adsorbed species.

According to this formula, if step velocity at the kink is same for different off cuts, growth on 8° off cut should be double than that of 4° off cut substrates. However, comparable growth rates for different off cuts were found for the epilayers using TFS. This weak off cut dependency of growth rates can be explained only if step velocity

(v_{step}) is higher for lower off cut substrates. However, as equation (5.2) suggests, for epitaxial growth governed by the surface diffusion of adatoms along the terrace, v_{step} will always be dependent on the terrace width, and hence the offcut angle. A derivative of the growth rate, R with respect to the terrace width shows that the dependence vanishes only if $\lambda_o >> \lambda_s$, which refers to a desorption-limited growth regime. Hence, we can deduce

1. For the TFS, the step velocity is not determined by the rate of surface diffusion, which has to be the same for all off cut angles. Rather, the growth takes place in a desorption-limited regime for all off cut angles, where the surface diffusion length of the adatoms are very small and only the adatoms formed near the step edge will participate in reaction. The higher level of desorption for TFS-based growth can be explained by the higher strength of Si-F bond compared to the other Si-X bonds (e.g., for DCS-based growth) or Si-H bond (for silane).
2. Because of the absence of lateral diffusion, the growth at the step edge (or kinks) proceeds at a near-equilibrium rate, which varies with the concentration of the available reactant species. Since the density of step kinks for a higher off cut surface is more than that for a lower off cut surface, for the same adatom flux, the concentration of the reactant species at the step edges will be more for lower off cut growth surface. The step velocity will then reflect this variation of reaction rate, and will be higher for lower off cut surface, compensating for the $\tan\theta$ term in equation (5.2). As a result, the overall growth rate will be independent of off cut angle.

3. The weak dependence of the doping levels on the off cut angles can also be explained by invoking the equilibrium reaction argument, where growth rate determines the doping concentration of the epilayer.

For the case of ~0° off cut (~0.5° miscut) substrates in Figure 5.4, homoepitaxial growth only took place at a C/Si ratio of 0.3 for the C/Si ratios used in the experiment. Growths found above C/Si ratios of 0.3 were mostly 3C type growth confirmed by Raman Spectroscopy (Harima, Nakashima, & Uemura, 1995; Nakashima & Harima, 1997) and discussed in the next section.

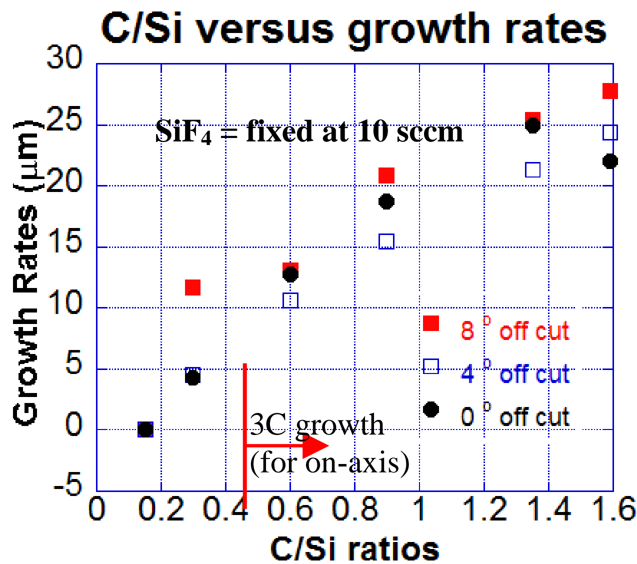

Figure 5.4 C/Si versus growth rate for various off cut substrates (3C growth is found above a C/Si ratio of 0.3 for on-axis substrates.

5.2.3 RAMAN ANALYSIS FOR POLYTYPE UNIFORMITY

The ratio of the 4H peak (E_2, transverse optic or TO mode at 776 cm-1) and 3C peak (E_1, transverse optic or TO mode at 796cm-1) provides indication of the polytypes present in the silicon carbide crystal (Harima et al., 1995; Iftekher et al., 2011; Rana,

Chandrashekhar, et al., 2012). If the 4H/3C peak ratio is higher, then it indicates lower formation of 3C which is desired for 4H-SiC epitaxial growth. No clear indication of influence of C/Si ratios on polytype uniformity (4H/3C) was found (will be presented later) for 8° and 4° off cuts. On, the other hand, for ~0° off cut substrate, step flow growth was only observed at a C/Si ratio of 0.3.

It is expected that 3C growth should be higher for lower off cut substrates since longer terrace in lower off cut substrates has the greater possibility to nucleate 3C during growth. In the SiC crystal, (0001) plane on the terrace is equivalent to (111) plane of cubic structure (Konstantinov et al., 1997) and hence terrace has higher probability of 3C formation during growth. However, contrarily, it was found from the Raman analysis that on average, 3C inclusion was higher for 8° off cut substrates compared to that of found for 4° off cut substrates (Figure 5.6). The maximum 4H/3C peak ratio was found for 8° substrate was 76 whereas the maximum ratio for 4° off cut substrates were higher (97) indicating improved homoepitaxy for lower off cut substrates. It was found that, 3C inclusion is lower even for epigrowth on ~0° off cut substrate compared to that of 8°- only when the growth was step flow mediated (Figure 5.7). We will try to explain this behavior in the following briefly.

In Chapter 4 we have shown that SiF_4 is a strong etchant of SiC substrate whereas propane mitigates the etching. A higher etching condition will result in increased etching and suppression of 3C nucleation on the longer terraces of lower off cut substrates. However, the reason for improved polytype uniformity (lower 3C) for the epilayers grown on 4° off cut substrates still cannot be explained by considering only the increased etching effect using TFS. If etching effect is taken account, then 3C on the terrace of both

4° and 8° growths should be suppressed and the polytype uniformity during growth should be comparable for both off cuts.

This higher polytype uniformity for the epilayers grown on lower off cut substrates (when step flow is present) is still need to be further studied for explanation. Here we speculate two possible reasons. In Chapter 1 we discussed how higher amount of BPDs intersect the surface for higher off cut substrate. Higher density of BPD intersects the substrate surface for 8° off cut compared to lower off cut substrates. Defects are the disorder in the crystal where polytype stacking sequence will be distorted. When the stacking sequences at the kinks are distorted, the polytype template present at the kinks for polytype replication for homoepitaxial growth is hampered (see Chapter 1 for the concept of polytype template). For a substrate with higher density of disorders (defects), more stacking disruption (see Chapter 1 for the concept of template mediated or step controlled growth). At these defects sites (with stacking disruption), when ad-atoms arrives, what polytype it may form is a question. 3C growth is more favorable to grow (energetically; growth takes place at lower temperatures, lower activation energy). When no good template is present (disrupted polytype stack sequence due to the defects), 3C formation may be more favorable, nucleating from the distorted stacking at the defect points.

In another speculation, we propose that due to the increased density of kinks for higher off cut substrates, when steps will flow (from the kinks), for 8° off cut, the step higher off cut substrates will have higher number of kinks present which will also have more 3C stackings for replication. Hence we propose that when step flow is ensured (with terrace nucleation is prevented) then polytype uniformity will be improved for

lower off cut substrates due to lower higher number of 3C presents due to higher number of kinks.

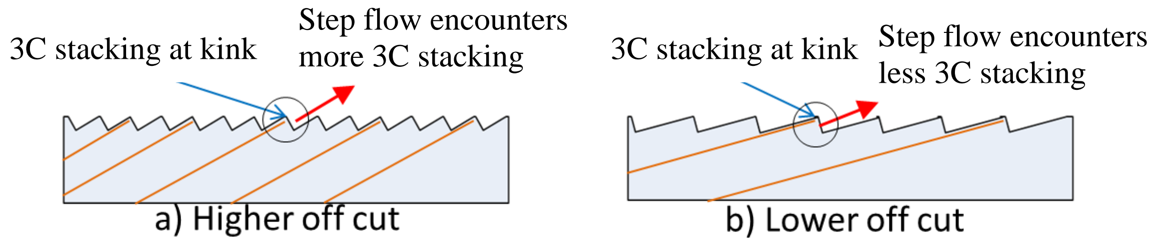

Figure 5.5 Increased 3C at the steps is shown due to the higher off cut substrates (a) compared to the lower off cut substrates (b) and considered to be the reason for lower 4H/3C for higher off cut substrates.

Though, ideally, no steps should be present for °0 off cut substrates, the off cut is not perfect (0.5° - 1°) in practice and steps are present on the surface. For the case of ~0 degree off cut substrates, a high 4H/3C ratio of 97 was observed only when step flow growth (2D) took place at only a low C/Si ratio of 0.3. At higher C/Si ratios, the step flow growth is lost and the growth was dominant by 3C growth (Figure 5.6 and Figure 5.7). Obviously, since the terrace width for vicinal on axis substrates much longer (~hundreds of nanometers) compared to 4° and 8° off cuts, 3C has much higher probability to nucleate on on-axis substrates. Due to this longer terrace condition, step flow will also take longer time to cross the terrace. At this condition where growth (3C) starts taking place on the terrace in higher amount due longer terrace length, the etch rate during the growth also has to be higher compared to higher 8° and 4° off cut substrates to keep the terrace free from 3C growth. This higher etching condition is only present at C/Si ratio of 0.3 or below in our case. However, as propane flow is increased, the etch rate is reduced (propane mitigates etching as discussed in Chapter 4). Further, the growth rate is also increased at a higher C/Si ratio due to increased availability of C species. So, as a

consequence, terrace nucleated 3C growth increases rapidly even for an increase of C/Si ratio of 0.3 to 0.6 due to the combined effect of reduced etching and increased 3C growth rate; as a result 4H/3C ratio (found from the Raman spectrum) is reduced dramatically from 97 to 0.5 (Figure 5.6 and Figure 5.7).

Finally, the effect of surface preparation has also to be considered to explain polytype uniformities related to different off cut substrates. It is to be noted that surface preparation prior to the growth (mainly by H_2 etching) determines the epilayer quality and greatly depends on the off cut of the substrates.

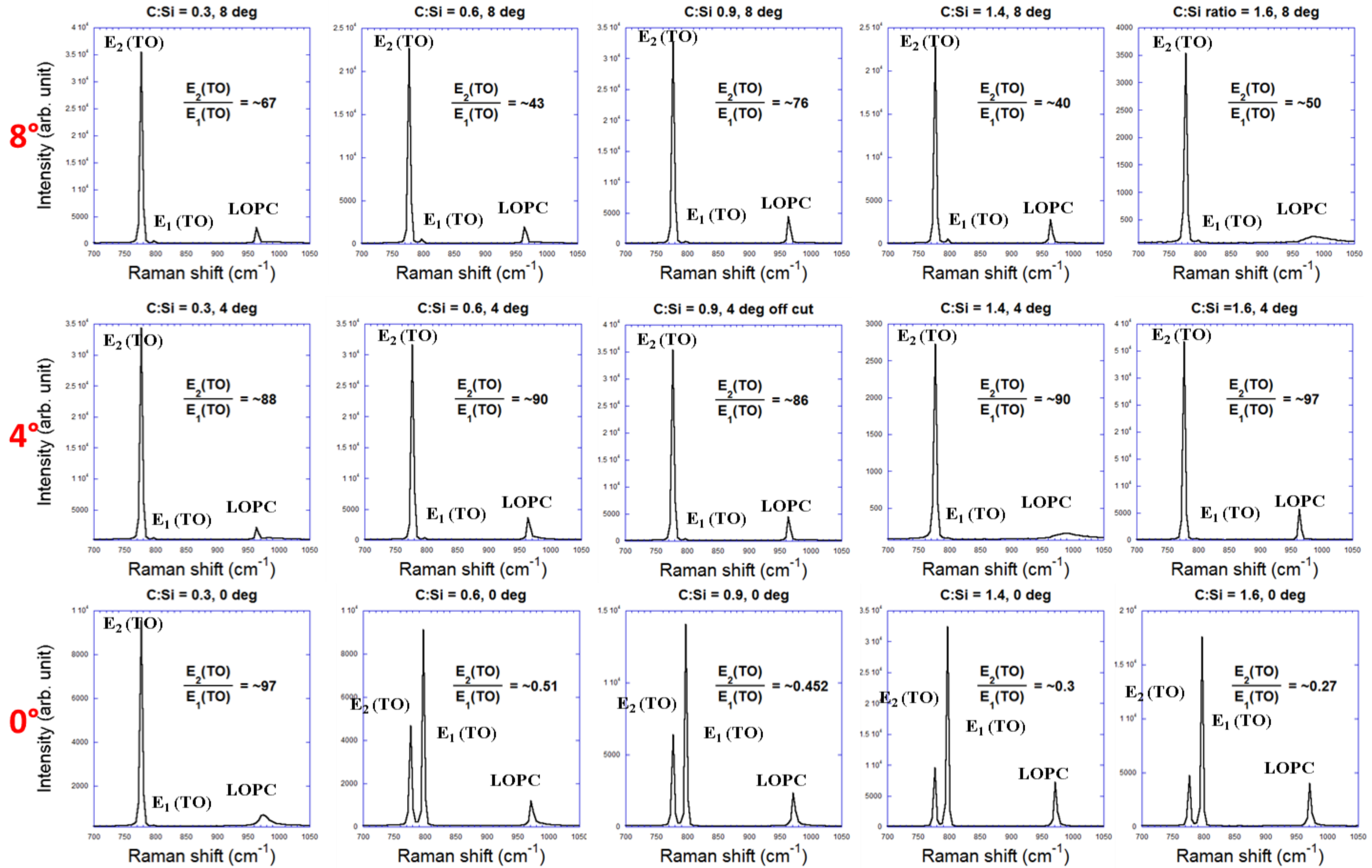

Figure 5.6 Raman analysis of various epilayers with different off cuts at different C/Si ratios

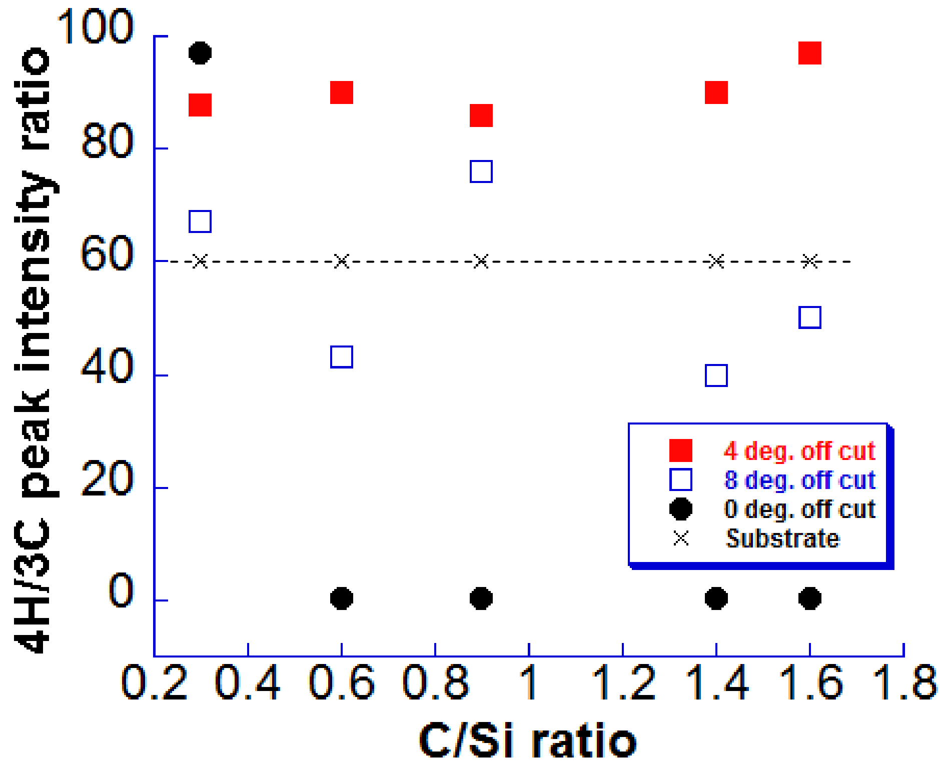

Figure 5.7 Bar graph showing the 4H/3C peak ratios found at various C/Si ratios for various off cut substrates. 4H/3C of the substrates (for all of cuts) are shown by dashed line.

In a Raman spectrum for SiC crystals, sharper and increased height of longitudinal optical phonon-plasmon coupled (LOPC) mode peak at ~964 cm^{-1} is the indication of lower doping concentration (Harima et al., 1995; Rana, Chandrashekhar, et al., 2012). From Figure 5.6, it can be found that for any off cut, LOPC mode peak became sharper and taller at higher C/Si ratios. LOPC peak denotes total impurity incorporation (N_D + N_A) rather than the net doping of the material ($N_D - N_A$). From Figure 5.6, observing the LOPC peaks, it can be seen that at higher C/Si ratio, though the epilayers became higher p-type (Figure 5.1) but the total impurity concentration (N_D + N_A) is decreased. Since nitrogen is more abundant (residual from atmosphere) compared to the p-type dopants (B or Al), we infer that the variation (increment or decrement) of nitrogen doping

concentration for various C/Si ratios is more significant than the variation of p-type dopant (B / Al). Hence, we postulate that as C/Si is increased, the (N_A-N_D) or net p-type doping concentration increases but (N_A+N_D) or overall impurity decreases. A detailed SIMS study is required to confirm the Raman data analysis for dopant shown in Figure 5.6.

5.3 C/Si VS. SURFACE MORPHOLOGY

5.3.1 (8°) OFF CUT

No correlation with C/Si ratio was observed (by AFM) for the surface morphologies of epilayer growths on 8° off cut substrates (Figure 5.8). Usually, step bunching is not occurred in epigrowth on 8° off cut substrates. However, surface morphology was found to be strongly influenced by the C/Si ratio for the lower off cut (4° and ~0° off cut substrates) as discussed in the next section.

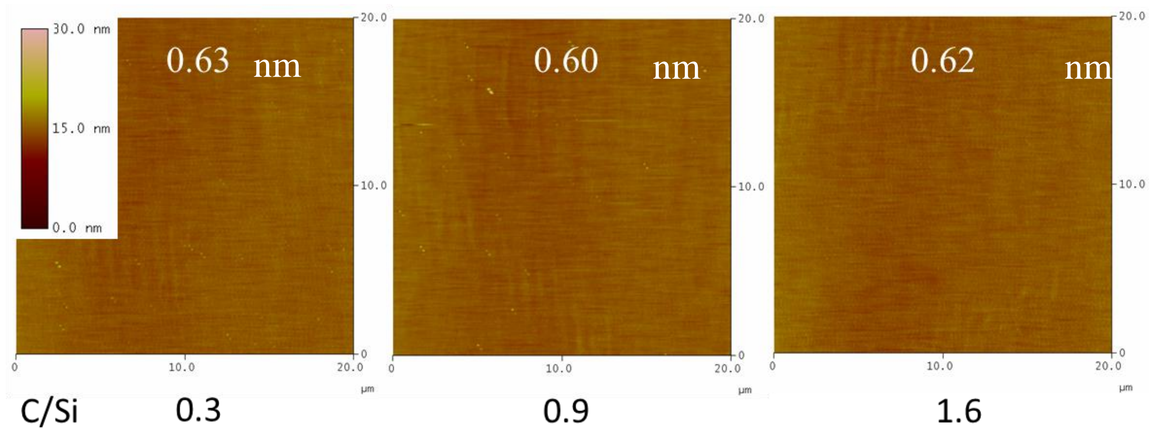

Figure 5.8 AFM study of epilayers grown on 8° off cut substrates at various C/Si ratios showing no strong correlation. Roughness (r.m.s) is shown in nm.

5.3.2. (4°) OFF CUT

Unlike the 8° off cut substrates, 4° showed some interesting morphological features in the AFM images with varying C/Si ratio. Before we proceed further, we discuss the concept of macro and micro steps (Figure 5.9).

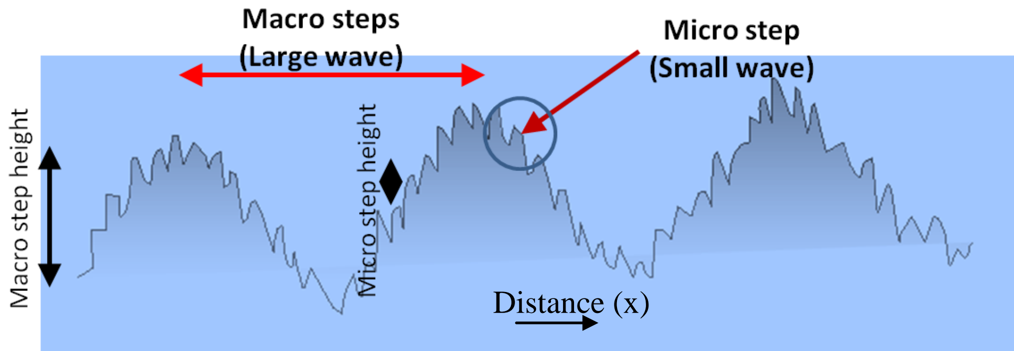

Figure 5.9 Graphical illustration of macro and micro steps.

Micro steps are essentially related to the steps created due to the off cut of the wafers. The height of these micro steps is ~1nm for 4H SiC which is the height of the 4H-SiC unit cell (see Chapter 1 for details for off cuts and related step geometry). On the other hand, macrosteps are generated due to step flows with different speeds, where steps coalesce or merge to each other rendering a larger step with a height of multiple microsteps in the range of ~5nm or above, which is called step bunching. Micro and macro steps are illustrated graphically in Figure 5.9. Macro steps are strongly related to growth conditions (e.g. C/Si ratio).

Figure 5.10 shows the AFM study of the epilayer surfaces found for different C/Si ratios. 1D analysis of the micro and macro steps of the epilayer formed at various C/Si ratios are presented in Figure 5.11. It can be seen in Figure 5.11 that both step height (amplitude) and step density (per unit length) of microsteps and macrosteps vary as a

function of C/Si ratios. It is observed that as the C/Si ratio is increased from 0.3 to 0.9, the macro step density reduces (Figure 5.10, Figure 5.11 and Table 2). The amplitude of these macrosteps is maximum (10nm) at the C/Si ratio of 0.9 (Figure 5.10 and 5.11). When C/Si ratio is increased further from 0.9 to 1.6, macrostep height is reduced gradually (Table 5.2). At a C/Si ratio of 1.6, the macrostep height is minimum (Figure 5.11). On the other hand micro step density increases when C/Si ratio is varied from 0.9

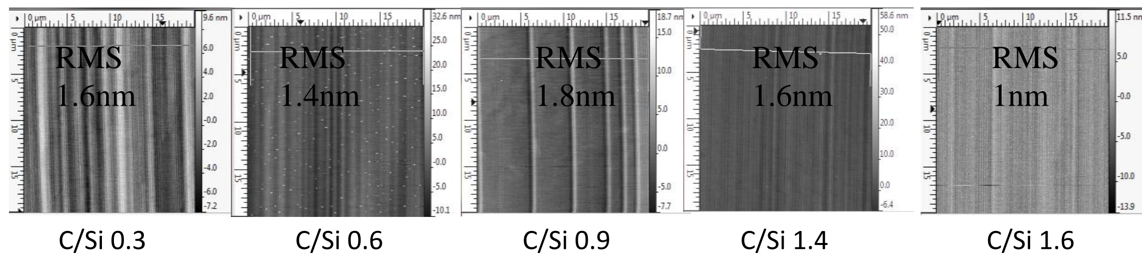

Figure 5.10 AFM images of the epilayer sufaces (4° off cut) for varoius C/Si ratios showing variation of step bunching on the surface. 1D analysis (white line at the top of each images) of these surfaces are shown in Figure 5.8.

Table 5.3 AFM surface analysis of epilayers grown on different off cuts.

C/Si ratio	**0.3**	**0.6**	**0.9**	**1.4**	**1.6**
Step density / 20um	9	17	6	10	13
Step height (nm)	8	5	10	5	4
Roughness	1.6	1.4	1.8	1.6	1

to 1.6. At a C/Si ratio of 1.6 (Table 5.2), even though microstep density increases but the surface roughness reaches minimum. This is due the reduced macrostep height (reduced step bunching) at a C/Si ratio of 1.6 (Figure 5.11). Variation of surface roughness based on the macrostep heights and variation of the roughness based on only the microstep

height for the variation of C/Si ratios are shown in Fig 5.12 (a and b). Microstep heights were found to be close to the unit cell height for all the C/Si ratios. However, macrostep heights were varied strongly with the variation of the C/Si ratios. From the surface study and relation of microsteps and macrosteps to the C/Si ratios (Figure 5.11 and 5.12) it can be understood that surface kinetics on the low off cut sample is extremely complicated and difficult to explain. Similar results are also observed for 4° off cut substrate in. W. Chen et al. (W. Chen & Capano, 2005) put an effort to explain the step bunching behavior of the surface found using 4° off cut substrates as following.

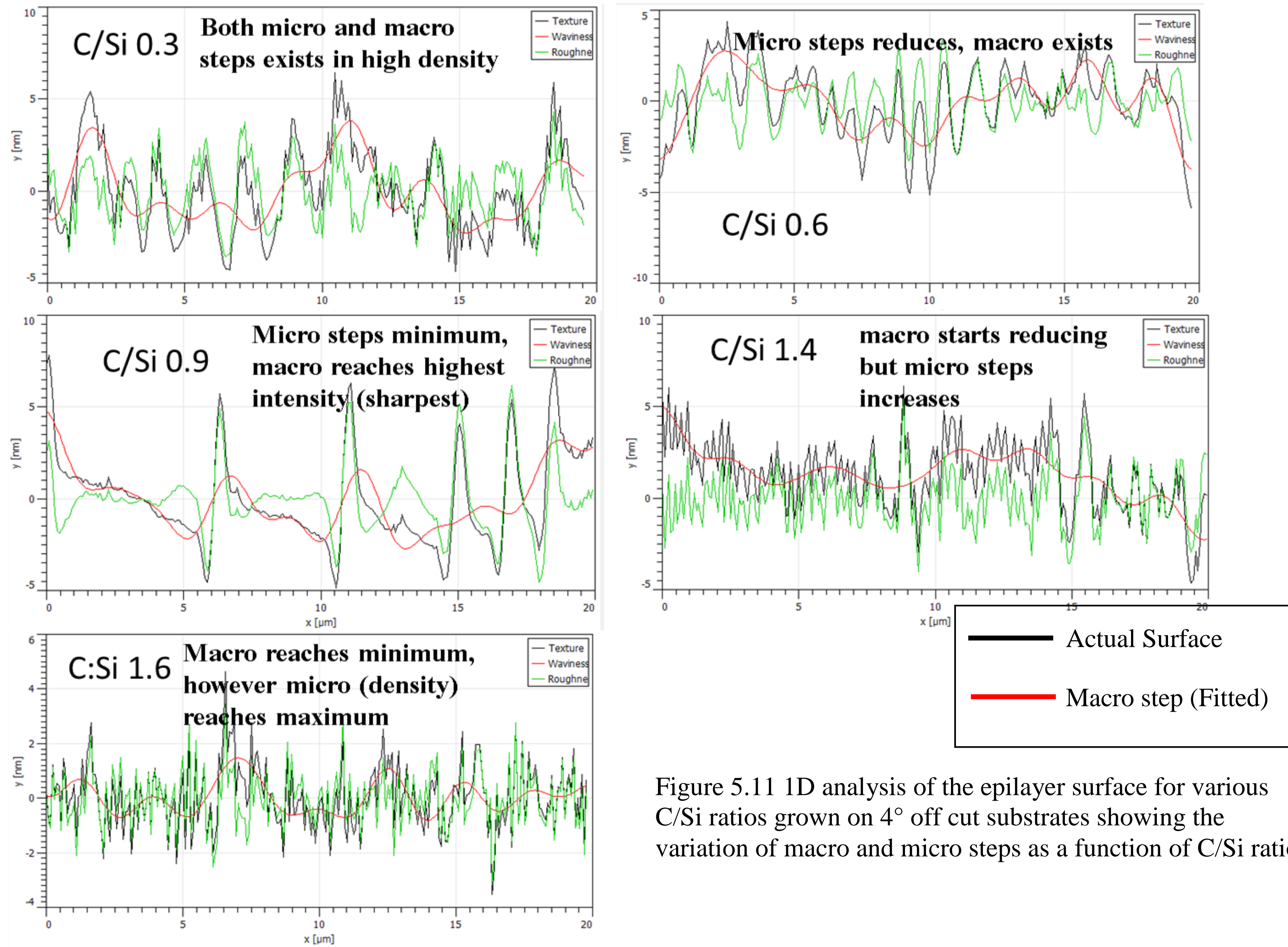

Figure 5.11 1D analysis of the epilayer surface for various C/Si ratios grown on 4° off cut substrates showing the variation of macro and micro steps as a function of C/Si ratios

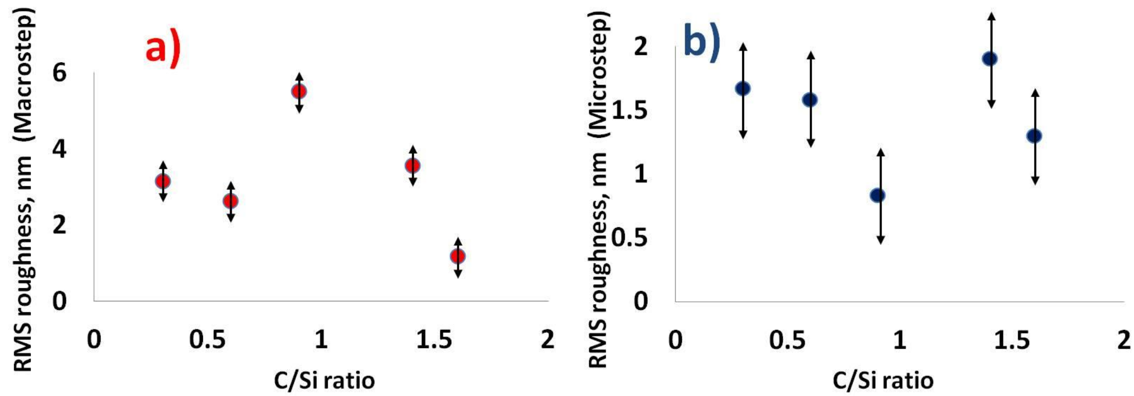

Figure 5.12 a) Roughness measured based on the macrostep peak and troughs (calculated manually) for different C/Si ratios. b) Roughness measured based on the microstep peaks and troughs (calculated manually) for different C/Si ratios. These figures demonstrates that macrostep height is a stronger function of C/Si ratio than the microstep height.

The reason for higher step bunching on lower off cut substrates are discussed in Chapter-4. Step bunching was explained by the Schwoebel effect. Step bunching is a process through which the surface energy is lowered during the growth. The elastic potential between two steps can be found from the equation (Marchenko & Parshin, 1980) as following.

$$U(x) = \frac{2(1-\sigma^2)}{\pi E}(f^2 + \beta a)^2 \frac{1}{x^2} \tag{5.2}$$

Where E = Young's modulus; Σ = Poison's ratio; β = surface tension at steps, a = step height; x = distance from the step. According to Equation 5.2, crystal surface has a varying elastic potential and the surface of a certain off cut substrate has a certain periodic elastic potential on the surface present prior to the growth. This potential changes dynamically during the growth based on various growth conditions (e.g. C/Si ratio) which results in varying step bunching. It was found that when bunched step grows

above a certain height then the step interaction between the macrostep and the microsteps may turn from repulsive to attractive interaction (Kukta, Peralta, & Kouris, 2002) and their dynamics may change during the growth. Hence prediction of step bunching is extremely complex as it varies during growth due to various growth conditions and may take unpredictable form after the growth. Variation of step bunching due to variation of C/Si ratio (Figure 5.7 and 5.8) indicates complex variation of step interactions during growth.

As the discussion in chapter 4, etch rate increases at lower C/Si ratio due to lower concentration of propane. In chapter 4 we have shown that, similar to the growth, step bunching may also occur due to etching. Hence, both etching and growth may influence the step bunching which are strong functions of C/Si ratio. A deeper investigation is required to predict the step dynamics of epitaxy on lower off cut substrates during growth, which might become useful to optimize the process to achieve good epilayer surface on low off cut substrates. It is interesting to see that no step-cross over was observed for these epilayers unlike reported in (W. Chen & Capano, 2005).

5.3.3 GROWTH ON VICINAL ON-AXIS (~0.5° OFF CUT) SUBSTRATES

Growth with polytype uniformity was only achieved at a C/Si ratio of 0.3 with a growth rate of ~4μm/hr. High amount of 3C inclusion was observed above a C/Si ratio of 0.3. The reason of increased 3C growth at higher C/Si ratio was assumed to be due to the combining effect of lower etch rate and higher growth rate at higher C/Si ratios. As shown in Figure 5.13, the growth is step mediated even for ~0° off cut substrates proving that steps are present even for the ~0° off cut substrates used in the experiments. From

the step analysis (terrace width = 140nm and height = 1 nm found from etched sample shown in Chapter 4) the off cut was found to be 0.5°. AFM images of the epilayer (Figure 5.13) shows steps on the epilayer to be parallel to each other. Typically no step crossing was observed for the epilayer grown at C/Si ratio of 0.3. Surface was mirror like for this growth. When the C/Si ratio was increased further, the epilayer surface degraded with faceted structures (Figure 5.13c) and good 4H growth is lost discussed in details earlier

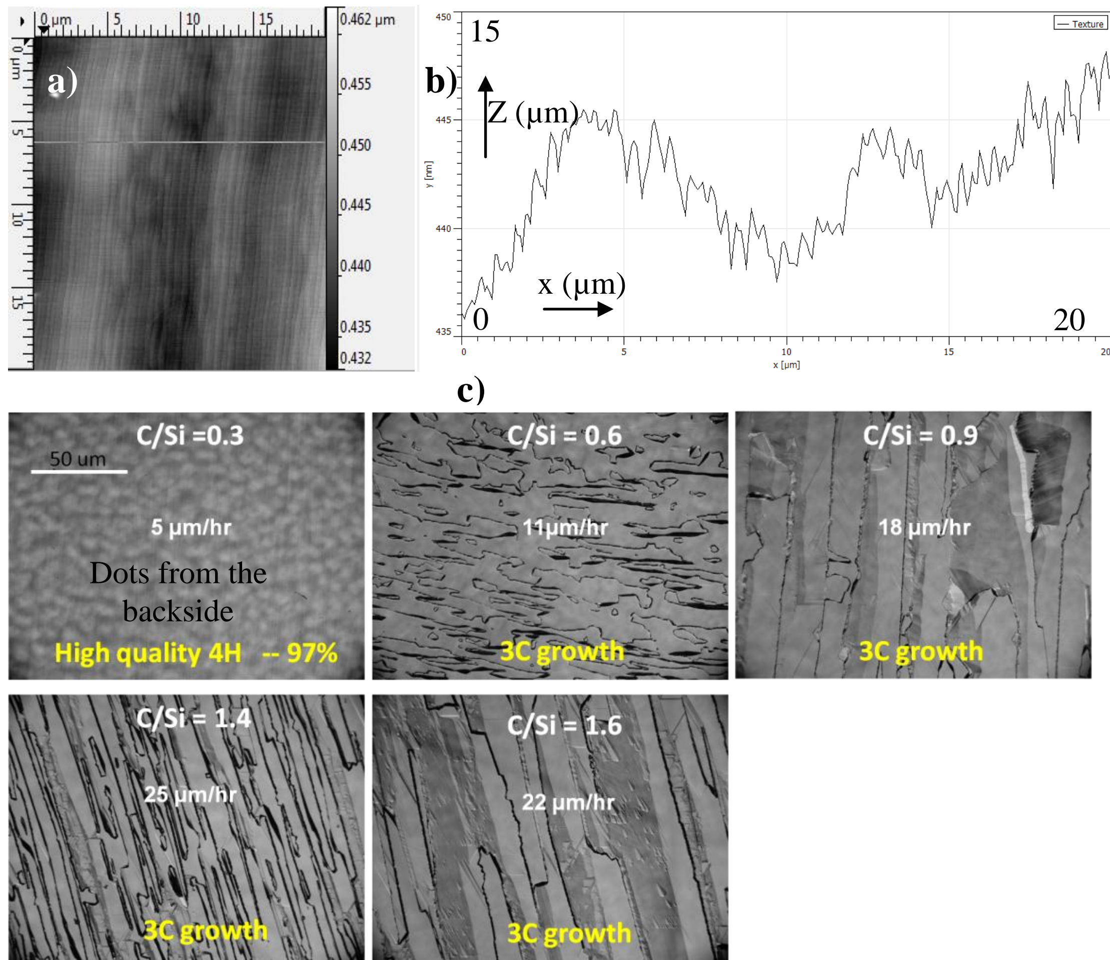

Figure 5.13 (a) AFM images of the epitaxial growth on the vicinal on-axis surface at a C/Si ratio of 0.3. b) 1D scan analysis of the surface along [11$\bar{2}$0]. (b) Nomarski images of the surface at different C/Si ratios.

by Raman analysis. A 4H/3C peak ratio was found to be ~97, indicating remarkably good polytype uniformity for the epilayer grown at a C/Si ratio of 0.3. Surface roughness was

found to be ~3nm (RMS). Macrosteps were observed for these epilayers with step height of 10nm compared to the microstep height of 1nm (Figure 5.13 b).

In summary, in this chapter we have discussed some critical issues of epitaxial growth on various off cut substrates using SiF_4 gas for various C/Si ratios. A very flat doping concentration versus C/Si ratio was found and shown to be an advantage to achieve doping uniformity over a large diameter substrate. Growth rate increases with increasing C/Si ratio (at fixed TFS flow rate) similar to the growth rates found using DCS unlike silane. Improved polytype uniformity was observed for lower off cut substrates (only low C/Si ratio for on axis). We postulate that high etch rate using SiF_4 during growth suppresses 3C nucleation on lower off cut substrates. While no significant variation of surface morphology was observed for the 8° off cut substrates, a complex variation of step bunching was observed for 4° off cut substrates which was due to the effect of both varying etch rates and growth rates at different C/Si ratios. Good epilayer growth on on-axis substrate was shown using SiF_4 gas at a C/Si ratio of 0.3. The polytype uniformity degraded dramatically above a C/Si ratio of 0.3 and assumed due to the combined effect of both reduced etch rates and higher growth rates at higher C/Si ratios.

5.3.4 SELECTION OF THE BEST C/Si RATIO FOR OPTIMUM GROWTH

Selection of the best C/Si ratio should be considered from (1) surface morphology (roughness, step-bunching, waviness, measured by AFM); (2) crystalline quality (XRD) and polytype uniformity (Raman); (3) doping (4) defects control (e.g., C/Si ratio may affect BPD conversion and growth pits generation.); (5) growth rate.

It is very important to select the best C/Si ratio for the growth based on the results presented earlier. For 8° off cut substrates, the main concern is the growth rate since surface morphology is not varied with C/Si ratio significantly. Hence, a C/Si ratio of 1.6 will be preferable for 8° off cut substrates since at this C/Si ratio the growth rate is higher. At higher C/Si ratios, the epilayer is p-type. However, the desired n-type doping can be achieved by adding nitrogen in the reactor.

In the case of 4° off cut substrates, both the surface morphology and growth rates are functions of C/Si ratios (where doping concentration can be adjusted by adding dopant). In general, the step bunching was found higher (with increased surface roughness) at lower C/Si ratios. Lowest surface roughness was achieved at a C/Si ratio of 1.6 (Figure 5.9a) with reduced macrostep height (Figure 5.9b). Raman spectra also demonstrate good polytype uniformity (Figure 5.5). Hence, a C/Si of 1.6 can be considered the optimized C/Si ratio for growth using 4° off cut substrates.

When on-axis (~0°) substrates were used, the choice of selecting C/Si ratio is limited. Step flow growth was found at a low C/Si ratio of 0.3.

We describe here the optimized condition where the doping concentration is ignored. Addition of nitrogen (Al or B for p-type) to achieve a desired doping concentration may require further optimization to achieve the best epitaxial layer.

In summary, in this chapter the detailed study is presented for the epilayer growth using SiF_4 gas. Growth rates, doping concentration, surface morphology etc. in relation to C/Si ratios was discussed. Growth rate was found to be increased at higher C/Si ratios indicating C-dependent growth rate. Doping concentration was found to be less

influenced by the C/Si ratio for SiF_4 than that of found using DCS. We concluded that F behaves as an acceptor in SiC epi growth if incorporated and reduces the n-type doping concentration. Lower doping concentration was easily achievable using SiF_4 over a longer range of C/Si ratios and better uniformity using SiF_4 compared to DCS. Higher polytype uniformity was found for the epilayer grown on lower off cut substrates when step flow growth (2D) took place. Surface morphology improved at higher C/Si ratios for the epilayer grown on 4° off-cut substrates compared to the epi grown on 8° off cut substrates. 4H-SiC growth was observed for ~0° off cut substrates only at a C/Si ratio below 0.3. At higher C/Si ratio (>0.3), 3C growth took place on the epi grown on ~0° substrates. Finally, based on the results presented in this chapter, optimized condition for the growth using SiF_4 was defined.

SUMMARY AND FUTURE PROSPECT

Silicon carbide (SiC) epitaxy is more challenging compared to other common semiconductor epitaxial growths due to the high temperature associated with the SiC growth. In this dissertation we have shown that at this high temperature condition conventional silicon gas precursor gases (e.g. silane and dichlorosilane) decompose very early during its flow towards the substrate. This early decomposition of silicon precursor induces excessive silicon gas phase nucleation in the reactor and generates particulate which eventually soils the epitaxial growth. We have first provided a scientific study of parasitic deposition in this work. In this work, we first proposed tetrafluorosilane gas as a silicon precursor suitable for high temperature SiC epitaxy. We provide evidence through our experimental results that the highest Si-X bond strength (highest dissociation bonding energy) of SiF_4 suppresses silicon gas phase nucleation and parasitic deposition in a best possible way.

Previously fluorosilane was considered not to be “a gas of choice” for SiC epitaxy due to its very strong Si-F bond (Pedersen et al., 2007), though, no research has been conducted previously for fluorosilane gases for SiC homoepitaxy. The Si-F bond in SiF_4 is indeed much stronger than its nearest halosilane bond Si-Cl (565 vs. 381 kJ/mol) in chlorosilanes. However, contrary to previous postulation we proved that, in the presence of propane and at high temperature condition required for SiC epitaxy, in fact

fluorosilane gas is a good choice for high temperature SiC epitaxial growth due to its strongest Si-X bond.

Silicon carbide epitaxial growth using CVD process is about 30 years old. The question arises that “Why SiF_4 was not paid much attention for SiC growth previously?” Historically, SiC epitaxy mainly took silicon CVD technology as the guide for its developments (Pedersen et al., 2011). Silicon industries commonly use chlorosilane gases (e.g. dichlorosilane or DCS) as silicon precursor for Si crystal growth. Fluorosilane gas cannot be used for Si growth since it is a Si etchant. Further for Si epitaxy, high bond strength is not essential since silicon growth temperature is much lower than the silicon carbide growth temperature. Hence, taking silicon CVD as guidance for silicon carbide CVD, fluorosilane gas was mainly left unattended and unexplored for silicon carbide epitaxy. In this research work we first report homoepitaxial growth using fluorosilane gas and provide detailed experimental and theoretical results and thus consummate the research for silicon carbide epitaxy using essential halosilane gases.

During the course if the research it was questioned by the critiques many times that why it is necessary to use a new gas since it is already reported high quality, thick epitaxy using chlorosilane gases exists. It has to be mentioned that despite numerous reports on very high quality thick epitaxy by various reports, commercially, high quality, cost effective thick epilayer is still not available. In existing literatures, no systematic study of parasitic deposition or reactor environment due to the growth were present. Hence despite reports of numerous high quality thick epitaxies, it is not possible to know that if those processes are practical in term of commercial production. In research lab it is fairly acceptable to grow few epilayers and discard the reactor parts heavily deposited

with parasitic materials, since cost is not an important factor for few growth runs. However, for commercial production, it is essential to grow bulk amount of epilayers in the number of millions. These epilayers have to be produced repetitively without increasing the production cost. Ensuring the cleanliness of the reactor parts with reduced parasitic deposition is a big consideration and a critical issue for industrial production, specifically for high temperature SiC CVD. Hence we argue that despite the available reports of high quality silicon carbide epitaxy by using chlorine precursor, the necessity of finding a new precursor gas for high quality epitaxy is not diminished. In this research we included two essential aspect of this novel fluorosilane gas.

-Study of silicon carbide growth using SiF_4

-Study of etching using SiF_4

Unlike other silicon precursor, etching is an essential part of SiF_4 chemistry and it is necessary to consider the etching effect of SiF_4 during the epitaxial growth as well. In this dissertation, we show tetrafluorosilane (SiF_4) to be an efficient SiC etchant of silicon carbide. We explain the silicon removal process from SiC surface during etching by SiF_4 based on the Gibbs free energy (ΔG) calculation of various etching reactions. It is shown that etching of Si from the SiC surface is favorable by SiF_4, whereas, comparably, etching of C by SiF_4 is much unfavorable. Hence SiF_4 selectively etches Si whereas H_2 removes C from surface. This selective etching of Si by SiF_4 may also find interest in future for other applications (e.g. epitaxial graphene growth by a precursor gas, which will be shown soon in a future publication in details) and may open new possibilities for large area, controlled graphene epitaxial growth (Appendix B).

Our research indicates that by using SiF_4- epitaxial growth, etching and even graphene growth is possible by using the same gas- thus gives a new dimension in silicon carbide epitaxy with new opportunities for the simplification of process related steps with a much greater controllability and flexibility for new applications.

In this research we conducted study of SiF_4 precursor for silicon carbide growth and etching. However, still the process needs further development as required for any new technology. Based on the knowledge gained from this research, the following future work is proposed.

STUDY OF THE CHEMICAL ROUTE/REACTION FOR THE GROWTH

The chemical process of silicon carbide growth using SiF_4 is much different than the chemical processes associated with the CVD growth found using chlorosilane gases. We believe that growth surface plays an important role for the decomposition of the gas since too strong Si-F bond does not decompose in the hydrogen gas stream even up to a temperature of 2000°C whereas the growth temperature is around 1600°C. A scientific investigation is required to find the exact chemical route for the growth using SiF_4

DEEPER INVESTIGATION OF FLUORINE INCORPORATION DURING GROWTH

We have performed an XPS (X-ray photo electron spectroscopy) analysis of an epilayer which indicates F incorporation (0.55%) on the surface of the epilayer. However it indicates only the result from the surface which might represent only the contaminated surface. A SIMS (Secondary Ion Mass Spectroscopy) depth profile study is essential to

know the actual F content in the material for various growth conditions (e.g. C/Si ratios, temperatures, pressures etc).

STUDY OF DOPING CONCENTRATION

One of the most important and interesting aspects of the growth using SiF_4 is the relation of doping concentration to C/Si ratio variation as shown and described in Chapter-5. Further investigation is required to know the reason behind the flat graph found for doping concentration vs. C/Si ratio for SiF_4 compared to DCS or silane.

GROWTH ON ON-AXIS SUBSTRATE

We present only preliminary results for on-axis growth in this research. However, detailed study is required for the growth on on-axis substrate using SiF_4 gas.

DEVICE CHARACTERIZATION

Preliminary I-V characteristics for the Schottky diodes fabricated on the epilayer grown using SiF_4 demonstrated improved device performance in terms of the uniformity of the Schottky barrier height over the sample. However, a detailed study is needed to be conducted in future to compare the electrical performance of devices fabricated on epilayer grown on SiF_4 to the epilayer grown using conventional gas for reverse leakage current, forward voltage drop, break down voltage, reliability etc.

Finally, we conclude that, study of a new precursor gas is always beneficial for the CVD growth community since it gives them wider options and more

flexibility to grow epilayers by different methods. We believe our contribution to the silicon carbide community by this research is the introduction of the strongest Si-X bond fluorosilane gas for epitaxial growth of silicon carbide and demonstration of its advantages. The use of fluorosilane gas gives the community to take the SiC growth forward beyond the regime of conventional silicon CVD. Silicon carbide epitaxy is significantly different than silicon epitaxy due to much higher temperature associated with it and has to be handled differently, and different precursor choice may find benefit. We believe the research presented in this dissertation will establish the foundation of the fluorinated precursors for the high temperature SiC epitaxy to take it to the next step for high quality material growth needed for high power, next generation electronics.

REFERENCES

A.A. Burk, J., & Rowland, L. B. (1996). The role of excess silicon and in situ etching on 4H SiC and 6H-SiC epitaxial layer morphology. *Journal of Crystal Growth, 167*, 586.

Bhatnagar, M., & Baliga, B. J. (1993). Comparison of 6H-SiC, 3C-SiC, and Si for Power Devices. *IEEE Transactions on Electron Devices, 40*, 645.

Bogdanov, M. V., Galyukov, A. O., Karpov, S. Y., Kulik, A. V., Kochuguev, S. K., Ofengeim, D. K., . . . Makarov, Y. N. (2001). Virtual reactor as a new tool for modeling and optimization of SiC bulk crystal growth. *Journal of Crystal Growth, 225*, 307.

Bondokov, R. T., Tipirneni, N., & Sudarshan, D. I. a. T. S. (2004). Modification of 6H-SiC Surface Defect Structure during Hydrogen Etching. *Materials Science Forum, 457-460*, 431.

Burk, A. A., Tsvetkov, D., Barnhardt, D., J., M., O'Loughlin, Garrett, L., . . . Palmour, J. W. (2012). SiC epitaxial layer growth in a 6x150 mm warm-wall planetary reactor. *Materials Science Forum, 717-720*, 75.

Chen, W., & Capano, M. A. (2005). Growth and characterization of 4H-SiC epilayers on substrates with different off-cut angles. *Journal of Applied Physics, 98*, 114907.

Chen, X., Li, J., Ma, D., Hu, X., Xu, X., & Jiang, M. (2006). Fine Machining of Large-Diameter 6H-SiC Wafers. *Journal of Material Science Technology, 22*, 681-684.

Cicala, G., Capezzuto, P., Bruno, G., Schiavulli, L., & Amato, G. (1996). Plasma deposition of amorphous SiC: H, F alloys from SiF 4?CH 4?H 2 mixtures under modulated conditions. *Journal of Applied Physics, 79*, 8856.

Collins, W. (2000). Silicon Compounds, Silicon Halides. *Kirk-Othmer Encycl. of Chemical Technologies*.

Crippa, D., Valente, G. L., Ruggiero, A., Neri, L., Reitano, R., Calcagno, L., G. Foti, M. Mauceri, S. Leone, G. Pistone, Via, F. la. (2005). New achievements on CVD based methods for SiC epitaxial growth. *Materials Science Forum, 483-485*, 67.

Daas, B. K., Nomani, W., Daniels, K. M., Sudarshan, T. S., Koley, G., & Chandrashekhar, M. (2012). *Molecular gas adsorption induced carrier transport studies of epitaxial graphene using IR reflection spectroscopy.* Paper presented at the Materials Science Forum.

Danielsson, O., Henry, A., & Janzen, E. (2002). Growth rate predictions of chemical vapor deposited silicon carbide epitaxial layers. *Journal of Crystal Growth, 243*, 170.

Ellison, A., Zhang, J., Henry, A., & Janzen, E. (2002). Epitaxial growth of SiC in a chimney CVD reactor. *Journal of Crystal Growth, 236*, 225.

Emtsev, K. V., Bostwick, A., Horn, K., Jobst, J., Kellogg, G. L., Ley, L., . . . Röhrl, J. (2009). Towards wafer-size graphene layers by atmospheric pressure graphitization of silicon carbide. *Nature materials, 8*(3), 203-207.

F. La, V., Galvagno, G., Foti, G., Mauceri, M., Leone, S., Pistone, G., . . . Crippa, D. (2006). 4H SiC epitaxial growth with chlorine addition. *Chemical Vapor Deposition, 12*, 509.

F. La, V., Galvagno, G., Roccaforte, F., Giannazzo, F., Franco, S. D., Ruggiero, A., . . . Crippa, D. (2006). High growth rate process in a SiC horizontal CVD reactor using HCl. *Microelectronic Engineering, 83*, 48-50.

F. La, V., Izzo, G., Mauceri, M., Pistone, G., Condorelli, G., Perdicaro, L., . . . Crippa, D. (2008). 4H-SiC epitaxial layer growth by trichlorosilane (TCS). *Journal of Crystal Growth, 311*, 107-113.

Fanton, M., Skowronski, M., Snyder, D., Chung, H. J., Nigam, S., Weiland, B., & Huh, S. W. (2004). Growth of Bulk SiC by Halide Chemical Vapor Deposition. *Materials Science Forum, 87*, 457.

Fanton, M. A., Weiland, B. E., & Redwing, J. M. (2008). Growth of thick p-type SiC epitaxial layers by halide chemical vapor deposition. *Journal of Crystal Growth, 310*, 4088- 4093.

Feron, O., Langlais, F., Naslain, R., & Thebault, J. (1999). On kinetic and microstructural transitions in the CVD of pyrocarbon from propane. *Carbon, 37*, 1343.

Forsberg, U., Danielsson, O., Henry, A., Linnarsson, M. K., & Janzen, E. (2002). Nitrogen doping of epitaxial silicon carbide. *Journal of Crystal Growth, 236*, 101.

Fujihira, K., Kimoto, T., & Matsunami, H. (2003). Growth and characterization of 4H-SiC in vertical hot-wall chemical vapor deposition. *Journal of Crystal Growth, 255*, 136.

Fujiwaraa, H., Dannoa, K., Kimotoa, T., Tojob, T., & Matsunami, H. (2005). Effects of C/Si ratio in fast epitaxial growth of 4H-SiC(0 0 0 1) by vertical hot-wall chemical vapor deposition. *Journal of Crystal Growth, 281*, 370.

Ganguly, G., De, S. C., Ray, S., & Barua, A. K. (1991). Polycrystalline silicon carbide films deposited by low?power radio?frequency plasma decomposition of SiF 4?CF 4?H 2 gas mixtures. *Journal of Applied Physics, 69*, 3915.

Ghandhi, S. K., & Field, R. J. (1984). A Re-examination of boundary layer theory for a horizontal CVD reactor. *Journal of Crystal Growth, 69*, 619.

Grim, J. R., Benamara, M., Skowronski, M., Everson, W. J., & Heydemann, V. D. (2006). Transmission electron microscopy analysis of mechanical polishing-related damage in silicon carbide wafers. *Semiconductor Science and Technology, 21*, 1709-1713.

Grisdale, R. O. (1953). The formation of black carbon. *Journal of Applied Physics, 24*, 1082.

Grovenor, C. R. M. (1994). *Microelectronic materials*: Institute of physics publishing.

Gutmann, V. (1967). Halogen Chemistry. *Academic press, Vol.2*, 171.

Ha, S., Mieszkowski, P., Skowronski, M., Rowland, L. B., Matsunami, H., Ueda, T., & Nishino, H. (2002). Dislocation conversion in 4H silicon carbide epitaxy. *Journal of Crystal Growth, 244*, 257-266.

Hallin, C., Owman, F., Mh-tenssorf, P., Ellison, A., Konstantinov, A., Kordinaa, & Janzen, E. (1997). In situ substrate preparation for high-quality SiC chemical vapour deposition. *Journal of Crystal Growth, 181*, 241-253.

Harima, H., Nakashima, S., & Uemura, T. (1995). Raman scattering from anisotropic LOphonon-plasmon-coupled mode in n type 4H- and 6H-SiC. *Journal of Applied Physics, 78*, 1996.

Hassan, J., Bergman, J. P., Henry, A., & Janzen, E. (2008). On-axis homoepitaxial growth on Si-face 4H-SiC substrates. *Journal of Crystal Growth, 310*, 4424-4429.

Henry, A., Hassan, J. u., Bergman, J. P., Hallin, C., & Janzen, E. (2006). Thick silicon carbide homoepitaxial layers grown by CVD techniques. *Chemical Vapor Deposition, 12*, 475.

Hirschfelder, J. O., Curtiss, C. F., & Bird, R. B. (1954). Molecular theory of gases and liquids. *Wiley, New York*.

Hori, T., Danno, K., & Kimoto, T. (2007). Fast homoepitaxial growth of 4H-SiC with low basal-plane dislocation density and low trap concentration by hot-wall chemical vapor deposition. *Journal of Crystal Growth, 306*, 297.

Huheey, J. E. (1972). Inorganic Chemistry Principles of structure and reactivity. *Prentice Hall*, 694.

Iftekher, C., M.V.S.Chandrasekhar, Klein, P. B., Caldwell, J. D., & Sudarshan, T. S. (2011). High growth rate 4H-SiC epitaxial growth using dichlorosilane in a hotwall CVD reactor. *Journal of Crystal Growth, 316*, 60-66.

Ito, M., Storasta, L., & Tsuchida, H. (2008). Development of 4H-SiC Epitaxial Growth Technique Achieving High Growth Rate and Large-Area Uniformity. *Applied Physics Express, 1*, 15001.

Johannes, W., & Julia R., W. (1964). Elementary dislocation theory. *Macmilan, New York*.

Kida, T., Nagasaka, Y., Sakurai, T., Yamakami, T., Hayashiby, R., Abe, K., & Kamimura, K. (2008). Growth and Characterization of SiC Films by Hot-Wire Chemical Vapor Deposition at Low Substrate Temperature Using SiF 4 /CH 4 /H 2 Mixture. *Japanese Journal of Applied Physics, 47*, 566.

Kimoto, T., Nishino, H., Yoo, W. S., & Matsunami, H. (1993). Growth mechanism of 6H-SiC in step-controlled epitaxy. *Journal of Applied Physics, 73*, 726.

Kimoto, T., Tamura, S., Chen, Y., Fujihira, K., & Matsunami, H. (2001). Fast Epitaxial Growth of 4H–SiC by Chimney-Type Vertical Hot-Wall Chemical Vapor Deposition. *Japanese Journal of Applied Physics, 40*, L374-L376.

kinetics.nist.gov/janaf/.

Klein, P., Shanabrook, B. V., Huh, S. W., Polyakov, A. Y., Skowronski, M., Sumakeris, J. J., & O'Loughlin, M. J. (2006). Lifetime-limiting defects in n? 4H-SiC epilayers. *Appled. Physics Letters, 88*, 52110.

Kolke, T., & Gardlner, W. C. (1980). Thermal decomposition of propane. *Journal of Physical Chemistry, 84*, 2005.

Konstantinov, A. O., Hallin, C., Pecz, B., Kordina, O., & Janzen, E. (1997). The mechanism for cubic SiC formation on off-oriented substrates. *Journal of Crystal Growth, 178*, 495.

Kordina, O., C. Hallin, A. H., Bergman, J. P., Ivanov, I., Ellison, A., Son, N. T., & Janzen, E. (1997). Growth of SiC by Hot-wall CVD and HTCVD. *Physica Status Solidi (B), 202*, 321.

Kotamraju, S., Krishnan, B., & Koshka, Y. (2009). Use of chlorinated carbon and silicon precursors for epitaxial growth of 4H-SiC at very high growth rates. *Physica Status Solidi RRL, 3*, 157.

Kukta, R. V., Peralta, A., & Kouris, D. (2002). Elastic interaction of surface steps: Effect of atomic-scale roughness. *Physical Review Letters, 88*, 186102.

Kumagawa, M., & Yamada, H. K. a. S. (1969). Hydrogen etching of silicon carbide. *Japanese Journal of Applied Physics, 8*, 421.

Larkin, D. J., Neudeck, P. G., Powell, J. A., & Matus, L. G. (1994). Site-compitition epitaxy for superior silicon carbide electronics. *Applied Physics Letters, 65*, 1659.

Laurence A Write, S. K., and Ian Williams. (2011). "Carbon footprinting": towards a universally accepted definition. *Carbon Management, 2*, 61-72.

Leone, S., Beyer, F. C., Pedersen, H., Kordina, O., Henry, A., & Janzen, E. (2010). High Growth Rate of 4H-SiC Epilayers on On-Axis Substrates with Different Chlorinated Precursors. *Crystal Growth and Design, 10*, 5334-5340.

Leone, S., H.Pedersen, A.Henry, & O.Kordina, E. J. (2009). Thick homoepitaxial layers grown on on-axis Si-face 6H- and 4H-SiC subsrates with HCl addition. *Journal of Crystal Growth, 312*, 24.

Lu, P., Edgar, J. H., Glembocki, O. J., Klein, P. B., Glaser, E. R., Perrin, J., & Chaudhuri, J. (2005). High-speed homoepitaxy of SiC from methyltrichlorosilane by chemical vapor deposition. *Journal of Crystal Growth, 285*, 506.

Marchenko, V. I., & Parshin, A. Y. (1980). Elastic properties of crystal surfaces. *Sov. Phys JETP, 52*, 129.

Margrave, J. L., & Wilson, P. W. (1971). Silicon difluoride, a carbene analog. Its reactions and properties. *Accounts of Chemical Research, 4*, 145.

Matsunami, H., & Kimoto, T. (1997). Step-controlled epitaxial growth of SiC: High quality homoepitaxy. *Materials Science and Engineering R: Reports, 20*, 125-166.

Musket, R. G., Yoshiyama, J. M., & Contolini, R. J. (2002). Vapor etching of ion tracks in fused silica. *Journal of Applied Physics, 91*, 5760.

Myers, R. L., -Ward, Kordina, O., Shishkin, Z., Rao, S. P., Everly, R., & Saddow, S. (2005). Increased growth rate in a SiC CVD reactor using HCl as a growth additive. *Materials Science Forum, 483-485*, 73.

Myers, R. L., Shishkin, Y., Kordina, O., & Saddow, S. E. (2005). High growth rates (> 30um/h) of 4H-SiC epitaxial layers using a horizontal hot-wall CVD reactor. *Journal of Crystal Growth, 285*, 486.

Nakajima, A., Yokoya, H., Furukawa, Y., & Yonezu, H. (2005). Step control of vicinal 6H-SiC (0001) surface by H 2 etching. *Journal of Applied Physics., 97*, 104919 - 104919-104915.

Nakamura, S.-i., Kimoto, T., Matsunami, H., Tanaka, S., Teraguchi, N., & Suzuki, A. (2000). Formation of periodic steps with a unit-cell height on 6H-SiC (0001) surface by HCl etching. *Applied Physics Letters, 76*, 3412.

Nakashima, S., & Harima, H. (1997). Raman investigation of SiC polytypes. *Physica Status Solidi A, 162*, 39-64.

Neudeck, P. G. (2006). The VLSI Handbook: Silicon carbide technology. *CRC Press LLC*, Chapter-5.

Nishizawa, S., & Pons, M. (2006). Numerical modeling of SiC CVD in a horizontal hot-wall reactor. *Microelectronic Engineering, 83*, 100.
O'Loughlin, M. J., K.G.Irvine, Sumakeris, J. J., Armentrout, M. H., Hull, B. A., & Jr., A. A. B. (2008). Silicon carbide hot-wall epitaxy for large-area, high-voltage devices. *Mater. Res. Soc. Symp. Proceding, 1069*, 115 1069-D1004-1001.
Ohno, T., Yamaguchi, H., Kuroda, S., Kojima, K., Suzuki, T., & Arai, K. (2004). Influence of growth conditions on basal plane dislocation in 4H-SiC epitaxial layer. *Journal of Crystal Growth, 271*, 1-7.
Oshima, C., & Nagashima, A. (1997). Ultra-thin epitaxial films of graphite and hexagonal boron nitride on solid surfaces. *Journal of Physics: Condensed Matter, 9*(1), 1.
Palisaitis, J., & Vasiliauskas, R. (2008). Epitaxial growth of thin films. *Physics of Advanced Materials Winter School*.
Pearton, S. J. (1997). *GaN and Related Materials*: Gordon and Breach Science Publishers.
Pedersen, H. (2008). Chloride-based Silicon Carbide CVD. *Thesis*.
Pedersen, H., Leone, S., Henry, A., Beyer, F. C., Darakchieva, V., & Janzen, E. (2007). Very high growth rate of 4H-SiC epilayers using the chlorinated precursor methyltrichlorosilane (MTS). *Journal of Crystal Growth, 307*, 334.
Pedersen, H., Leone, S., Kordina, O., Henry, A., Nishizawa, S.-i., Koshka, Y., & Janzen, E. (2011). Chloride-Based CVD Growth of Silicon Carbide
for Electronic Applications. *Chemical Reviews, 112*, 2434-2450.
Pedersen, H., Leone, S., O.Kordina, Henry, A., Nishizawa, S., Koshka, Y., & Janzen, E. (2012). Gas-Phase Modeling of Chlorine-Based Chemical Vapor Deposition of Silicon Carbide. *Chemical Review, 112*, 2434.
Putte, P. V., Gilling, L. J., & Bloem, J. (1975). Growth and etching of silicon in chemical vapour deposition system; The influence of thermal diffusion and temperature gradient. *Journal of Crystal Growth, 31*, 299.
Ramachandran, V., Brady, M. F., smith, A. R., & Greve, R. M. F. a. D. W. (1998). Preparation of atomically flat surfaces on silicon carbide using hydrogen etching. *Journal of Electronic Materials, 27*, 308.
Rana, T., Chandrashekhar, M., & Sudarshan, T. S. (2012). Elimination of silicon gas phase nucleation using tetrafluorosilane (SiF4) precursor for high quality thick silicon carbide (SiC) homoepitaxy. *Physica Status Solidi A, 209*, 2455.
Rana, T., Song, H. Z., Chandrashekhar, M. V. S., & Sudarshan, T. S. (2012a). Behavior of particles in the growth reactor and their effect on silicon carbide epitaxial growth. *Materials Science Forum, 717-720*, 153.
Rana, T., Song, H. Z., Chandrashekhar, M. V. S., & Sudarshan, T. S. (2012b). Comparison of 4H silicon carbide epitaxial growths at various growth pressures using dicholorosilane and silane gases. *Materials Science Forum, 717-720*, 117.
Robinson, J. A., Wetherington, M., Tedesco, J. L., Campbell, P. M., Weng, X., Stitt, J., . . . VanMil, B. L. (2009). Correlating Raman spectral signatures with carrier mobility in epitaxial graphene: A guide to achieving high mobility on the wafer scale. *Nano letters, 9*(8), 2873-2876.
Robinson, P. H. (1976). US Patent 3945864,1976

Robinson, P. H., & Goldsmith, N. (1975). Silicon epitaxial growth using dichlorosilane. *Journal of electronic material, 4*, 313.
Sanchez, E. K., Ha, S., Grim, J., Skowronski, M., Vetter, W. M., Dudley, M., & Mitchel, R. B. a. W. C. Assessment of Polishing-Related Surface Damage in Silicon Carbide.
Sato, M., & Uwaha, M. (2001). Growth law of step bunches induced by the Ehrlich-Schwoebel effect in growth. *Surface Science, 493*, 494-498.
Schwoebel, R. L. (1966). Step motion on crystal surfaces. *Journal of Applied Physics, 37*, 3682-3686.
Shephered, W. H. (1965). Vapor phase deposition and etching of silicon. *J. Electrochem. Soc., 112*, 988.
Shrivastava, A. (2008). *Epitaxial growth and characterization of 4H-silicon carbide on low off-axis substrates for high-power devices.* 3336623 Ph.D., University of South Carolina, Ann Arbor. Dissertations & Theses @ University of South Carolina; ProQuest Dissertations & Theses Full Text database.
Skelland, A. H. P. (1985). *Diffusional Mass Transfer*.
Spencer, H. B., Toguri, J. M., & Kurtis, J. A. (1969). Diffusivity measurements of the argon mercury vapor system. *Canadian Journal of Chemistry*, 47
Starke, U., Schardt, J., Bernhardt, J., Franke, M., & Heinz, K. (1999). Stacking transformation from hexagonal to cubic SiC induced by surface reconstruction: A seed for heterostructure growth. *Physical Review Letters, 82*, 2107-2110.
Sundaresan, S., Sturdevant, C., Marripelly, M., Lieser, E., & Singh, R. (2012). 12.9 kV SiC PiN diodes with low on-state drops and high carrier lifetime. *Materials Science Forum, 717-720*, 949.
Swihart, M. T., & Carr, R. W. (1998). On the mechanism of homogeneous decomposition of the chlorinated silanes. Chain Reactions Propagated by Divalent Silicon Species. *Journal of Physical Chemistry A, 102*, 1542.
Syvajarvi, M., Yakimova, R., & Janzen, E. (2002). Step-bunching in SiC epitaxy: anisotropy and influence of growth temperature. *Journal of Crystal Growth, 236*, 297-304.
Timms, P. L., Kent, R. A., Ehlert, T. C., & Margave, J. L. (1965). Silicon-Fluorine Chemistry. I. Silicon Difluoride and the Perfluorosilanes. *Journal of the American Chemical Society, 87*, 2824-2828.
Valente, G., Cavallotti, C., Masi, M., & Carra, S. (2001). Reduced order model for the CVD of epitaxial silicon from silane and chlorosilanes. *Journal of Crystal Growth, 230*, 247.
VanMil, B. L., K.K.Lew, R.L.Myers, R.T.Holm, D.K.Gaskill, Eddy, C. R., . . . P.Zhao. (2009). Etch rates near hot-wall CVD growth temperature for Si-face 4H-SiC using H2 and C3H8, Journal of Crystal Growth. *Journal of Crystal Growth, 311*, 238-243.
Veneroni, A., & Masi, M. (2006). Gas Phase and Surface Kinetics of Epitaxial Silicon Carbide Growth Involving Chlorine Containing Species. *Chemical Vapor Deposition, 12*, 562-568.
Veneroni, A., Omarini, F., & Masi, M. (2005). Silicon carbide growth mechanisms from SiH_4, $SiHCl_3$ and nC_3H_8. *Crystal. Research. Technology, 40*, 967.

Vorob'ev, A. N., Karpov, S. Y., Bord, O. V., Zhmakin, A. I., Lovtsus, A. A., & Makarov, Y. N. (2000). Modeling of gas phase nucleation during SiC CVD. *Diamond and related materials, 9*, 472.

W. T. Read, J. (1953). *Dislocations in crystals*.

Wang, R., & Ma, R. (2007). Kinetics of halide chemical vapor deposition of silicon carbide film. *Journal of Crystal Growth, 308*, 189.

Wang, R., & Ma, R. (2008). An integrated model for halide chemical vapor deposition of silicon carbide epitaxial films. *Journal of Crystal Growth, 310*, 4248.

www.compoundsemiconductor.net/csc/features-details/19734837/Exploiting-the-high-temperature-promise-of-Si.html.

www.compoundsemiconductor.net/csc/indepth-details/19735741/GaN-substrates-to-challenge-silico.html.

www.cree.com.

www.cree.com/news-and-events/cree-news/press-releases/2013/march/2nd-gen-mosfet.

www.eia.gov/tools/faqs/faq.cfm?id=105&t=3.

www.eia.gov/tools/faqs/faq.cfm?id=427&t=3.

www.energy.gov.

www.genesicsemi.com/index.php/news/03-05-13.

Yamamoto, T., Kimito, T., & Matsunami, H. (1998). Materials Science Forum. *Impurity Incorporation Mechanism in Step-Controlled Epitaxy Growth Temperature and Substrate Off-Angle Dependence, 264*, 111.

Yershov, I. A., Orlov, A. N., Petrov, Y. N., & Prokhorov, A. M. (1993). Dissociation of SiF4 Molecules in the Gas Phase under the Action of Continuous-Wave CO2-Laser Radiation: Frequency Dependence. *Laser physics, 3*, 204.

Zhang, & Sudarshan, T. S. (2005). Basal plane dislocation-free epitaxy of silicon carbide. *Applied Physics Letters, 87*, 151913.

Zhao, J. H., Alexandrov, P., & Li, X. (2003). Demonstration of the First 10-kV 4H-SiC Schottky Barrier Diodes. *IEEE Electron Device Letters, 24*, 402.

APPENDIX A --SILICON CARBIDE CRYSTAL PLANES AND DIRECTIONS

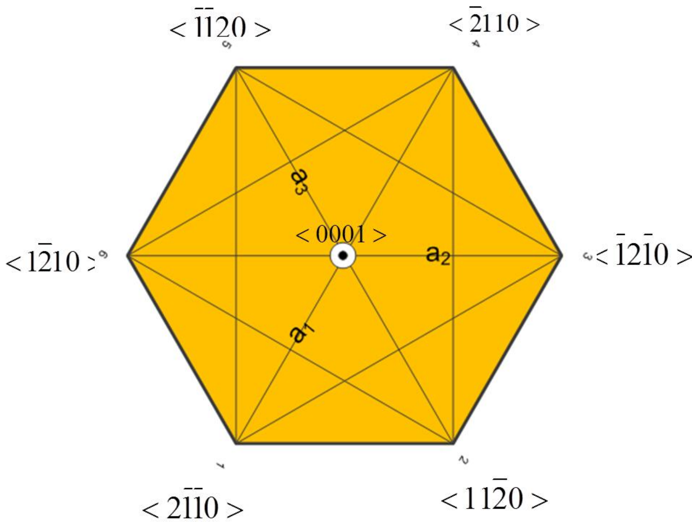

Figure A.1 Crystal directions on the basal plane of hexagonal SiC crystal

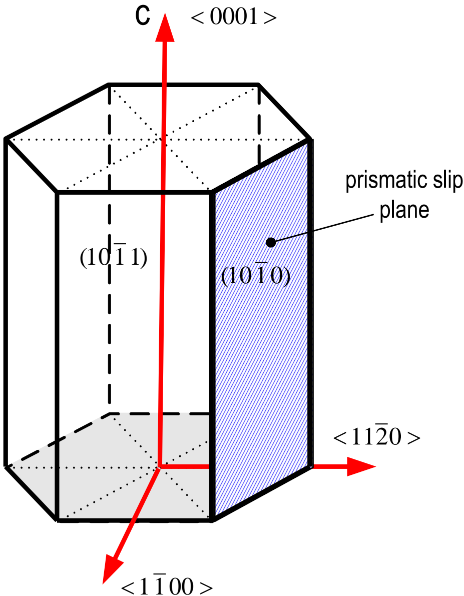

Figure A.2 Various crystal planes of hexagonal SiC crystal

APPENDIX B – EPITAXIAL GRAPHENE GROWTH BY SiF_4 GAS

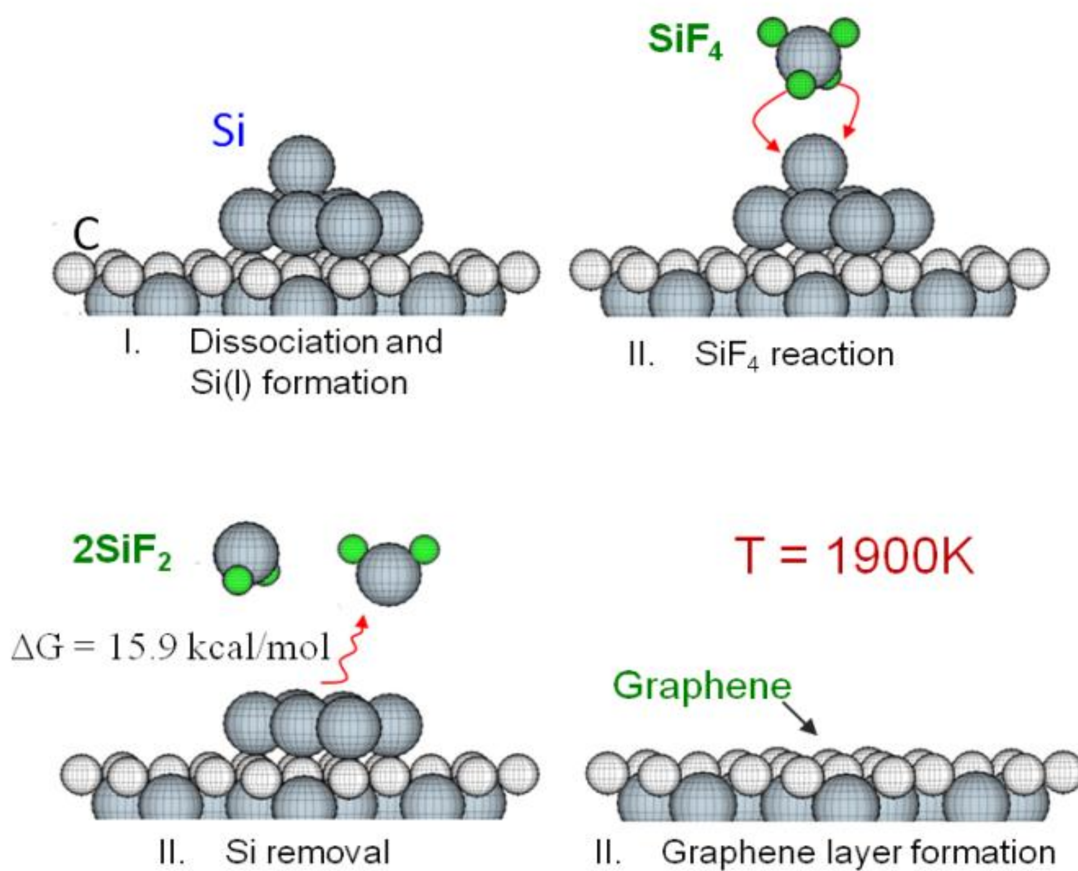

Figure B.1 Steps of the graphene growth by TFS (SiF_4) gas n an inert ambient.

APPENDIX C – SAFETY ISSUES USING SiF_4 GAS

Safety is the most important factor in any circumstances. CVD furnace, especially for SiC epitaxy, where temperature is high and flammable gases are flowing, the situation is particularly dangerous and extreme care has to be taken in order to prevent any life threatening accident. For any other gases, TFS based CVD is also needed to be handled with extreme care. Some important precautions are presented below.

1. CVD furnace should never be unattended during the growth.
2. Reactor should be pumped for high vacuum (~10^{-6} torr) before starting the growth.
3. H_2, HF, DCS etc. gas sensors should be checked before starting the growth.
4. Proper filters to trap by product gases HCl, HF (if any) needed to be used.
5. Reactor must be pumped and flushed properly before unloading the sample. For this process overnight pumping (turbo pump) is recommended.
6. Graphite parts must be baked at 750°C - 1000ºC to remove residual moisture.
7. Exhausted pumps should be regularly checked for operation.
8. Safety equipments, e.g. fire extinguisher, emergency stop switch etc. should be checked before starting the growth process.
9. Water flow for the reactor cooling has to be ensured before starting the growth during the whole process.

APPENDIX D – DRAWING OF SPLIT TUBE ASSEMBLY

Date: 02/31/12......................
Part number:......................

UNIVERSITY OF SOUTH CAROLINA

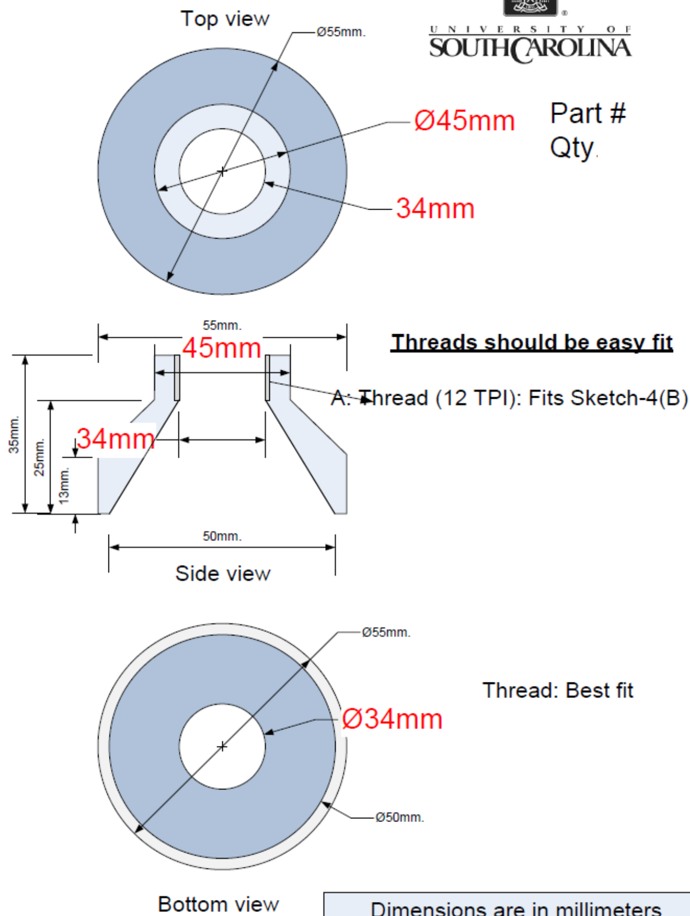

Dimensions are in millimeters
(+/-0.1mm)
High purity, high density graphite
SiC coating
Contact: Tawhid Rana
University of South Carolina
Phone: 803-777-8480
rana@email.sc.edu

Not drawn to scale

Figure D.1 Sketch of the injector.

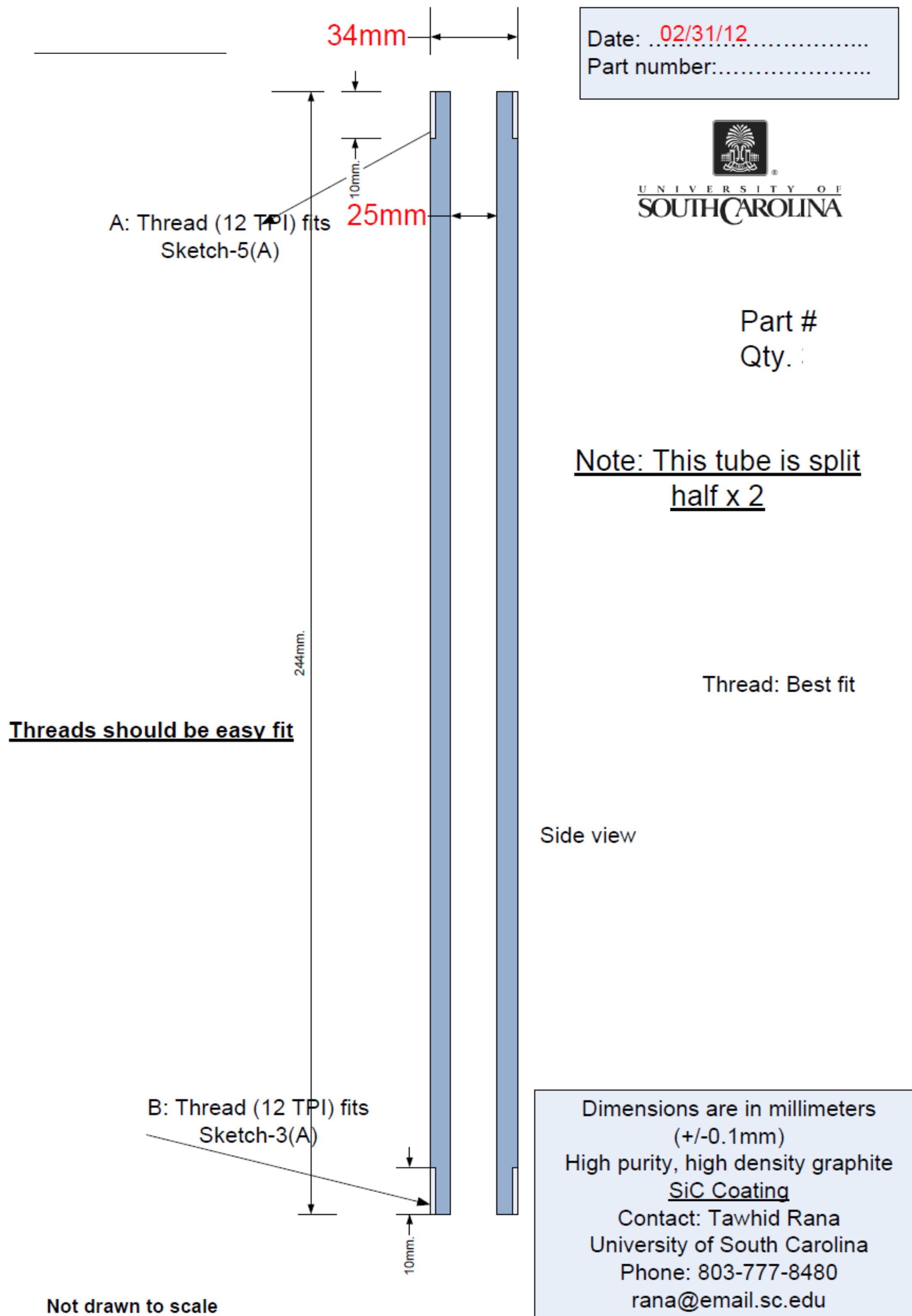

Figure D.2 Sketch of injector split tube.

Date: 02/31/12..................
Part number:.....................

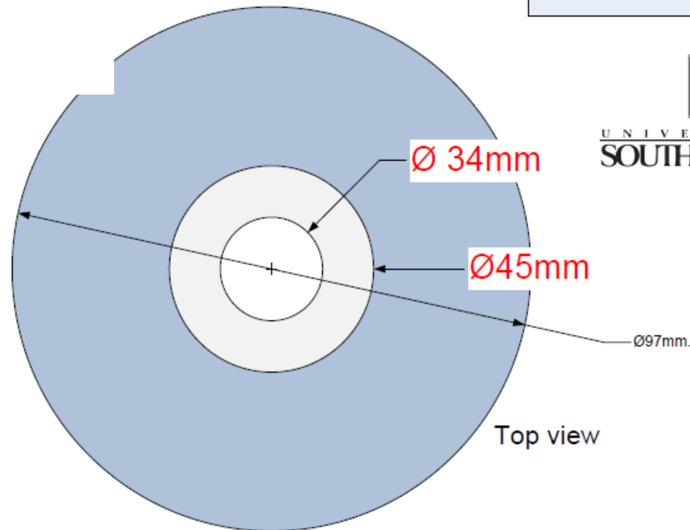

Part #
Qty. 1

Thread: Best fit

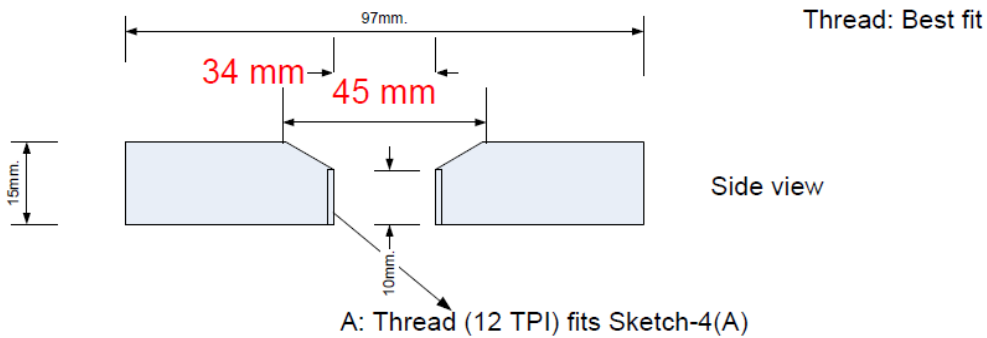

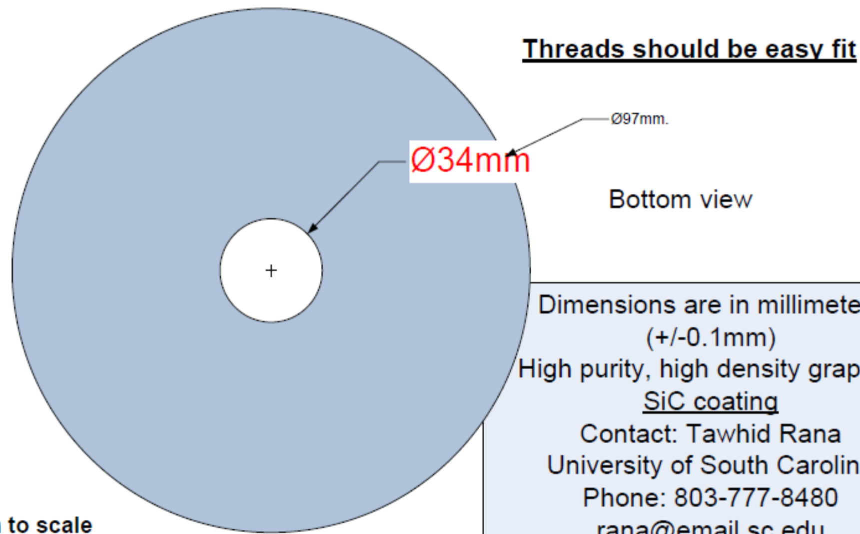

Dimensions are in millimeters
(+/-0.1mm)
High purity, high density graphite
SiC coating
Contact: Tawhid Rana
University of South Carolina
Phone: 803-777-8480
rana@email.sc.edu

Not drawn to scale

Figure D.3 Sketch of top plate of the gas injector.

APPENDIX E – CHEMICAL VAPOR DEPOSITION MANUAL[1]

In electronic device preparation it is required to grow a thin layer on semiconductor substrate. Chemical vapor deposition or CVD is a widely used technique to grow epilayer on semiconductor substrates.

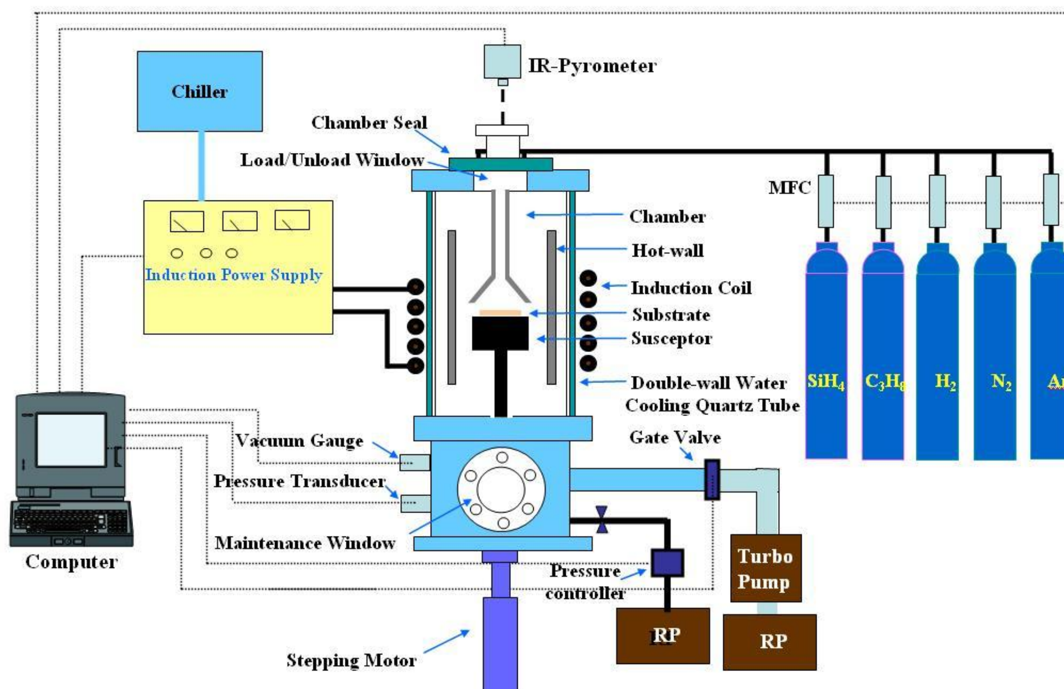

Figure E.1: Block diagram of CVD system

The goal of CVD is to grow a layer on top of the substrate by replicating substrate's atomic arrangement. It uses source gases which contains elements of the desired material.

[1] This section is adapted from Appendix A (Shrivastava, 2008), originally written by the candidate (group member) for the same CVD reactor. Please note that reactor geometry, processes are modified time to time and this manual may not be directly followed.

Source gases are carried into the reaction chamber by carrier gas H_2. Precise control of temperature, pressure and their respective duration and substrate position are required during the whole process.

Basic components of a CVD system are

1. Furnace
2. Vacuum pumps
3. Temperature controlling facilities.
4. Gas flow controlling facilities.
5. Pressure controlling facilities.
6. Computer based control system.

Operation of a CVD can be dissected into four basic parts

1. Temperature Ramp up
2. Hydrogen Etching
3. Growth at High temperature
4. Temperature ramp Down

COMPONENT LIST:

RACK-1

1. Temperature sensor
2. Turbo pump controller unit
3. Cold cathode pressure measurement unit
4. MKS multi gas controller
5. MKS 600 series pressure controller
6. Smart UPS 1400
7. Smart UPS 2200
8. Gas flow indicator panel

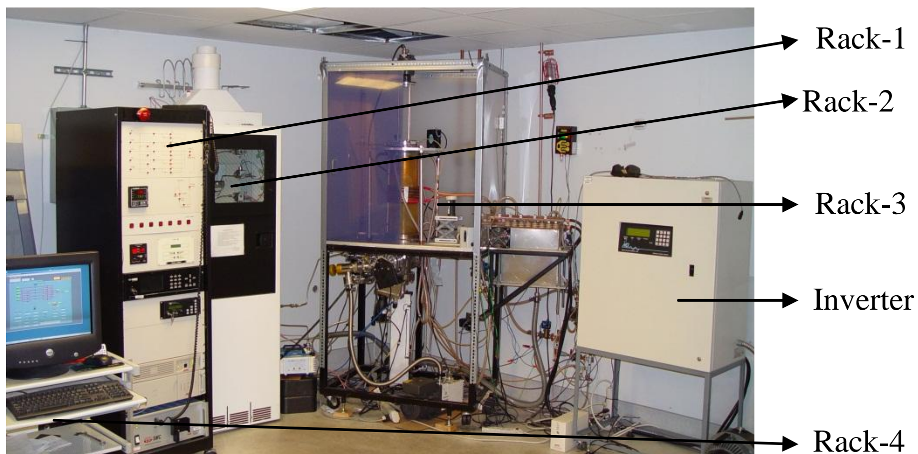

Figure E.2 CVD reactor system used for the experiments.

RACK-2

1. MFC controllers,
2. Electrical valves
3. Pipe connections
4. Manual valves

RACK-3

1. Pyrometer
2. Reactor furnace
3. Gas nozzle
4. Hot wall
5. Susceptor
6. Glass rod sample raiser
7. Turbo pump
8. Rotary vane pump

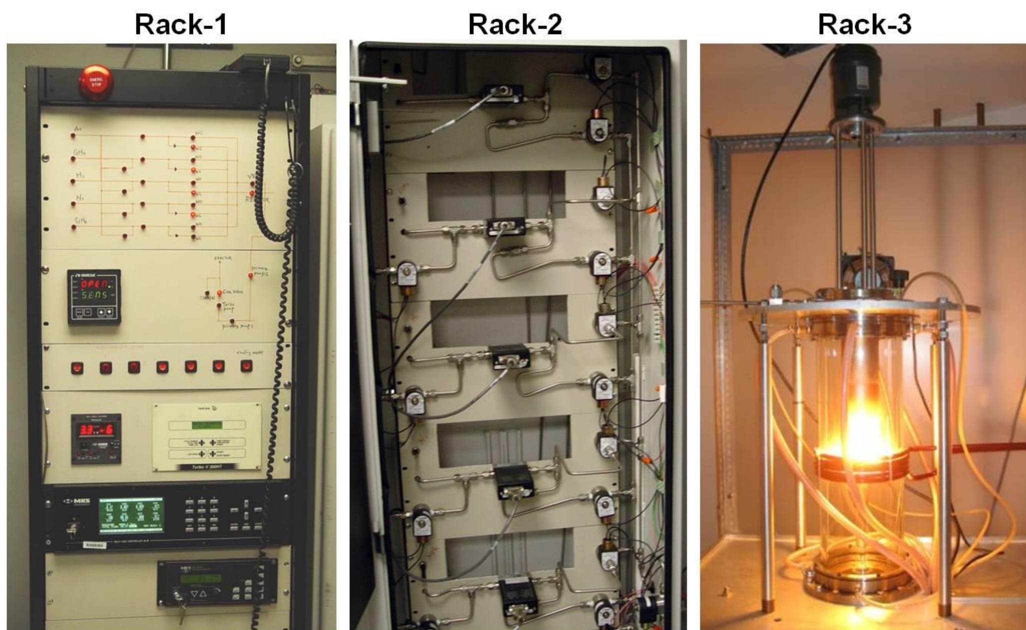

Figure E.3 Rack-1, Rack-2 and Rack-3 of the CVD system at USC

RACK-4

9. PC with interfaces
10. Lab CVD software
11. MKS software
12. Labview Recipe maker
13. Labview Recipe viewer

GAS TANK CABINET

1. H_2 Gas cylinder
2. $SiCl_2H_4$ (DCS) gas cylinder
3. SiF_4 (TFS) gas cylinder
4. Ar gas cylinder
5. SiH_4 gas cylinder
6. C_3H_8 gas cylinder
7. Pressure controllers

SAFETY DEVICES

1. H_2 detectors
2. $SiCl_2H_4$ gas detector
3. SiH_4 gas detector
4. C_3H_8 gas detector
5. HF gas detectors

SOFTWARE (LABVIEW)

1. CVD (LABVIEW)

CVD program which is used to control different electrical valves for different stages by graphical interface. A recipe can be loaded and run for automatic CVD process

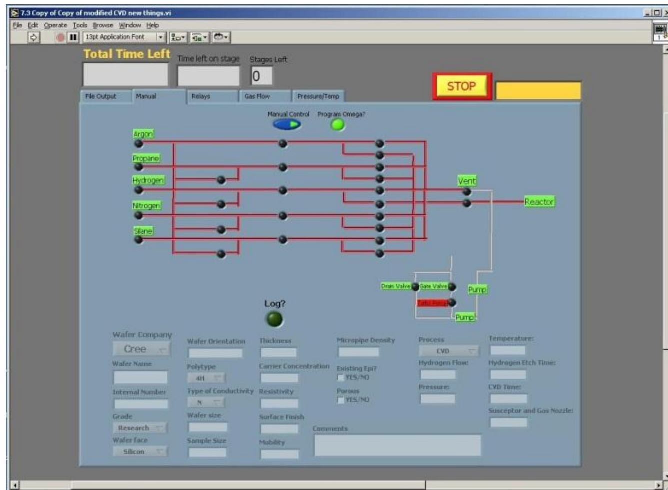

Figure E.4: CVD program by lab view

2. MKS CONTROLLER

This is the software for MFC (Mass flow controller). MFCs inside rack-2 are controlled by this software which determines gas flows during the process.

Figure E.5: MFC software (MKS controller)

3. PROFILE VIEWER

Profile viewer is Labview software which is used to tweak existing CVD recipes. It can only change gas flow, temperature, duration of the stages.

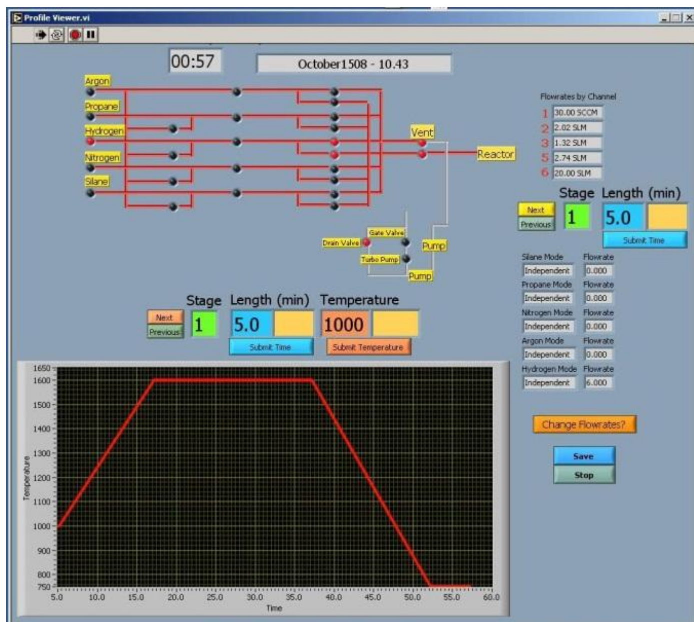

Figure E.6: Profile viewer (Labview)

STEP BY STEP GROWTH PROCESS

SAMPLE CLEANING AND PLACEMENT

1. Clean the sample (in boiling TCE, Acetone, Methanol, DI water, Aqua regia, DI water, HF, DI water, ultra-sonic cleaning)

2. Clean the susceptor.

3. Clean air nozzle.

4. Put the sample on susceptor manually, very gently on the susceptor.

5. Put gas nozzle and hotwall on top of the susceptor.

6. Close the cover and tight up the screws.

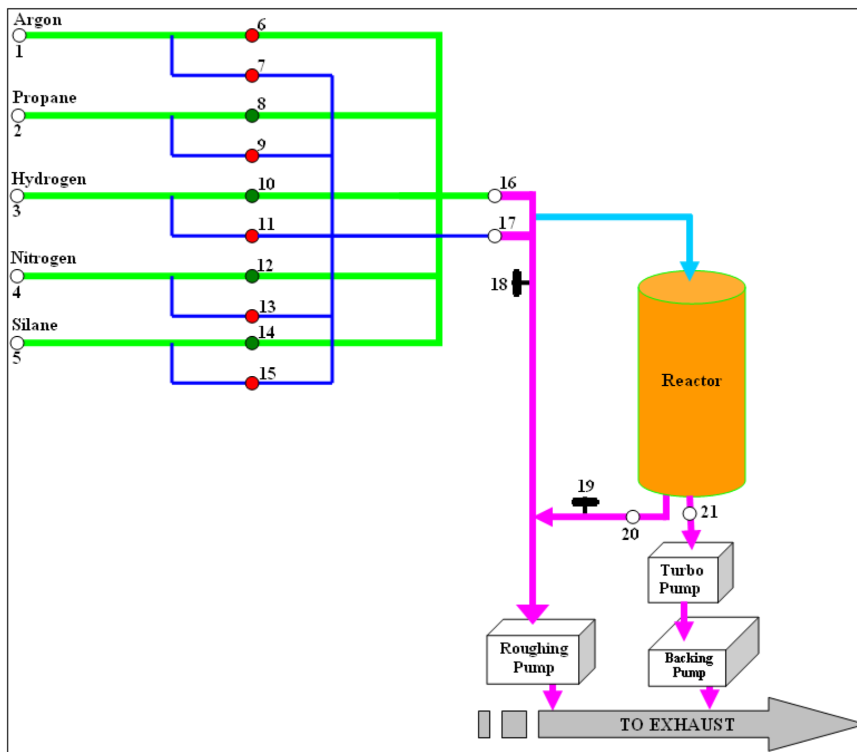

Figure E.7 Simplified block diagram of CVD system.

SYSTEM EVACUATION: LOW VACUUM

1. Slowly adjust MKS pressure controller (Figure E.8) and reduce the pressure to 0torr.

2. Open MKS software and click run button. (Figure E.5)

3. Make H_2 independent (Figure E.5).

4. Update each MFC (from software) and open it for flowing/pumping down by the maximum flow rates SLM/SCCM for the respective gases (Figure E.5).

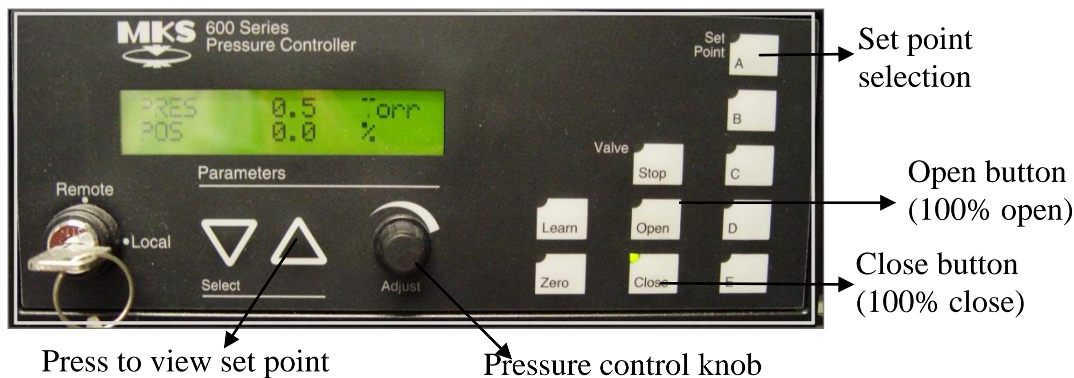

Figure E.8: pressure controller front panel.

5. Open CVD program (Figure E.4); open drain valve, reactor valve and second line of all gases. The second lines are connected to the reactor while first lines are connected to vent.

6. Wait until pressure reaches around 1 torr.

7. Press “Close” button in MKS unit (Figure E.10).

8. Open gate valve. Wait until pressure reaches ~0.5 torr.

SYSTEM EVACUATION: HIGH VACUUM

1. Turn on turbo-V 300HT controller by pressing start button in Varian turbo pump control panel (Figure E.9).

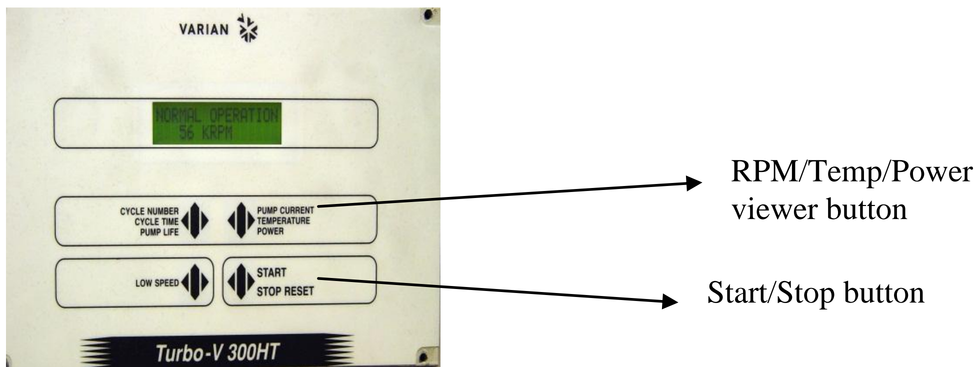

Figure E.9: Varian turbo pump control panel

2. Turn on high vacuum toggle valve after 10 minutes (Figure E.10).

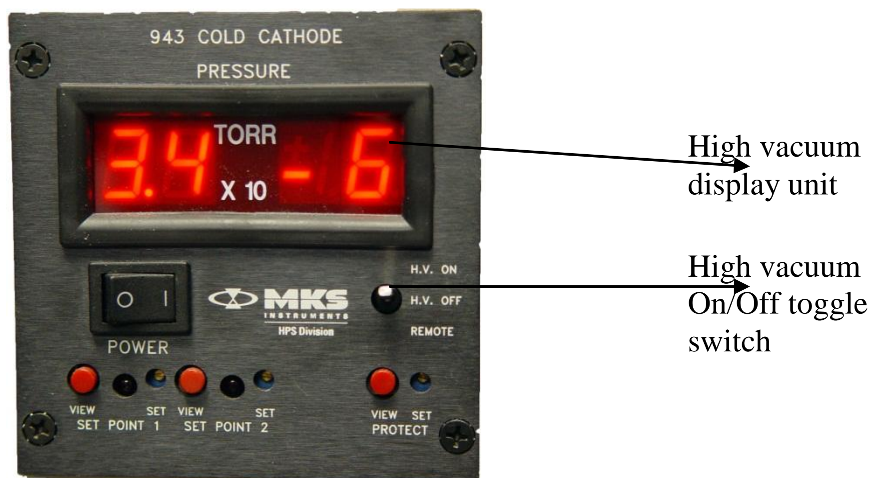

Figure E.10: Cold Cathode Pressure unit.

3. Wait until the vacuum reaches around 5e-6 torr (display unit in Figure E10 or any other pressure monitor unit).
4. Press ‘log’ button in Labview software (Figure E4) and provide all the necessary information regarding growth such as temperature, C/Si ratio etc.
5. Connect pyrometer.

6. Turn on cooling water (20 psi respectively), cooling fan and inverter.

GAS FLOW: INCREASING AMBIENT PRESSURE FOR GROWTH

1. Open H_2 cylinder main valve in the gas cabinet (Figure E.13)
2. Open MKS controller software (Figure E.5).
3. Close all lines except H_2 in MKS software.
4. Update for H_2 in MKS software by 0.5 slm.
5. Open H_2 reactor line.
6. Open H_2 main valve and wait till flow becomes stable in Figure E.11.

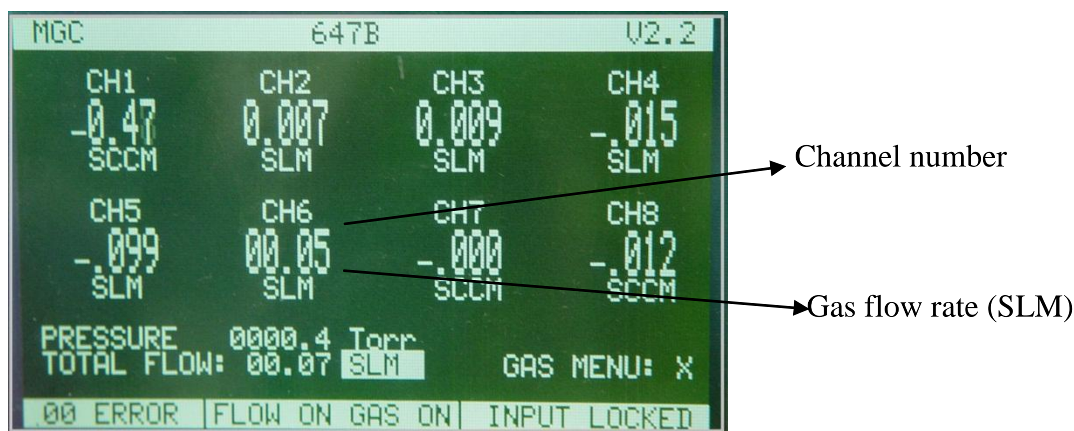

Figure E.11: Gas flow meter display unit.

7. Close gate valve in Rack-3.
8. Turn off turbo pump (Figure E.9).
9. Close cold cathode pressure gauge (Figure E.12).
10. Open second line first and then the first line of H_2 to pass gas through reactor (Figure E4).
11. Wait until pressure reaches 300 torr (Check display in Figure E.8)

12. Gradually increase H_2 flow rate by increasing the flow in increment of 0.5 slm in MKS controller software up to 10 slm.

STARTING THE CVD PROCESS

1. Check all the safety issues such as gas leak, cooling system etc. Close the furnace protective door.
2. Open Propane and Silane/DCS/TFS gas cylinders main valves.
3. Stop and close MKS software (Figure E.5).
4. Click ‘manual control’ in Labview^{TM} and a window pops up (Figure E4).
5. Select desired recipe and load it. It will give a number. Press OK.
6. Close the vent knob in the rack 3.
7. Wait until the gas flow is stable and then open the vent knob inside the rack 3.
8. Observe temperature, pressure, gas flow etc as process goes on.

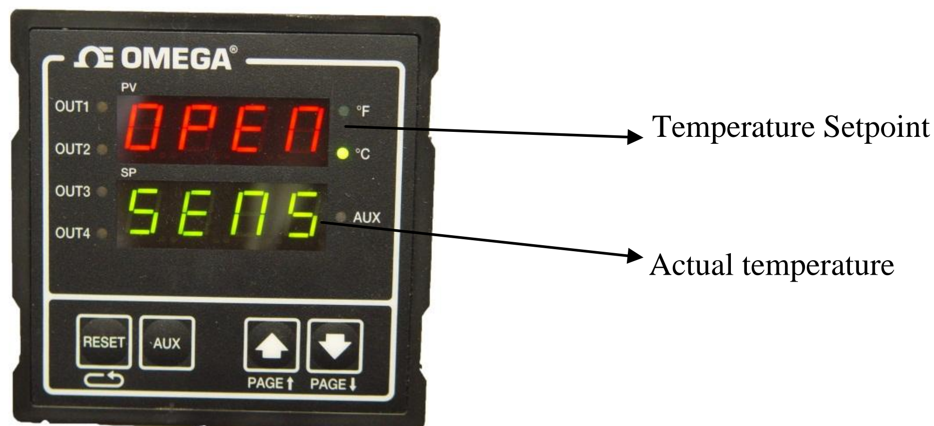

Figure E.12: Temperature sensor display.

9. Wait until it reaches growth temperature (usually 1550-1600°C).

10. Wait until process stops.
11. Close H_2, Propane and Silane/DCS/TFS gas cylinders.
12. Wait for at least 20 minutes after all the processes stop.
13. Turn off cooling water, cooling fan, inverter switches.

SYSTEM EVACUATION : LOW VACUUM

1. Slowly reduce pressure by adjusting MKS pressure controller (Figure 8).
2. Open MKS software (Figure E.5)
3. Make H_2 Independent (Figure E.5).
4. Open all the gas lines in Figure 4 let them flow through vent.
5. Purge all the gas lines by Ar for 3 times.
6. Press 'Close' button in MKS unit (Figure E.11).
7. Open gate valve to let backing pump pumps more up to ~0.5 torr.

SYSTEM EVACUATION: HIGH VACUUM

1. Turn on turbo pump.
2. Wait until it reaches around 5e-6 torr.

BRINGING THE SAMPLE OUT

1. Open the lid cover very slowly by unscrewing the bolts.
2. Bring the gas nozzle out very carefully so that it does not touch the hot wall.

3. Bring out the hotwall.

4. Bring the sample out carefully.

5. Close the lid again.

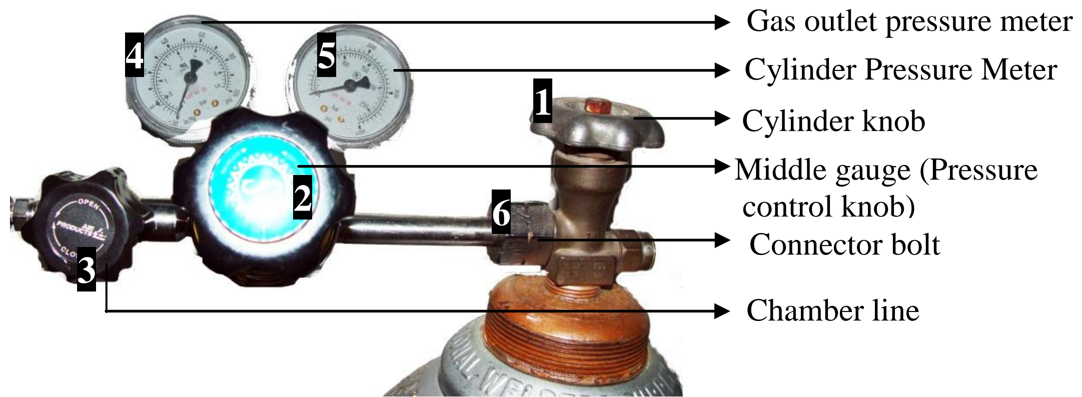

Figure E.13: Gas cylinder valves and meters.